

# Time scale interaction in low-order climate models

Tijdschaalinteractie in lage orde klimaatmodellen  
(met een samenvatting in het Nederlands)

Proefschrift

ter verkrijging van de graad van doctor aan de Universiteit Utrecht op  
gezag van de Rector Magnificus, Prof. dr. W.H. Gispen, ingevolge het  
besluit van het College voor Promoties in het openbaar te verdedigen op  
maandag 10 juni 2002 des middags te 14.30 uur

door

Lennaert van Veen

geboren op 27 maart 1972 te Leiden

Promotoren: Prof. Dr. F. Verhulst  
Faculteit der Wiskunde en Informatica,  
Universiteit Utrecht  
Prof. Dr. J. D. Opsteegh  
Faculteit der Natuur- en Sterrenkunde,  
Universiteit Utrecht;  
Koninklijk Nederlands Meteorologisch Instituut

Dit proefschrift werd mede mogelijk gemaakt door financiële steun van de Nederlandse Organisatie voor Wetenschappelijk Onderzoek.

2000 Mathematics Subject Classification: 86A05, 86A10, 37N10, 65P20, 65P30, 37G35, 34E20.

ISBN 90-393-3029-8

*Omnia sol temperat.*

Leescommissie: Prof. Dr. H. W. Broer  
Prof. Dr. O. Diekman  
Prof. Dr. ir. H. A. Dijkstra  
Dr. Yu. A. Kuznetsov  
Dr. L. R. M. Maas

# Contents

Chapter 1. Introduction	1
Bibliography	7
Chapter 2. Baroclinic flow and the Lorenz-84 model	9
1. Introduction	9
2. The QG two layer model	11
3. The Galerkin approximation	15
4. The six dimensional truncation	16
5. The reduced system	26
6. Reduction to the Lorenz-84 model	28
7. Conclusion	33
8. Acknowledgments	35
Bibliography	37
Chapter 3. Active and passive ocean regimes in a low-order climate model	39
1. Introduction	39
2. The Lorenz-84 general circulation model	41
3. The box model for a single ocean basin	42
4. The coupled equations	43
5. Perturbation theory	45
6. Bifurcations of equilibrium points	45
7. Chaotic attractors	46
8. Intermittency	47
9. Power spectra in the passive and the active regime	52
10. Conclusion and discussion	52
11. Acknowledgments	55
Bibliography	57
Chapter 4. Overturning and wind driven circulation in a low-order ocean-atmosphere model	59
1. Introduction	59
2. Description of the model	61
3. Asymptotic analysis with a passive atmosphere	68
4. Bifurcation analysis of the coupled system	72

5. Conclusion	79
6. Acknowledgments	80
Bibliography	81
Samenvatting	83
Dankwoord	87
Curriculum Vitae	89

## CHAPTER 1

# Introduction

Over the last decades, the study of climate variability has attracted ample attention. Temperature records show signs of global warming, starting around the end of the nineteenth century. The observation of this structural climatic change has led to questions about its causes and the mechanisms involved. Perhaps the most important issue is, to what extent climatic change is due to anthropogenic influence, connected to the industrial revolution, and to what extent to natural variability. This issue is becoming more and more important, as speculations arise about the link between climatic change and catastrophes such as floods and droughts. The task to understand interactions in the complex climate system is particularly difficult because of the lack of observational data, spanning a period of time typical for natural climate variability.

One way around this problem is to represent the earth's climate in a computer model, as a set of prognostic equations. By means of numerical integration the past and future climate can then be reconstructed. Also, numerical experiments can be conducted in which a number of quantities are kept fixed in order to investigate the sensitivity of the climate system to isolated physical effects.

A disadvantage of this approach is that, if the model under consideration is to faithfully represent the real climate system, it has to be large in terms of the number of degrees of freedom. Depending on their extent of realism, so called General Circulation Models (GCM's) have from a few thousand up to a few million degrees of freedom. This puts them out of reach of the ordinary analysis of dynamical systems theory. Instead, statistical analysis is used to study the model's output. The measurement of, for example, correlation coefficients, combined with the physical theory behind the processes represented in the model may lead to insight into the mechanism of climatic change and variability. The mathematical structure behind it, however, remains unclear. As a rule of thumb, the bigger the model, the harder it is to investigate its dynamics mathematically. Such a mathematical investigation can validate conclusions drawn on basis of experiments conducted with the model, as it focusses on stability of its behaviour to perturbations and genericity of its behaviour in a wider class of models.

The problem, that mathematical analysis is harder for more realistic models, also frustrates the study of weather, restricted to a time scale of days or weeks. As weather has a considerable impact on daily life, meteorology dates back to long before the computer era. Numerous approximations and simplifications have been devised to render the equations for atmospheric flow solvable by hand. In classical

studies such as Philips [1954]; Charney [1959]; Lorenz [1960] solutions are obtained by imposing symmetries, considering limits of physical parameters and exploiting perturbation theory. Their approach and results are now common knowledge in meteorology.

Computers made it possible to investigate solutions, out of reach of perturbation theory. At first, however, numerical computations were slow and painstaking. Forward integration of a set of three prognostic equations was a considerable task. Edward Lorenz had such a model at hand. He split the forward integration into parts and had them overlap in order to check the numerics. According to the popular anecdote this is how he came across the phenomenon of sensitive dependence on initial conditions, nowadays a major paradigm in meteorology and climatology. On a present day desktop computer, the whole computation he had in mind would take less than one second and this sensitive dependence may well go unnoticed.

Thus, the study of the equations governing atmospheric flow, without resort to massive numerical simulations, has led to many fundamental insights in meteorology. The study of extremely simplified climate models, as presented in this thesis, should likewise lead to an understanding of the mechanisms of climatic change. One feature climate models share is the presence of widely different time scales. Components of the climate system, which can often be considered fixed in the context of weather forecasts, have to be taken into account explicitly. Throughout this thesis the emphasis will be on the question to what extent the slow time scales play a role in the model's dynamics. In climate models, the slow time scales may be related to, e.g., ice sheet dynamics, variations in solar heat flux or ocean dynamics. In this work, the slow time scales will only be related to ocean dynamics and the fast time scale to atmospheric dynamics. The question is thus if the ocean plays an active or a passive role in the combined system [Marotzke, 1994].

An important class of extremely simplified models (for a review, see Olbers [2001]) is formed by Low-Order Models (LOM's). Low-order refers to the number of degrees of freedom. In conformance with mathematical literature I will refer to models of low order as those with a number of degrees of freedom not much greater than 10. This is a subjective definition which serves its purpose in the context of this work. The equations governing the dynamics of the atmosphere and the ocean are partial differential equations, with an infinite number of degrees of freedom. I will loosely refer to them as Fluid Dynamical (FD) equations, a notion which will be specified in chapters 2 and 4.

The set of LOM's can be subdivided in *conceptual* and *scalable* models. Conceptual models are formulated in an ad hoc fashion. The terms in the prognostic equations are chosen such that they represent certain isolated physical processes. Examples of such models are Stommel's model for the ocean [Stommel, 1961], in which the ocean is thought of as a number of boxes, connected by pipes, and the Daisyworld model [Watson and Lovelock, 1983], in which the face of the earth is covered by black and white daisies, competing for space. Scalable models are derived from a FD model by means of Galerkin truncation. The variables of the FD model, such as temperature and velocity fields, are projected onto a finite number



of basis functions, which describe spatial structures. The expansion coefficients are the variables of the LOM. Some basis functions, common in fluid dynamics, are:

- Fourier modes, as in Lorenz [1963], a description of the three degrees of freedom model mentioned above, and in chapter 2 of this thesis,
- orthogonal polynomials, as in Maas [1994], see chapter 4 of this thesis, and
- eigenfunctions of covariance operators, here referred to as Empirical Orthogonal Functions (EOF's), see Preisendorfer [1988].

These sets of basis functions can be ordered by the spatial scale they take into account. In the case of Fourier functions, for instance, this ordering is simply given by the wave number. The spatial scales are tied to time scales through the typical velocity of the fluids or masses of air under consideration. Hence, the reduction to finite order is, at the same time, a selection of relevant time and spatial scales. Contrary to conceptual models, the dynamics of scalable models is determined by the FD model. Also, the number of degrees of freedom of scalable models can be increased at will in order to investigate the robustness of their behaviour. Thus, stronger statements about the real climate system can be inferred from the study of scalable models.

There is no definite answer to the question, to what extent the solutions of a LOM represent solutions of the parent FD model. In general, experience shows that the solutions of a FD model settle down on a finite dimensional, attracting set in phase space. For certain FD models, rigorous analysis yields an upper bound for the dimension of this set [Temam, 1988]. This means, that the dynamics of the FD model can at least be captured by a model of finite order. Such upper bounds, however, are large compared to the definition of low-order put forward here. Therefore, we can not expect the LOM's to quantitatively reproduce solutions of the FD model.

The question, how to represent the effect of omitted degrees of freedom in a LOM is known as the closure problem. Some of the proposed solutions are inclusion of stochastic forcing terms in the LOM [De Swart and Grasman, 1987], statistical optimisation of the LOM's coefficients [Achatz and Branstator, 1999] and approximation of inertial manifolds by means of a modified Galerkin method [Foias et al., 1988]. In this thesis, I will not address the closure problem. The LOM's studied here are not intended to yield quantitatively correct predictions about the real climate system. The Galerkin method is regarded as a means to select time and spatial scales, and thereby the physical processes of interest. It is checked, however, that the LOM's output has the right order of magnitude.

As mentioned above, the low-order climate models in this thesis are coupled ocean-atmosphere models. The atmosphere model, studied here, was introduced by Lorenz [1984]. Lorenz only hinted at the possibility to derive the model as a Galerkin truncation of a FD model. In Chapter 2 of this thesis this link is made explicit. In doing so, the physics behind the model and its scaling are described in detail. It is shown, that the Lorenz-84 model describes the jet stream in the mid-latitude atmosphere, and planetary waves, which can grow if the jet stream becomes dynamically unstable [Peixoto and Oort, 1992, chapter 7]. The typical time scale,

associated with variability of the jet stream, also called the synoptic scale, is about one week. In subsequent chapters this will be the fast, atmospheric time scale.

The Lorenz-84 model will be coupled to two different low-order ocean models. In chapter 3, it is coupled to Stommel's two box model [Stommel, 1961]. Stommel's model mimics the large scale overturning, or thermohaline circulation in the North Atlantic ocean [Peixoto and Oort, 1992, chapter 8]. The typical time scale of variability of the thermohaline circulation is of the order of centuries. This will be the longest time scale in the coupled models.

In chapter 4, the Lorenz-84 model is coupled to an ocean model formulated by Maas [1994]. Contrary to the two box model, this is a scalable model. Consequently, considerable effort is put into a physical description of the coupling. Apart from the overturning circulation, Maas' model is capable of representing a wind driven gyre. The coupling works in two ways: through exchange of heat at the surface and through wind shear forcing. The latter acts on a time scale in between the fast atmospheric time scale and the slow overturning time scale. The intermediary time scale is set to about one year.

The LOM's in this thesis are sets of coupled, nonlinear, Ordinary Differential Equations (ODE's) on one, two and three widely separate time scales, respectively. These can be analysed with the aid of dynamical systems theory [Wiggins, 1990]. The emphasis will be on bifurcation analysis, i.e. the analysis of the dependence of the qualitative behaviour of the models on their parameters [Kuznetsov, 1998]. Also, the time scale separation leads to the presence of small parameters in the equations. The consequences for the behaviour of the coupled models are briefly explored by means of singular perturbation theory [Wiggins, 1994].

In chapter 2, the bifurcation structure of the Lorenz-84 model is investigated in some detail. Here, the focus is on the routes to chaotic behaviour in this model. In the subsequent chapters, the bifurcation structure of the coupled models is then compared to that of the uncoupled models. Keeping in mind the issue of time scale interaction, two differences stand out. In both coupled models, prominent intermittent behaviour is observed. This behaviour occurs near a point in parameter space at which the stability of periodic motion is lost. The slow subsystem, i.e. the ocean model, repeatedly pushes the fast subsystem, i.e. the atmosphere model, through a sequence of bifurcations. Thus, the ocean model plays an active role in the coupled system. Secondly, in the Lorenz-Maas model a periodic solution is shown to exist, with a period on the slow, overturning time scale. The atmospheric variables are at instantaneous equilibrium with the feedback of the ocean, and the behaviour of the coupled model is thus dictated by internal ocean dynamics. Both these phenomena occur near a critical point of the coupled system, in agreement with the general idea that in climate models the slow components can play an active role near such critical points and are passive otherwise.

There is not much literature on low-order models of ocean-atmosphere interaction. Models, studied in this field, are often extensions of the box-type approach [Huang and Stommel, 1992; Nakamura et al., 1994; Rivin and Tziperman, 1997; Titz et al., 2002]. To my knowledge, the Lorenz-Maas model, introduced in chapter 4, is

the only scalable low-order model which includes overturning and wind driven circulation in the ocean. Accordingly, a number of extensions of this model is proposed, such as the inclusion of salinity and wave-wave interaction in the atmosphere.

The chapters of this thesis are based on the following papers:

- Chapter 2:  
Veen, L. van [2002] “Baroclinic flow and the Lorenz-84 model”, to appear in the *Internat. J. Bifur. Chaos*.
- Chapter 3:  
Veen, L. van, Opsteegh, T., and Verhulst, F. [2001] “Active and passive ocean regimes in a low-order climate model”, *Tellus* **53A**, 616-628
- Chapter 4:  
Veen, L. van [2002] “Overturning and wind driven circulation in a low-order ocean-atmosphere model”, submitted to *Dyn. Atmos. Oceans*.



## Bibliography

- Achatz, U. & Branstator, G. [1999] “A two-layer model with empirical linear corrections and reduced order for studies of internal climate variability,” *J. Atmos. Sci.* **56**, 3140–3160.
- Charney, J. [1959] *On the general circulation of the atmosphere*, chapter in *The atmosphere and sea in motion*, Rossby Memorial Volume, ed. Bolin, B., pp 178–193 Rockefeller Institute Press.
- De Swart, H. E. & Grasman, J. [1987] “Effect of stochastic perturbations on a low-order spectral model of the atmospheric circulation,” *Tellus* **39A**, 10–24.
- Foias, C., Jolly, M. S., Kevrekidis, I. G., Sell, G. R. & Titi, E. S. [1988] “On the computation of inertial manifolds,” *Phys. Lett. A* **131**, 433–436.
- Huang, R. X. & Stommel, H. M. [1992] “Convective flow patterns in an eight-box cube driven by combined wind stress, thermal, and saline forcing,” *J. Geoph. Res.* **97C**, 2347–2364.
- Kuznetsov, Yu. A. [1998] *Elements of applied bifurcation theory* (Springer, New York).
- Lorenz, E. N. [1960] “Maximum simplification of the dynamic equations,” *Tellus* **12**, 243–254.
- Lorenz, E. N. [1963] “Deterministic non-periodic flows,” *Journal of Atmospheric Science* **20**, 130–141.
- Lorenz, E. N. [1984] “Irregularity: a fundamental property of the atmosphere,” *Tellus* **36A**, 98–110.
- Maas, L. R. M. [1994] “A simple model for the three-dimensional, thermally and wind-driven ocean circulation,” *Tellus* **46A**, 671–680.
- Marotzke, J. [1994] *Ocean models in climate problems*, chapter in *Ocean processes in climate dynamics: global and Mediterranean examples*, eds. Malanotte-Rizzoli, P. and Robinson, A. R., pp 79–109 NATO ASI Series C, Vol. 419, Kluwer Academic Publishers.
- Nakamura, M., Stone, P. H. & Marotzke, J. [1994] “Destabilization of the thermohaline circulation by atmospheric eddy transports,” *Journal of Climate* **7**, 1870–1882.
- Olbers, D. [2001] “A gallery of simple models from climate physics,” *Progress in Probability* **49**, 3–63.
- Peixoto, J.P. & Oort, A.H. [1992] *Physics of climate* (American Institute of Physics).

- Philips, N. A. [1954] “Energy transformations and meridional circulations associated with simple baroclinic waves in a two-level, quasi-geostrophic model,” *Tellus* **6**, 273–286.
- Preisendorfer, R. W. [1988] *Principal component analysis in meteorology and oceanography* (Elsevier, Amsterdam) ed. Mobley, C. D.
- Rivin, I. & Tziperman, E. [1997] “Linear versus self-sustained interdecadal thermohaline variability in a coupled box model,” *J. Phys. Oceanogr.* **27**, 1216–1232.
- Stommel, H. [1961] “Thermohaline convection with two stable regimes of flow,” *Tellus* **13**, 224–230.
- Temam, R. [1988] *Infinite-dimensional dynamical systems in mechanics and physics* (Springer-Verlag).
- Titz, S., Kuhlbrodt, T., Rahmstorf, S. & Feudel, U. [2002] “On freshwater-dependent bifurcations in box models of the interhemispheric thermohaline circulation,” *Tellus* **54A**, 89–98.
- Watson, J. & Lovelock, J. E. [1983] “Biological homeostasis of the global environment: the parable of daisyworld,” *Tellus* **35B**, 284–289.
- Wiggins, S. [1990] *Introduction to applied nonlinear dynamical systems and chaos* (Springer-Verlag).
- Wiggins, S. [1994] *Normally hyperbolic invariant manifolds in dynamical systems* (Springer Verlag).

## CHAPTER 2

# Baroclinic flow and the Lorenz-84 model

To appear in the *Internat. J. Bifur. Chaos*.

ABSTRACT. The bifurcation diagram of a truncation to six degrees of freedom of the equations for quasi-geostrophic, baroclinic flow is investigated. Period doubling cascades and Shil'nikov bifurcations lead to chaos in this model. The low dimension of the chaotic attractor suggests the possibility to reduce the model to three degrees of freedom. In a physically comprehensible limit of the parameters this reduction is done explicitly. The bifurcation diagram of the reduced model in this limit is compared to the diagram of the six degrees of freedom model and agrees well. A numerical implementation of the graph transform is used to approximate the three dimensional invariant manifold away from the limit case. If the six dimensional model is reduced to a linearisation of the invariant manifold about the Hadley state, the Lorenz-84 model is found. Its parameters can then be calculated from the physical parameters of the quasi-geostrophic model. Bifurcation diagrams at physical and traditional parameter values are compared and routes to chaos in the Lorenz-84 model are described.

### 1. Introduction

The equations for atmospheric flow form one of the most intensely studied dynamical systems of the last century. Both their practical importance and their mathematical richness have attracted much attention. The atmospheric equations are studied in various forms, depending on the physical domain, and the time and length scales of interest. The starting point of the analysis in this paper is a model which describes midlatitude atmospheric flow on a synoptic scale, a few thousand kilometers in space and a week or so in time. A phenomenological description of the typical flow patterns in this range can be found in Peixoto and Oort [1992], chapter 7. The model consists of the filtered equations, derived from the basic atmospheric equations under the assumption of quasi-geostrophic (QG) and hydrostatic balance (see Holton [1992]).

In the absence of dissipative processes and forcing through solar heating, the filtered equations are energy preserving. The dominant dissipative terms are friction at the earth's surface, internal friction and Newtonian cooling. The solar heating induces a strong temperature gradient in the meridional direction. Additional temperature gradients in the zonal direction can be induced by, e.g. land-sea contrast. The response to this forcing is a strong westerly circulation, called the jet stream. This circulation can become dynamically unstable so that traveling waves develop.

The jet stream pattern is nearly equivalent barotropic, which means that its height dependence can be represented by multiplication by a scale function. In other words, at each surface of constant height, the velocity field has the same shape, but may have a different amplitude. In contrast, the traveling waves can be baroclinic, which means that their phase depends on the vertical coordinate. Typically, they exhibit a westward tilt with height. Theoretical studies of the filtered equations indicate, that the baroclinicity of these traveling waves changes in the course of their life cycle [Frisius, 1998]. In the growing, strongly baroclinic, phase, they extract energy from the jet stream. In the decaying phase, they can become equivalent barotropic and transfer energy back into the jet stream.

The focus of this study is on the interaction of the jet stream and the baroclinic waves and its representation in a low order model. With the aid of discretisation in the vertical and Galerkin truncation in the horizontal coordinates, we approximate the filtered equations by a finite number of ordinary differential equations (ODE's). The discretisation can be done without violating the energy preserving nature of the filtered equations, as described in Lorenz [1960]. The number of layers is fixed to two, the minimal number necessary to describe baroclinic waves.

The two layer model is considered on an  $f$ -plane, a rectangular domain on which the Coriolis force is taken to be constant. The partial differential equations of the two layer model are then projected onto Fourier modes. In each layer, we use one zonally symmetric pattern, representing the jet stream, and two patterns which combine to represent a traveling wave. Thus, the ODE model has six degrees of freedom. The solar forcing is represented by constant terms, which are used as bifurcation parameters.

The bifurcation diagram is organised by its codimension two points, namely fold-Hopf, 2:1 resonance and a neutral saddle-focus on a homoclinic bifurcation line. Two routes to chaos are readily identified: period doubling cascades and a Shil'nikov type bifurcation. An inspection of the spectra of equilibria and periodic orbits found, and the calculation of the Kaplan-Yorke dimension of the chaotic attractor, leads to the conjecture, that there is a three dimensional, globally attracting, invariant manifold in the phase space of the six dimensional model.

In order to calculate a first approximation of this invariant manifold, a small parameter is introduced into the equations. In the limit where this parameter tends to zero, an analytic expression is obtained. This limit has a clear physical interpretation in terms of the energy transfer between the jet stream pattern and the traveling waves. Numerical evidence for the persistence of the invariant manifold away from this limit is obtained by the use of techniques introduced by Broer et al. [1997] and Foias et al. [1988].

Reducing the six dimensional model to the invariant manifold, in the limit where the small parameter tends to zero, a three dimensional model is obtained. Its bifurcation diagram is compared to the corresponding diagram of the six dimensional model in order to see if the qualitative dynamics is retained. This comparison is convincing. Particularly, the codimension two points are still present.

If the six dimensional model is reduced to a linearisation of the invariant manifold about the Hadley state, the Lorenz-84 model emerges. This model was introduced



by Lorenz [1984] as the simplest model capable of representing the basic features of midlatitude, synoptic flow. To the author's knowledge, no derivation of the Lorenz-84 model from atmospheric flow equations has been presented before. A rather *ad hoc* link was established by Wiin-Nielsen [1992, 1994], but in his work the reduction to three degrees of freedom is not based on physical or mathematical arguments. The link established here enables us to calculate the parameters in the Lorenz-84 model from the physical parameters in the filtered equations. As it turns out, one of the parameters comes out significantly different from its traditional, yet unmotivated, value. A continuation in this parameter relates the bifurcation diagram found at the traditional parameter value, presented in Shilnikov et al. [1995], to the one found at the physical value. The latter still bears resemblance to the bifurcation diagram of the six dimensional model, but the neutral saddle-focus transition is no longer there. Hence the route to chaos through a Shil'nikov type bifurcation is absent. It is shown, that chaos through period doubling cascades, the Ruelle-Takens scenario and intermittency does occur in the Lorenz-84 model.

The derivation presented here is not unlike the derivation of the Lorenz-63 model from the fluid dynamical equations governing Rayleigh-Bénard convection [Saltzman, 1962; Lorenz, 1963]. There too, the Galerkin truncation calculated has six degrees of freedom and can be reduced to a three dimensional invariant manifold. In that case, however, the invariant manifold is linear.

Galerkin truncations of the filtered equations have been studied on various domains and at various truncation numbers, see De Swart [1988] and references therein. One lesson to be learned from these studies, is that severe truncations, such as the one studied here, can only be regarded as qualitative models. A quantitative comparison to solutions of the filtered equations may be sensible at a truncation number in the order of a hundred or higher, depending on the basis functions used (see, e.g., Achatz and Branstator [1999] and Itoh and Kimoto [1996]). Low order models, however, allow us to isolate a physical process, such as the interaction between the jet stream and baroclinic waves, and represent it in a simple way. Because of this conceptual simplicity, and the fact that they are easy to integrate numerically, low dimensional truncations are widely used for testing and illustrating new ideas in dynamical systems theory, meteorology and climatology. The Lorenz-84 model for instance, has been used to investigate low-frequency atmospheric variability [Pielke and Zeng, 1994], measures of predictability [González-Miranda, 1997; Anderson and Hubeny, 1997], time scale interaction in the climate system [Roebber, 1995; van Veen et al., 2001] and the influence of periodic forcing [Broer et al., 2001]. It has also been formulated in the context of symplectic diffusion [Pelino and Pasini, 2001]. The link with the filtered equations, presented here, validates the use of the Lorenz-84 model in these contexts.

## 2. The QG two layer model

As a starting point for the calculations we take the quasi-geostrophic two layer model, described by Lorenz [1960]. Alternative derivations of this model can be found e.g. in Holton [1992], chapter 8, or the review article by De Swart [1988].

In Lorenz' article the stress is on the energy conserving nature of the nonlinear interaction terms, in De Swarts review article strong scaling arguments are provided.

**2.1. Setup of the model.** In the quasi-geostrophic approximation, the dry atmosphere is described by the velocity field,  $\mathbf{v}$ , and the temperature field,  $T$ . It is convenient to use the streamfunction,  $\Psi$ , the velocity potential,  $\chi$ , and the potential temperature,  $\Theta$ , as variables. As a vertical coordinate we use pressure instead of height. The velocity and the temperature can then be expressed as

$$\begin{aligned} \mathbf{v}_r &= \mathbf{k} \times \nabla \Psi & \mathbf{v}_d &= \nabla \chi \\ \mathbf{v} &= \mathbf{v}_r + \mathbf{v}_d + \omega \mathbf{k} & T &= \Theta \left( \frac{p}{p_s} \right)^{\frac{c_p - c_v}{c_p}} \end{aligned} \quad (1)$$

Here  $\mathbf{v}_r$  and  $\mathbf{v}_d$  are the divergence free and the irrotational part of the horizontal velocity,  $p$  is pressure,  $p_s$  is surface pressure,  $\omega = dp/dt$  is the vertical velocity,  $\mathbf{k}$  is the vertical unit vector and  $c_v$  and  $c_p$  are the specific heat of dry air at constant volume and pressure, respectively.

At the earth's surface, the lower boundary, we impose that  $p = p_s$  is constant and  $\omega = 0$ . At the upper boundary we have  $p = 0$  and  $\omega = 0$ . Discretisation of the vertical in layers means that we replace each function of three spatial variables by a number of functions of longitude and latitude only. In the simplest case we take two layers, the minimal number necessary to describe baroclinic waves.

The two layers are bounded by three isobaric surfaces at  $p_0 = p_s$ ,  $p_2 = p_s/2$  and  $p_4 = 0$  (see figure 1). Vertical derivatives are replaced by linear interpolations, e.g. in the continuity equation:

$$\nabla^2 \chi + \frac{\partial \omega}{\partial p} = 0 \rightarrow \begin{cases} \nabla^2 \chi_3 + \omega(p_2) = 0 \\ \nabla^2 \chi_1 - \omega(p_2) = 0 \end{cases} \Rightarrow \nabla^2 (\chi_1 + \chi_3) = 0 \quad (2)$$

The streamfunction and the potential temperature in the lower and the upper layer are denoted by  $\Psi_{1,3}$  and  $\Theta_{1,3}$ , respectively. The pressure in the lower and the upper layer is set to  $p_1 = 3p_s/4$  and  $p_3 = p_s/4$ . The equations are written in terms of vertical means and differences, defined as

$$\begin{aligned} \Psi &= 1/2(\Psi_3 + \Psi_1) && \text{the barotropic streamfunction,} \\ \tau &= 1/2(\Psi_3 - \Psi_1) && \text{the baroclinic streamfunction,} \\ \Theta &= 1/2(\Theta_3 + \Theta_1) && \text{the mean potential temperature,} \\ \sigma &= 1/2(\Theta_3 - \Theta_1) && \text{the static stability.} \end{aligned} \quad (3)$$

The static stability,  $\sigma$ , will be taken constant.

In addition to the conservative dynamics described in Lorenz [1960], we introduce linear damping through friction at the earth's surface, the terms proportional to  $C$ , friction at the boundary of the two layers, the term proportional to  $C'$  and Newtonian cooling, the term proportional to  $h_N$ . The temperature forcing is given

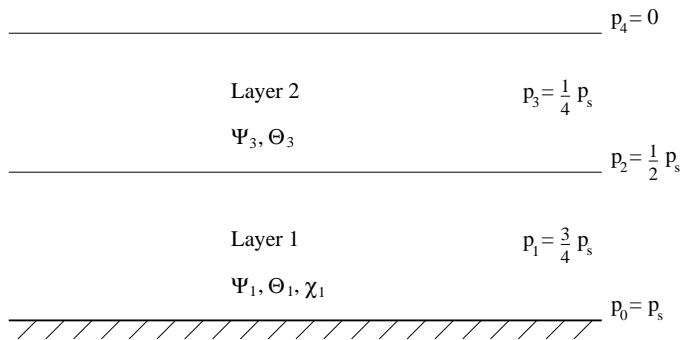


FIGURE 1. The vertical discretisation in pressure coordinates. If the static stability,  $\sigma$ , is fixed, equations (4) and (5) determine  $\Psi$ ,  $\tau$ ,  $\Theta$  and  $\chi_1$ .

by  $\Theta^*$ . The resulting equations are

$$\frac{\partial}{\partial t} \nabla^2 \Psi = -J(\Psi, \nabla^2 \Psi + f) - J(\tau, \nabla^2 \tau) - C \nabla^2 (\Psi - \tau) \quad (4.1)$$

$$\frac{\partial}{\partial t} \nabla^2 \tau = -J(\tau, \nabla^2 \Psi + f) - J(\Psi, \nabla^2 \tau) + \nabla \cdot (f \nabla \chi_1) + C \nabla^2 (\Psi - \tau) - 2C' \nabla^2 \tau \quad (4.2)$$

$$\frac{\partial}{\partial t} \Theta = -J(\Psi, \Theta) + \sigma \nabla^2 \chi_1 - h_N (\Theta - \Theta^*) \quad (4.3)$$

where the *Jacobian operator*,  $J$ , is defined as  $J(A, B) = \nabla A \cdot \nabla B \times \mathbf{k}$  for any pair of functions  $A, B$ . The Coriolis parameter has been denoted by  $f$ .

Furthermore we have the thermal wind equation, relating the shear streamfunction to the mean potential temperature

$$bc_p \nabla^2 \Theta = \nabla \cdot (f \nabla \tau) \quad (5)$$

Where  $b = \frac{1}{2} \left[ \left( \frac{p_1}{p_s} \right)^{\frac{c_p - c_v}{c_p}} - \left( \frac{p_3}{p_s} \right)^{\frac{c_p - c_v}{c_p}} \right] \approx 0.124$  results from the discretisation scheme in the vertical.

**2.2. Domain and boundary conditions.** The set of equations (4) will be considered on an  $f$ -plane, a rectangular domain centered about a fixed latitude  $\phi_0$  on which the Coriolis parameter is approximated by the constant value  $f_0$ . This domain has length  $L$  in the zonal direction and  $D$  in the meridional direction. On this plane we will use Cartesian coordinates  $x \in [0, L]$  and  $y \in [0, D]$ . In the following we set  $\phi_0 = 45^\circ$ .

In the zonal direction we take periodic boundary conditions. In the meridional direction we have

$$\frac{\partial \Psi}{\partial x} = \frac{\partial \tau}{\partial x} = \frac{\partial \chi_{1,3}}{\partial y} = 0 \quad \text{at } y = 0, D \quad (6.1)$$

This means that there is no mass flux through the boundaries. The second condition was put forward by Philips [1954], and imposes that there is no net flow along the

Length	$D$	$5 \cdot 10^3 \text{ km}$
Time	$\Sigma^{-1}$	7 days
Temperature	$R = \frac{f_0 \Sigma D^2}{bc_p}$	34.3K
Mass	$M = \frac{\rho_0 D^2}{2g} \frac{f_0 R}{\Sigma \sigma}$	$7.7 \cdot 10^{18} \text{ kg}$

TABLE 1. Scaling for the synoptic physics described by (4). In the right column the numerical values used.

boundaries:

$$\int_0^L \frac{\partial \Psi}{\partial y} dx = \int_0^L \frac{\partial \tau}{\partial y} dx = 0 \quad \text{at } y = 0, D \quad (6.2)$$

It follows from the thermal wind equation (5), and the restriction that there be no net heat flux through the boundaries, that  $\Theta$  satisfies

$$\frac{\partial \Theta}{\partial x} = 0 \quad \int_0^L \frac{\partial \Theta}{\partial y} dx = 0 \quad \text{at } y = 0, D \quad (6.3)$$

With these boundary conditions we can consider  $\Theta$  to describe deviations from the spatially averaged potential temperature.

**2.3. Scaling.** In table (1) the scales, suitable for the synoptic physics are listed. In the right column the numerical values, used below, are listed. In the following all quantities are dimensionless, unless otherwise indicated. The dimensionless length of the domain will be denoted by  $s = L/D$ .

**2.4. Equations for  $\Psi$  and  $\tau$ .** Under the boundary conditions (6), the thermal wind relation (5) takes the simple form  $\Theta = \tau$ . This identity can be used to eliminate the velocity potential  $\chi_1$  from equations (4.2) and (4.3). This results in a closed set of prognostic equations for  $\Psi$  and  $\tau$

$$\frac{\partial}{\partial t} \nabla^2 \Psi = -J(\Psi, \nabla^2 \Psi) - J(\tau, \nabla^2 \tau) - C \nabla^2 (\Psi - \tau) \quad (7.1)$$

$$\begin{aligned} \frac{\partial}{\partial t} (1 - \alpha \nabla^2) \tau = & -J(\Psi, \tau) + \alpha J(\tau, \nabla^2 \Psi) + \alpha J(\Psi, \nabla^2 \tau) - h_N (\tau - \tau^*) \\ & - \alpha C \nabla^2 (\Psi - \tau) + 2\alpha C' \nabla^2 \tau \end{aligned} \quad (7.2)$$

where  $\alpha = \sigma/f_0$  and  $\tau^* = \Theta^*$ . In this scaling  $f_0^{-1} \approx 1.6 \cdot 10^{-2}$  is the Rossby number. We will study the lowest dimensional nontrivial spectral truncation of these equations.

**2.5. Energy.** In the absence of friction and forcing, the prognostic equations (7) conserve the sum of kinetic and available potential energy, defined respectively as

$$K = \alpha \int_0^1 \int_0^s (\nabla \Psi \cdot \nabla \Psi + \nabla \tau \cdot \nabla \tau) dx dy \quad A = \int_0^1 \int_0^s \Theta^2 dx dy \quad (8)$$

in units  $MD^2\Sigma^2$ . The simplified models will be shown to have a corresponding conserved quantity.

### 3. The Galerkin approximation

In order to approximate equations (7) by a finite number of ODE's we do a Galerkin projection onto Fourier modes. On this basis the variables are given by

$$\begin{aligned}\Psi(x, y, t) &= \sum_{n,m} \psi(m, n, t) \exp[i(mkx + nly)] \\ \tau(x, y, t) &= \sum_{n,m} \theta(m, n, t) \exp[i(mkx + nly)]\end{aligned}\quad (9)$$

where  $k = 2\pi/s$ ,  $l = \pi$ . The boundary conditions, and the restriction that  $\Psi$  and  $\tau$  are real variables impose that

$$\begin{aligned}\psi(m, -n) &= -\psi(m, n) & \theta(m, -n) &= -\theta(m, n) & \text{if } m \neq 0 \\ \psi(0, n) &= \psi(0, -n) & \theta(0, n) &= \theta(0, -n) \\ \psi(m, n) &= \psi^*(-m, -n) & \theta(m, n) &= \theta^*(-m, -n)\end{aligned}\quad (10)$$

This Fourier decomposition is equivalent to the introduction of a basis of eigenfunctions of the Laplacian operator on our domain, with the specified boundary conditions. The eigenfunctions are  $\phi_{0n} = \cos nly$  for zonal wavenumber zero, and  $\phi_{mn} = e^{imkx} \sin nly$  otherwise.

If we apply the zonally symmetric forcing  $\theta^* = \frac{1}{2} \Delta T \phi_{01}$ , with temperature contrast  $\Delta T$  between the boundaries, there is an exact solution to equations (7). It is given by

$$\Psi = \tau = \frac{1}{2} \frac{h_N \Delta T}{h_N + 2\alpha l^2 C'} \phi_{01}\quad (11)$$

This solution is called the Hadley state and describes a strong jet in the upper layer, rising air at the south boundary and sinking air at the north boundary. The eigenfunctions with nonzero zonal wavenumber describe traveling waves which can grow if the Hadley circulation becomes dynamically unstable.

The projection of equations (7) is given by

$$\begin{aligned}\lambda_{cd} \dot{\psi}(c, d) &= -\lambda_{cd} C (\psi(c, d) - \theta(c, d)) \\ &+ kl \sum_{pqrs} \lambda_{rs} (ps - qr) \delta(p + r - c) \mu(q + s - d) \{ \psi(r, s) \psi(p, q) + \theta(r, s) \theta(p, q) \} \\ \bar{\lambda}_{cd} \dot{\theta}(c, d) &= -h_N (\theta(c, d) - \theta^*(c, d)) - \alpha \lambda_{cd} C (\psi(c, d) - \theta(c, d)) + 2\alpha C' \lambda_{cd} \theta(c, d) \\ &+ kl \sum_{pqrs} (ps - qr) \delta(p + r - c) \mu(q + s - d) \{ 1 - \alpha ([p^2 - r^2] k^2 + [q^2 - s^2] l^2) \} \psi(p, q) \theta(r, s)\end{aligned}$$

where  $\delta$  is the Kronecker delta,  $\theta^*$  is the Fourier transform of  $\tau^*$  and  $\mu$  is defined as

$$\mu(a) = \int_0^1 e^{ialy} dy = \begin{cases} 1 & \text{if } a = 0 \\ 0 & \text{if } a \text{ is even} \\ \frac{-2}{\pi ia} & \text{if } a \text{ is odd} \end{cases}\quad (13)$$

The eigenvalues of the operators on the left hand side of equations (7) have been denoted by  $\lambda_{ab} = -(a^2 k^2 + b^2 l^2)$  and  $\bar{\lambda}_{ab} = 1 - \alpha \lambda_{ab}$ .

#### 4. The six dimensional truncation

The smallest nontrivial truncation of equations (12) has six degrees of freedom. We set  $s = 2$  and define

$$\begin{aligned} x_1 &= 2\psi(0, 1) & y_1 &= 2\theta(0, 1) & T_1 &= 2\theta^*(0, 1) \\ x_2 &= 2\sqrt{2}\operatorname{Re}\psi(1, 1) & y_2 &= 2\sqrt{2}\operatorname{Re}\theta(1, 1) & T_2 &= 2\sqrt{2}\operatorname{Re}\theta^*(1, 1) \\ x_3 &= 2\sqrt{2}\operatorname{Im}\psi(1, 1) & y_3 &= 2\sqrt{2}\operatorname{Im}\theta(1, 1) & T_3 &= 2\sqrt{2}\operatorname{Im}\theta^*(1, 1) \end{aligned} \quad (14)$$

These variables satisfy the following equations

$$\dot{x}_1 = -C(x_1 - y_1) \quad (15.1)$$

$$\lambda_{11}\dot{x}_2 = -\lambda_{11}C(x_2 - y_2) + \lambda_{10}\delta(x_1x_3 + y_1y_3) \quad (15.2)$$

$$\lambda_{11}\dot{x}_3 = -\lambda_{11}C(x_3 - y_3) - \lambda_{10}\delta(x_1x_2 + y_1y_2) \quad (15.3)$$

$$\bar{\lambda}_{01}\dot{y}_1 = -\alpha\lambda_{01}(Cx_1 - [C + 2C']y_1) - h_N(y_1 - T_1) + \delta(x_3y_2 - x_2y_3) \quad (15.4)$$

$$\bar{\lambda}_{11}\dot{y}_2 = -\alpha\lambda_{11}(Cx_2 - [C + 2C']y_2) - h_N(y_2 - T_2) + \delta(\bar{\lambda}_{10}x_1y_3 - \nu_{10}x_3y_1) \quad (15.5)$$

$$\bar{\lambda}_{11}\dot{y}_3 = -\alpha\lambda_{11}(Cx_3 - [C + 2C']y_3) - h_N(y_3 - T_3) - \delta(\bar{\lambda}_{10}x_1y_2 - \nu_{10}x_2y_1) \quad (15.6)$$

where  $\delta = 8kl/(3\pi)$  and  $\nu_{ab} = 1 + \alpha\lambda_{ab}$ . When we put dissipation and forcing to zero, the ODE system (15) has a conserved quantity  $L$ , defined by

$$L = -\alpha\lambda_{01}x_1^2 - \alpha\lambda_{11}(x_2^2 + x_3^2) + \bar{\lambda}_{01}y_1^2 + \bar{\lambda}_{11}(y_2^2 + y_3^2) \quad (16)$$

which corresponds to the projection of the sum of kinetic and available potential energy defined in equation (8). Using  $L$  as a Lyapunov function we can show, that a trapping region for equations (15) is defined by

$$L \leq \frac{3\|\mathbf{T}\|^2}{(h_N - 2\alpha\lambda_{11}C')^2} \quad (17)$$

where  $\|\cdot\|$  denotes the  $L_2$  norm, and we have assumed that  $0 < h_N \leq C$ ,  $0 < 2C' \leq C$  and  $\sigma \leq 1$ , a realistic range for the parameters. Note, that the divergence of the vector field, defined by equation (15), is constant and negative. Therefore, volume elements always shrink.

**4.1. Bifurcation diagram.** In diagram (8)(top) the partial bifurcation diagram of system (15) is shown. This diagram, and all other diagrams below, have been calculated using the software package AUTO (Doedel et al. [1986]). To obtain this picture, we varied  $T_1$  and  $T_2$ , setting  $T_3 = 0$ . Due to a discrete symmetry in equations (15), given by

$$\begin{aligned} \mathbf{x} &\rightarrow \mathbf{x}' = \mathbf{R}\mathbf{x} \\ \mathbf{y} &\rightarrow \mathbf{y}' = \mathbf{R}\mathbf{y} \\ \mathbf{T} &\rightarrow \mathbf{T}' = \mathbf{R}\mathbf{T} \end{aligned} \quad \text{where } \mathbf{R} = \begin{pmatrix} 1 & 0 & 0 \\ 0 & 0 & -1 \\ 0 & 1 & 0 \end{pmatrix}, \quad (18)$$

setting  $T_2 = 0$  and varying  $T_3$  yields the same diagram. This symmetry corresponds to a translation  $x \rightarrow x' = x + 1/2$  in the physical domain. Furthermore, we have set  $C = 3.5$ ,  $h_N = 0.7$ ,  $C' = 0.5$  and  $\sigma = 0.9$ . This corresponds to a damping time scale of two days at the earth's surface and two weeks at the layer interface. The thermal

damping time scale is ten days and the temperature difference between the layers is about 34K.

If we put  $T_2 = 0$  and increase  $T_1$  from zero, at first a stable equilibrium is the unique limit set in the phase space of system (15). This equilibrium corresponds to the Hadley state (11). At the Hopf bifurcation line, marked h, this equilibrium becomes unstable and a stable periodic orbit is created. This is our model's baroclinic instability. The periodic orbit corresponds to a traveling baroclinic wave.

The two line segments fe, joint at cusp point c, denote a fold bifurcation of the equilibrium. Within the V-shaped region, bounded by curve fe, there are three equilibria, one of which is stable. At the codimension two point, marked fh, the Hopf line and the fold line are tangent. At this point an equilibrium exists with one zero eigenvalue and a complex pair on the imaginary axis. The unfolding of this point can be found in Kuznetsov [1998], chapter 8. In the following, we will adopt the notation of this book for normal form coefficients. An algorithm for computing the normal form coefficients of fold-Hopf points is described in Kuznetsov [1999] and implemented in the forthcoming release of CONTENT (Kuznetsov and Levitin [1997]). In this case, we have normal form coefficients  $s = 1$  and  $\theta < 0$ .

A torus bifurcation line emerges from point fh, and connects to the flip bifurcation line marked  $f_1$ . Above the torus bifurcation line, the periodic orbit created on Hopf curve h is unstable, below the torus bifurcation line it is stable and coexists with a saddle type, two dimensional torus. At the point where the torus and the flip bifurcation lines meet, the periodic orbit has two Floquet multipliers equal to minus unity. This point is marked  $r_1$  for 1 : 2 resonance. At this point, we have normal form coefficient  $s = -1$ . Connected to the resonance point  $r_1$  there is torus bifurcation line of the period doubled orbit, which leads to another 1 : 2 resonance point,  $r_2$ . In fact, flip bifurcation lines  $f_1$  and  $f_2$  are the first two of a period doubling cascade. There seems to be an accumulation of 1 : 2 resonance points directly to the right of  $r_2$ . Such an accumulation has been described in the context of a biological model in Kuznetsov [1998], chapter 9.6. Wicczorek et al. [2001] found it in a rate equation model for a semiconductor laser. They also provide a partial unfolding of this codimension two phenomenon.

From codimension two point fh two homoclinic bifurcation lines emanate. Both homoclinic connections are attached to a saddle focus. Along  $H_2$  the unstable manifold of the saddle focus is one dimensional and the saddle value,  $\sigma$ , is negative. On this line a stable periodic orbit is created. Along  $H_1$ , the saddle focus has a complex pair of eigenvalues with positive real part. The saddle value is positive along the larger part  $H_1$  and another stable periodic orbit is created. However, near the leftmost turning point of this curve, the saddle value changes sign. On a small segment it is negative, indicating that Shil'nikov type chaos can occur. In the literature, this type of Shil'nikov bifurcation, with complex unstable leading eigenvalues, is uncommon.

The points, where the saddle value is zero, are called neutral saddle focus, or Belyakov, transitions. What is known about the unfolding of this transition is summed up in Champneys and Kuznetsov [1994]. In figure (2) the transition points are shown in more detail, along with a phase portrait. An infinite number of

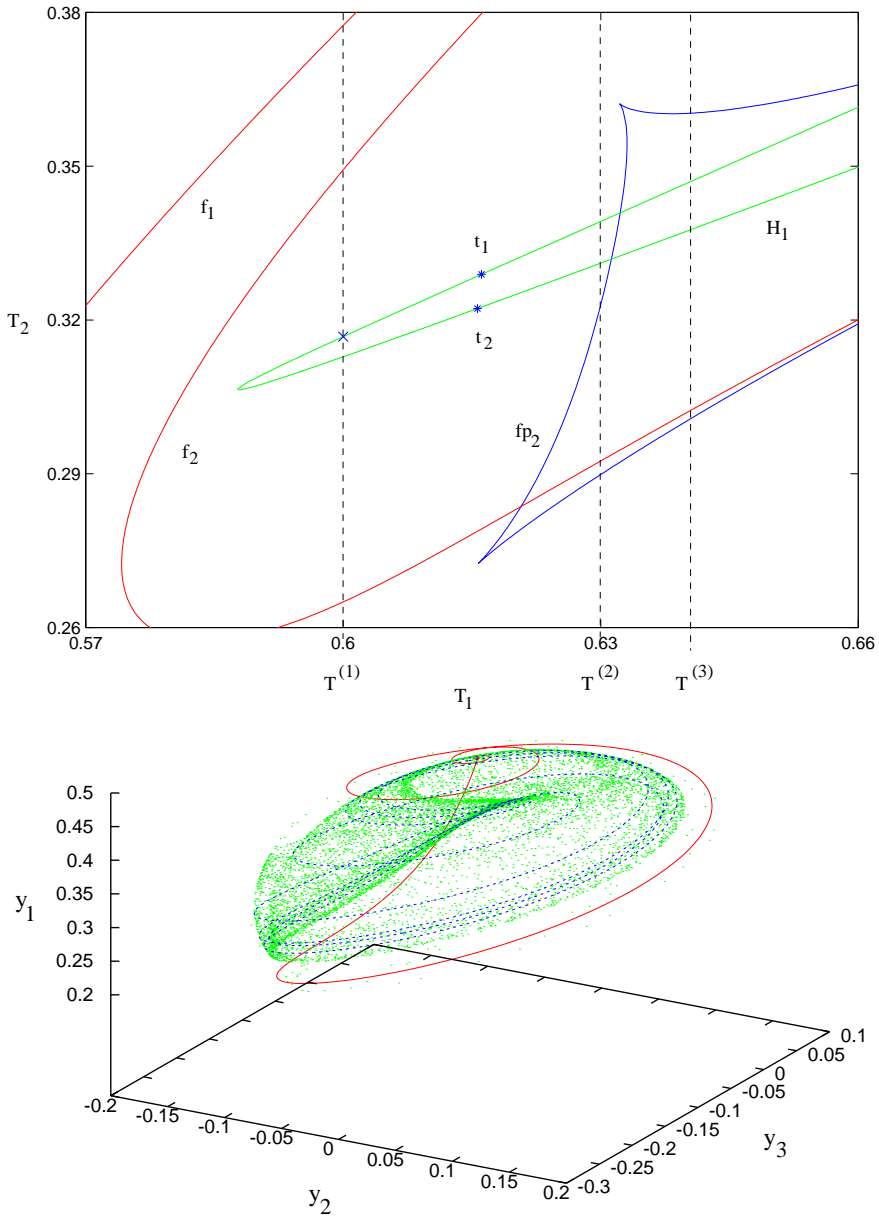


FIGURE 2. Top: detail of bifurcation diagram (8)(top). The neutral saddle focus transitions have been marked  $t_{1,2}$ . To the left of these transitions the saddle value is negative and the Shil'nikov condition is satisfied. Bottom: phase portrait at  $(T_1, T_2) = (0.6, 0.3168)$ . These parameter values have been marked with a cross in the top picture. Solid: the homoclinic orbit. Dashed: the periodic solution after four period doublings, i.e. the fifth branch in the top picture of figure (3). Dotted: points on the chaotic attractor.



cusps of fold lines of periodic orbits are expected to accumulate here, corresponding to the creation of successive folds of the branch of periodic solutions which becomes homoclinic on  $H_1$ . However, as described in Glendinning and Sparrow [1984], the neutral saddle focus transition is continuous, and these cusp bifurcations correspond to orbits of very high period which are hard to detect numerically. Looking at sections like in figure (4), the case with negative saddle values cannot be distinguished from the case with positive saddle value.

In figure (3) a cross section of diagram (8)(top) is shown. We have fixed  $T_1 = T^{(1)}$  and let  $T_2$  vary as indicated in diagram (8)(top). The top picture shows a number of branches of the period doubling cascade, as well as the primary homoclinic branch corresponding to curve  $H_1$ . The bottom picture, on the same horizontal scale, is a limit point diagram. This picture was obtained by calculating the Poincaré map on the plane  $\mathcal{S} = \{(\mathbf{x}, \mathbf{y}) \in \mathbb{R}^6 | y_2 = 0\}$ . After a sufficiently long integration, to filter out transients, the value of  $y_1$  was plotted at a number of iterations of the Poincaré map. The behaviour is chaotic between the accumulation points of the period doubling cascade and changes qualitatively near the Shil'nikov bifurcation.

The lines marked  $fp_1$  and  $fp_2$  denote fold bifurcations of periodic orbits. Near the cusps of these fold lines, the periodic orbit, created at Hopf line  $h$ , and its period doubled versions, switch branches with periodic orbits that become homoclinic near  $H_1$ . This process is illustrated in figure (4). In the top left picture, where we have  $T_1 = T^{(2)}$ , none of the branches of the period doubling cascade are connected to the homoclinic branch, see also figure (3)(top). For  $T_1 > T^{(2)}$ , however, the first period doubled branch becomes homoclinic on curve  $H_1$ . The period doubled branch and the homoclinic branch collide in a transcritical bifurcation. This process is repeated for the branch of the basic cycle, continued from Hopf line  $h$ . Therefore, the flip bifurcation lines  $f_{1,2,\dots}$  do not simply form a cascade and an inverse cascade. At the fold lines  $fp_{1,2}$  the simple structure of figure (3)(top) at  $T_1 = T^{(1)}$  is rearranged.

Summarising, the qualitative dynamics of system (15) is as follows. Left of the Hopf line  $h$ , and within the V-shaped region bounded by fold curve  $fe$ , there is a stable equilibrium. To the right of curve  $h$ , and below curve  $fe$ , the behaviour is periodic before crossing flip bifurcation curve  $f_1$ . When crossing  $f_1$  near the leftmost fold of the homoclinic curve  $H_1$ , where the saddle value is positive, a combination of period doubling and Shil'nikov chaos is encountered, as demonstrated in figures (2) and (3). To the right of the neutral saddle focus transition points, the behaviour is alternately periodic and chaotic. Due to the branch switching, shown in figure (4), the parameter space is divided into small chaotic and periodic windows.

In figure (5) the Kaplan-Yorke dimension of the attractor is shown for  $T_1 = T^{(1)}$  and values of  $T_2$  at which complex dynamics arise. Most remarkably, the attractor dimension does not exceed three. Also, the equilibria and periodic orbits studied in diagram (8)(top) have a feature in common. They all have three strongly contracting directions. These observations suggest, that the dynamics of system (15) take place on a three dimensional invariant manifold. In the next section we will present an approximate, three dimensional invariant manifold of this system, which enables us to reduce the model to three degrees of freedom.

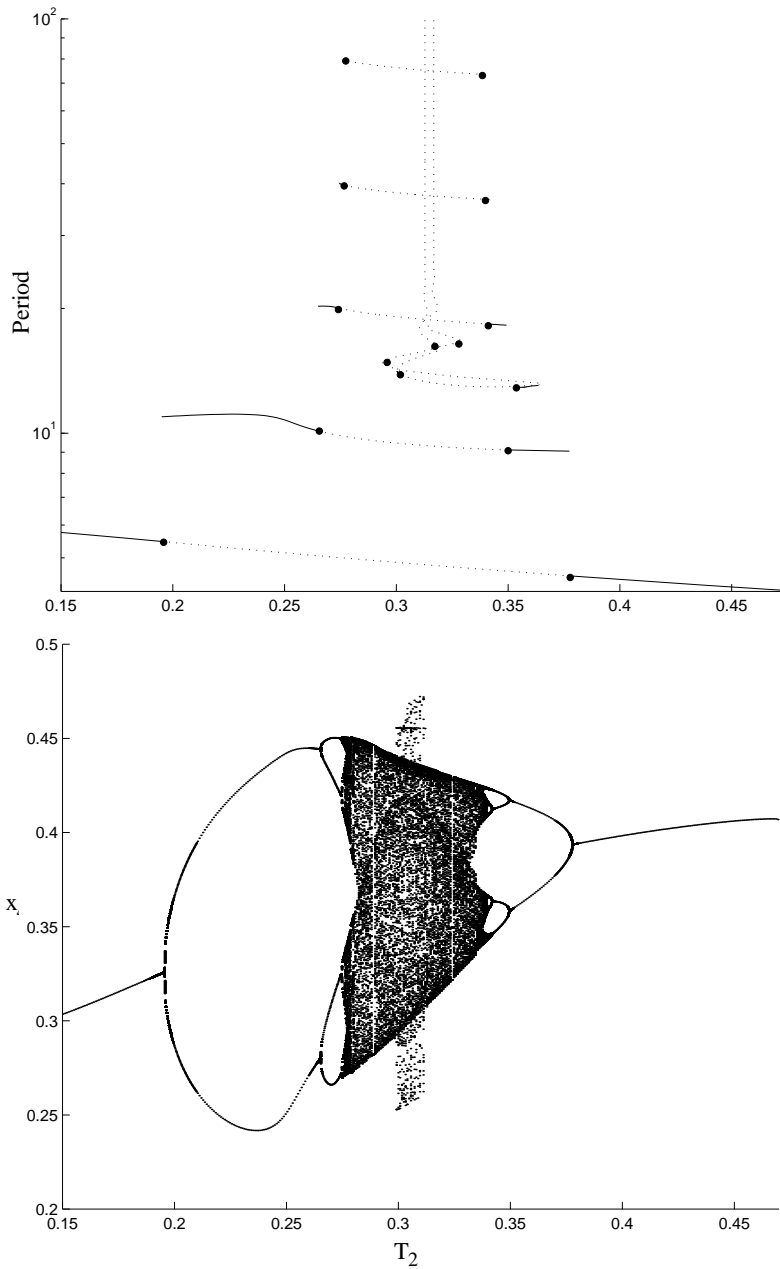


FIGURE 3. Top: continuation of the periodic orbit created on curve  $h$ , along the line  $T_1 = T^{(1)}$  in diagram (8)(top). Solid lines denote stable branches, dotted lines denote unstable branches, Hopf bifurcation point are marked with dots. Also shown is the primary homoclinic branch corresponding to curve  $H_1$ . Bottom: limit point diagram of the Poincaré map on  $\mathcal{S}$ .

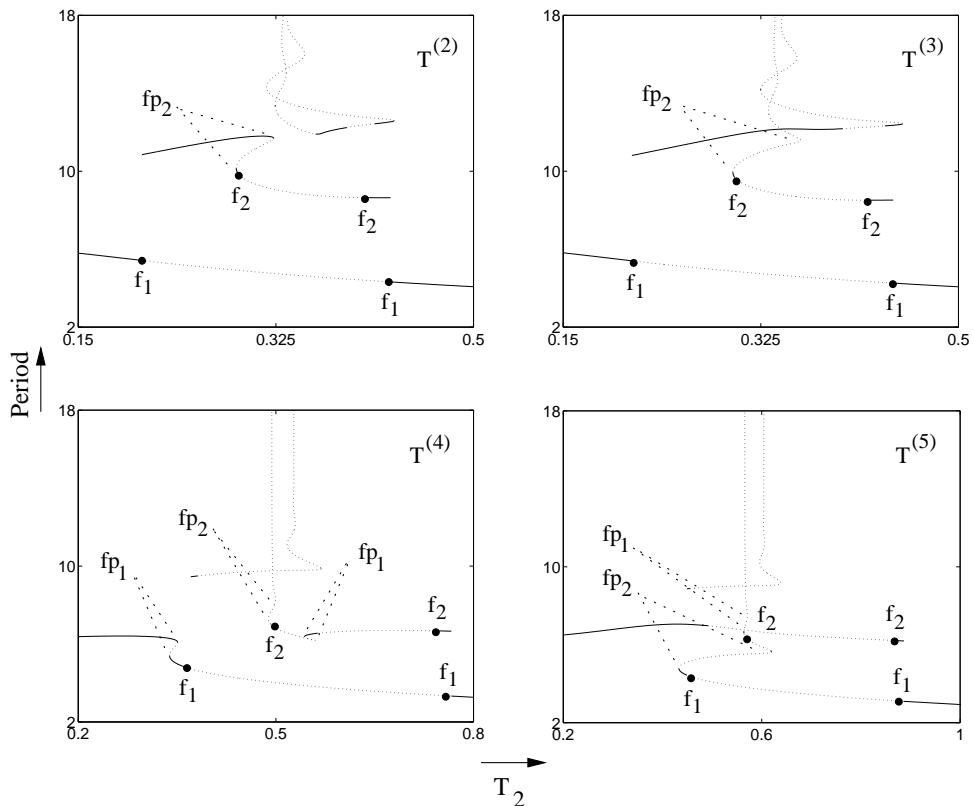


FIGURE 4. Cross sections of diagram (8)(top). Dots denote flip bifurcations, solid lines stable branches and dotted lines unstable branches. The labels  $f_{1,2}$  and  $fp_{1,2}$  refer to diagram (8)(top). Top left:  $T_1 = T^{(2)} = 0.63$ . The basic cycle, born on Hopf line  $h$ , and its period double version, are not connected to the homoclinic branch. Top right:  $T_1 = T^{(3)} = 0.64$ . The period doubled cycle now becomes homoclinic on  $H_1$ . Bottom left:  $T_1 = T^{(4)} = 0.88$ . The branch of the basic cycle folds. Bottom right:  $T_1 = T^{(5)} = 0.98$ . From one end,  $T_2$  increasing from zero, the branch of the basic cycle ends in a period halving bifurcation. From the other end,  $T_2$  decreasing, the branch of the basic cycle becomes homoclinic on  $H_1$ .

**4.2. Reduction to an invariant manifold.** With the parameters set to the values, specified in section (4.1), we can scale the constants in equations (15.1)-(15.3) as

$$\bar{C} = \epsilon C \quad \kappa = \epsilon \frac{\delta \lambda_{10}}{\lambda_{11}} = \epsilon \frac{\delta}{2} \quad (19)$$

where  $\epsilon \approx 1/4$  and  $\bar{C} \approx \kappa \approx 1$ . System (15) is then written symbolically as

$$\epsilon \dot{\mathbf{x}} = \bar{\mathbf{f}}(\mathbf{x}, \mathbf{y}) \quad (20.1)$$

$$\dot{\mathbf{y}} = \mathbf{g}(\mathbf{x}, \mathbf{y}) \quad (20.2)$$

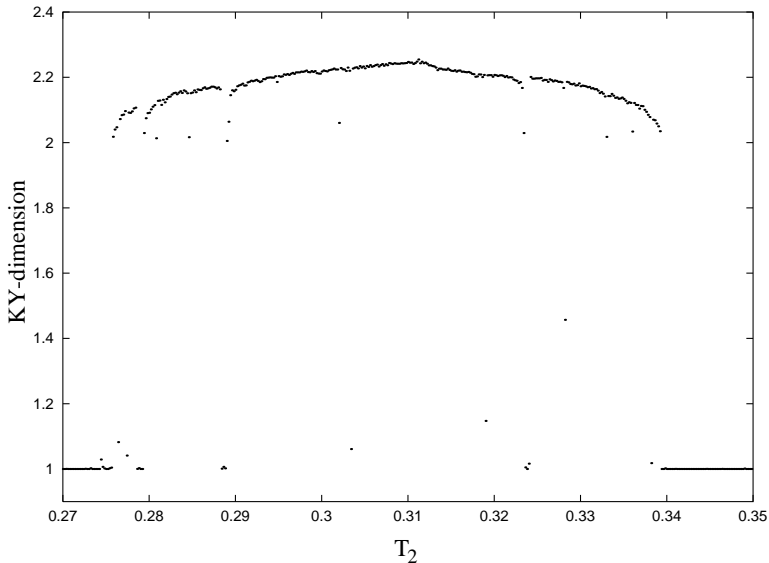


FIGURE 5. Numerical estimate of the Kaplan-Yorke dimension, obtained from an integration during  $\Delta t = 1.5 \cdot 10^4$  at each parameter value  $T_2$ , for fixed  $T_1 = T^{(1)}$ .

where  $\bar{\mathbf{f}}$  is defined as

$$\bar{f}_1 = -\bar{C}(x_1 - y_1) \quad (21.1)$$

$$\bar{f}_2 = -\bar{C}(x_2 - y_2) + \kappa(x_1 x_3 + y_1 y_3) \quad (21.2)$$

$$\bar{f}_3 = -\bar{C}(x_3 - y_3) - \kappa(x_1 x_2 + y_1 y_2) \quad (21.3)$$

We assume, that there exists a globally attracting, three dimensional invariant manifold in system (20), denoted by  $W_\epsilon$ . This manifold is represented as the graph of a function,  $\phi_\epsilon$ , of the baroclinic components:

$$W_\epsilon = \{(\mathbf{x}, \mathbf{y}) \in \mathbb{R}^6 \mid \mathbf{x} = \phi_\epsilon(\mathbf{y})\} \quad (22)$$

and satisfies

$$\bar{\mathbf{f}}(\phi_\epsilon, \mathbf{y}) = \epsilon \mathbf{D}\phi_\epsilon \cdot \mathbf{g}(\phi_\epsilon, \mathbf{y}) \quad (23)$$

The solution of (23) can be approximated asymptotically. Substituting the regular expansion  $\phi_\epsilon = \phi_0 + \epsilon\phi_1 + \dots$ , we find

$$\phi_0(\mathbf{y}) = \begin{pmatrix} 1 & 0 & 0 \\ 0 & A(y_1) & B(y_1) \\ 0 & -B(y_1) & A(y_1) \end{pmatrix} \mathbf{y} \quad (24)$$

where  $A$  and  $B$  are defined as

$$A(y_1) = \frac{\bar{C}^2 - \kappa^2 y_1^2}{\bar{C}^2 + \kappa^2 y_1^2} = \cos \gamma \quad \text{and} \quad B(y_1) = \frac{2\bar{C}\kappa y_1}{\bar{C}^2 + \kappa^2 y_1^2} = \sin \gamma. \quad (25)$$

This zeroth order approximation has a clear physical interpretation. It describes a zonally symmetric part of the flow which is equivalent barotropic (i.e.  $\Psi_3 \propto \Psi_1$ ) and a phase shift,  $\gamma$ , between the traveling waves in the upper and the lower layer.

The nonlinear terms in equations (15) can be divided into two groups: one represents advection of waves with the zonally symmetric flow (the terms proportional to  $x_1$ ) and the other represents energy exchange between waves and the zonally symmetric flow. The nonlinear terms in equation (15.4) belong to the second group. If the phase shift is zero, these terms cancel, and the wave components are decoupled from the zonally symmetric components. Thus, the function  $\phi_0$  describes how the energy transfer depends on the strength of the zonally symmetric flow.

The asymptotic expansion of  $\phi_\epsilon$  can not accurately describe the solution of equation (23) at the realistic parameter value  $\epsilon = 0.25$ . Therefore, we use a numerical algorithm to continue the solution, known analytically in the limit of  $\epsilon \downarrow 0$ . The algorithm is similar to the graph transform described in Broer et al. [1997]. In contrast to the systems considered in their work, however, ours is a continuous time system. Therefore, we apply the graph transform to the map, induced by an implicit Euler step which approximates the flow of system (20) over a finite time interval. This approach was already used by Foias et al. [1988] to approximate inertial manifolds by their modified Galerkin method.

Another difference is the choice of coordinates. Here, we do not represent the (approximate) invariant manifold as the graph of a section of the normal bundle of some given approximation. Instead, we globally represent it as the graph of a function  $\phi_\epsilon(\mathbf{y})$ . This can be done provided that  $D\phi_\epsilon$  has full rank. For small  $\epsilon$  this condition is satisfied, as we have  $\det D\phi_\epsilon = 1 + O(\epsilon)$ . When increasing  $\epsilon$  the condition has to be checked numerically.

Suppose that, for some fixed value of  $\epsilon$ , we have an approximation,  $W$ , of  $W_\epsilon$ . By assumption,  $W_\epsilon$  is globally attracting so that the image of  $W$  under the flow over a finite time interval of system (20) lies closer to  $W_\epsilon$  than  $W$ . Thus, by approximating the flow of system (20), we can calculate an improved approximation  $\bar{W}$ . To this end we use the map  $E : \mathbb{R}^6 \rightarrow \mathbb{R}^6$ , where  $(\bar{\mathbf{x}}, \bar{\mathbf{y}}) = E((\mathbf{x}, \mathbf{y}))$  is the solution of

$$\bar{\mathbf{x}} = \mathbf{x} + \frac{\Delta}{\epsilon} \bar{\mathbf{f}}(\bar{\mathbf{x}}, \bar{\mathbf{y}}) \quad (26.1)$$

$$\bar{\mathbf{y}} = \mathbf{y} + \Delta \mathbf{g}(\bar{\mathbf{x}}, \bar{\mathbf{y}}) \quad (26.2)$$

which defines an implicit Euler time step. The step size,  $\Delta$ , is a free parameter. The improved approximation is then defined as  $\bar{W} = E(W)$ .

In order to represent  $\bar{W}$  as the graph of a function  $\bar{\phi}(\mathbf{y})$ , we map a point  $(\phi(\mathbf{y}), \mathbf{y}) \in W$  onto the point  $(\bar{\phi}(\mathbf{y}), \mathbf{y}) \in \bar{W}$ , where  $\bar{\phi}$  is the solution of

$$\bar{\phi} = \phi(\mathbf{y} - \Delta \mathbf{g}(\bar{\phi}, \mathbf{y})) + \frac{\Delta}{\epsilon} \bar{\mathbf{f}}(\bar{\phi}, \mathbf{y}) \quad (27)$$

In other words, for a given vector  $\mathbf{y}$  we look for the point  $(\phi(\mathbf{y}'), \mathbf{y}') \in W$  which is mapped according to (26) onto  $(\bar{\phi}(\mathbf{y}), \mathbf{y}) \in \bar{W}$ . In figure (6) this procedure is sketched.

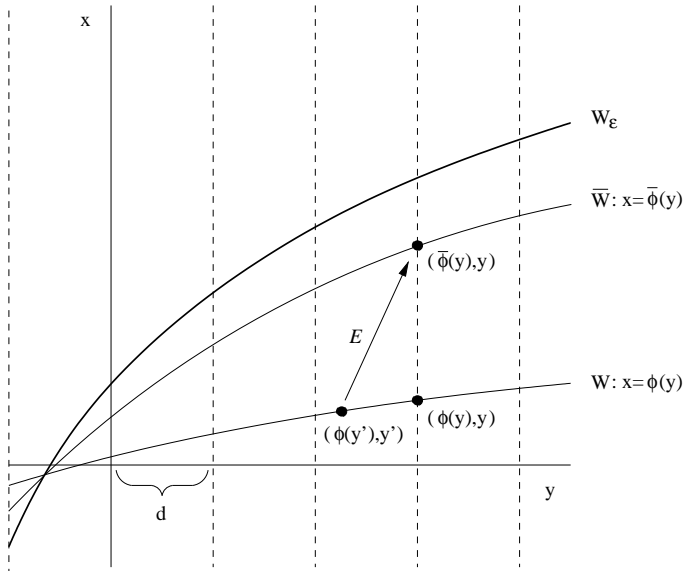


FIGURE 6. Schematic picture of the graph transform. Note, that equilibria of system (20) are intersection points of  $W$ ,  $\bar{W}$  and  $W_\epsilon$ . The dashed lines represent the mesh  $\mathbf{y}_{ijk}$ .

Differentiating equation (27) with respect to  $\mathbf{y}$ , we find

$$\left(\mathbb{I} - \frac{\Delta}{\epsilon} D_x \bar{\mathbf{f}} + \Delta D\phi|_{\mathbf{y}'}, D_x \mathbf{g}\right) D_y \bar{\phi} = D\phi|_{\mathbf{y}'} (\mathbb{I} - \Delta D_y \mathbf{g}) + \frac{\Delta}{\epsilon} D_y \bar{\mathbf{f}} \quad (28)$$

from which we can calculate  $D_y \bar{\phi}$ , and thus the tangent space  $T_{(\bar{\phi}, \mathbf{y})} \bar{W}$ , from  $D_y \bar{\phi}$  and the Jacobian of system (20). This enables us to define a local error function. Let  $F = (\bar{\mathbf{f}}/\epsilon, \mathbf{g})$  denote the vector field (20) and  $\mathcal{P}$  the orthogonal projection onto the tangent space at  $(\bar{\phi}, \mathbf{y})$ . Then we define the error function

$$e(\mathbf{y}) = \frac{2}{\pi} \arccos \frac{\|\mathcal{P}F(\bar{\phi}, \mathbf{y})\|}{\|F(\bar{\phi}, \mathbf{y})\|} \quad (29)$$

We will represent the approximate invariant manifold on a cubic lattice in  $\mathbb{R}^3$ . The vertices of this lattice are located at  $\mathbf{y}_{ijk} = d(i, j, k)^T$ , where  $d$  is the lattice spacing and  $i, j, k$  are integers. We consider a finite number of lattice points, demanding that all points  $(\phi_0(\mathbf{y}_{ijk}), \mathbf{y}_{ijk})$  lie within the trapping region defined in section (4). In fact, inequality (17) is a fairly coarse estimate. In order to reduce computation time and data storage, we use a sharper estimate, obtained by numerical computation of the eigenvalues of the linear part of equations (15.1)-(15.6). To an approximate solution  $\bar{\phi}$  we can then assign the error

$$\mathcal{E} = \max_{ijk} e(\mathbf{y}_{ijk}) \quad (30)$$

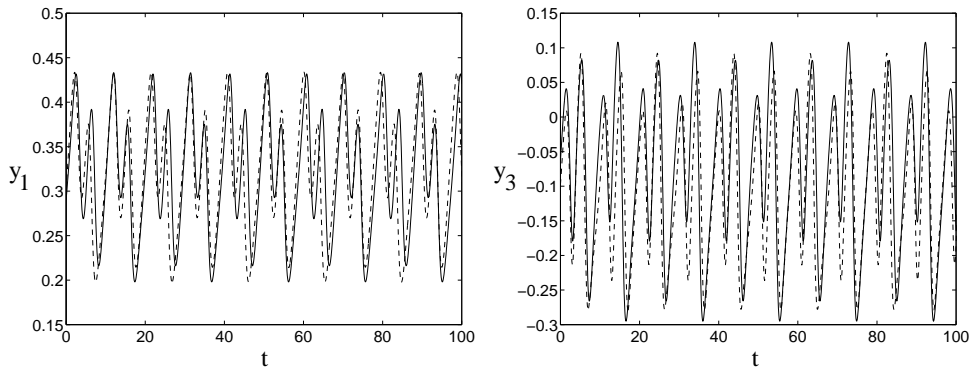


FIGURE 7. Time series of the zonally symmetric component,  $y_1$ , and a wave component,  $y_3$ . Solid: solution of system (20) at  $(T_1, T_2) = (0.6, 0.25)$  and  $\epsilon = 0.1$ . Dashed: solution of  $\dot{\mathbf{y}} = \mathbf{g}(\phi_\epsilon(\mathbf{y}), \mathbf{y})$ , using the approximate solution  $\phi_\epsilon$  of equation (23) obtained by the graph transform method. Linear interpolation is used inbetween lattice points.

In order to approximate the invariant manifold for finite  $\epsilon$ , we will proceed in steps. First of all, we fix an initial value for  $\epsilon$  and calculate  $\phi_1$  and  $D\phi_1$  on each lattice point. Next, we solve equation (27), by Newton iteration, and subsequently (28), to find the next approximation  $\bar{\phi}$  and its derivatives. A suitable initial guess for the Newton iteration is obtained by linearisation in  $\xi = \mathbf{y}' - \mathbf{y}$ . This yields

$$\begin{pmatrix} \bar{\phi}(\mathbf{y}) \\ \mathbf{y} \end{pmatrix} = E \begin{pmatrix} \phi(\mathbf{y}') \\ \mathbf{y}' \end{pmatrix} \approx E \begin{pmatrix} \phi(\mathbf{y}) \\ \mathbf{y} \end{pmatrix} + DE \cdot \begin{pmatrix} D\phi \\ \mathbb{I} \end{pmatrix} \cdot \xi \quad (31)$$

from which we can estimate  $\xi$  and, subsequently,  $\bar{\phi}$ . The graph transform is iterated until the global error is smaller than a fixed threshold  $\mathcal{E}_{max}$ . If this is achieved, we increase epsilon and iterate the process.

When solving equation (27), evaluation of  $\phi$  and  $D\phi$  inbetween lattice points is necessary. This is done by linear interpolation. To this end, each cube in the lattice is divided into six tetraeders of equal volume. The associated error is expected to be of order  $O(d^2)$ . At the edge of the domain we consider, it may happen that evaluation of  $\phi$  outside this domain is required. If so, we solve equation (27), substituting  $\phi(\mathbf{y}') \rightarrow \phi(\mathbf{y}) + D\phi \cdot \xi$ . The derivatives of  $\bar{\phi}$  are then calculated by finite difference. This, however, introduces an error, which disables us to continue the invariant manifold up to  $\epsilon = 0.25$ .

For example we approximate the invariant manifold at fixed parameter values  $(T_1, T_2) = (0.6, 0.25)$ . The step size is fixed to  $\Delta = 0.0025$  and the increment of  $\epsilon$  is chosen in the range  $[0.001, 0.005]$ . The maximal error is fixed to  $\mathcal{E}_{max} = 0.05$ . At each value of  $\epsilon$  about six iterations of the graph transform are needed. The computations were done with a lattice spacing of  $d = 0.01$ , in the trapping region  $L \leq 0.52$ . Thus, about  $5 \cdot 10^5$  points on the manifold are calculated.

In figure (7) the result of this computation is illustrated. Shown are the stable periodic orbit of system (20) at  $\epsilon = 0.1$  and  $(T_1, T_2) = (0.6, 0.25)$  and a forward

integration of the system  $\dot{\mathbf{y}} = \mathbf{g}(\phi_\epsilon(\mathbf{y}), \mathbf{y})$ . To find the latter integral curve we approximated every point of  $\phi_\epsilon(\mathbf{y})$  required for numerical integration by linear interpolation inbetween lattice points.

### 5. The reduced system

In the following, we will describe system (20), reduced to the approximate invariant manifold  $W_0$ . This reduction can be done analytically, so that we can compare bifurcation diagrams. Physically, an argument to study the system reduced to  $W_0$ , rather than to the numerically approximated  $W_\epsilon$ , is that the quantitative error, introduced by setting  $\epsilon = 0$ , is smaller than the error introduced by the Galerkin approximation. Equations (15) form a qualitative model of one aspect of the atmospheric circulation, namely the interaction between the jet stream and the baroclinic waves. A further simplification is justified if it keeps the qualitative behaviour in tact.

Substituting expression (24), we find that the reduced system,  $\dot{\mathbf{y}} = \mathbf{g}(\phi_0(\mathbf{y}), \mathbf{y})$ , is given by

$$\dot{y}_1 = -c_1 y_1 - d_1 (y_2^2 + y_3^2) + \bar{T}_1 \quad (32.1)$$

$$\dot{y}_2 = -c_2 y_2 + c_3 y_3 + d_3 y_1 y_3 + d_2 y_1 y_2 + \bar{T}_2 \quad (32.2)$$

$$\dot{y}_3 = -c_2 y_3 - c_3 y_2 - d_3 y_1 y_2 + d_2 y_1 y_3 + \bar{T}_3 \quad (32.3)$$

where we have introduced

$$\begin{aligned} c_1 &= (-2\alpha\lambda_{01}C' + h_N)/\bar{\lambda}_{01} & \bar{T}_1 &= h_N T_1 / \bar{\lambda}_{01} & d_1 &= \delta B / \bar{\lambda}_{01} \\ c_2 &= (-\alpha\lambda_{11}[C(1-A) + 2C'] + h_N)/\bar{\lambda}_{11} & \bar{T}_2 &= h_N T_2 / \bar{\lambda}_{11} & d_2 &= \delta\nu B / \bar{\lambda}_{11} \\ c_3 &= -\alpha\lambda_{11}CB/\bar{\lambda}_{11} & \bar{T}_3 &= h_N T_3 / \bar{\lambda}_{11} & d_3 &= \delta[\bar{\lambda}_{10} - \nu_{10}A]/\bar{\lambda}_{11} \end{aligned} \quad (33)$$

Again, we have a Lyapunov function

$$L = y_1^2 + \frac{\bar{\lambda}_{11}}{\nu_{10}\bar{\lambda}_{01}}(y_2^2 + y_3^2) \quad (34)$$

and a trapping region defined by

$$L \leq \left( \frac{\bar{\lambda}_{11}}{\nu_{10}\bar{\lambda}_{01}} \right)^2 \frac{\|\bar{T}\|^2}{c_1^2} \quad (35)$$

In contrast to equations (15), the divergence of the vector field of this reduced system can change sign, so that volume elements are not necessarily shrinking.

As explained in section (4.2), the amplitude of the nonlinear interaction depends on  $y_1$  through  $A$  and  $B$ . In figure (9) the dependence of the interaction coefficient in (32.1) is shown. This figure illustrates the life cycle of the baroclinic waves. The linear stability of the Hadley circulation is determined by the effective damping coefficient of the wave components  $y_{2,3}$ , given by  $c_2 - d_2 y_1$ . If this number is positive, the waves are damped. If it is negative, a perturbation of the Hadley circulation will lead to growing waves. If  $y_1$  is small, there is little energy transfer and the waves are damped. As  $y_1$  is forced by the meridional temperature gradient,  $\bar{T}_1$ , it grows and



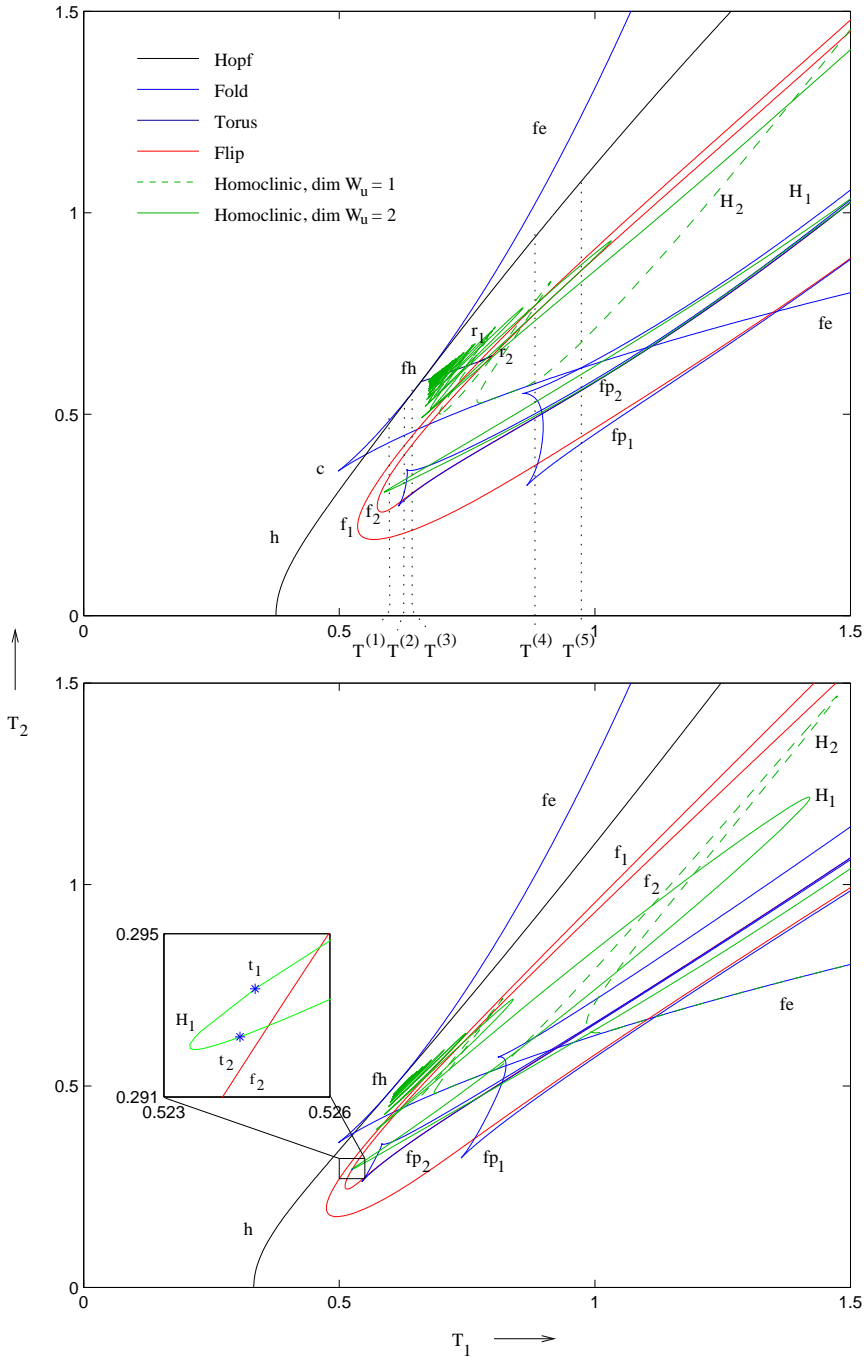


FIGURE 8. Top: partial bifurcation diagram of system (15). The dotted lines at  $T_1 = T^{(1...5)}$  refer to figures (3)-(5). Bottom: bifurcation diagram of system (32). The enlargement shows the neutral saddle focus transitions  $t_{1,2}$ .

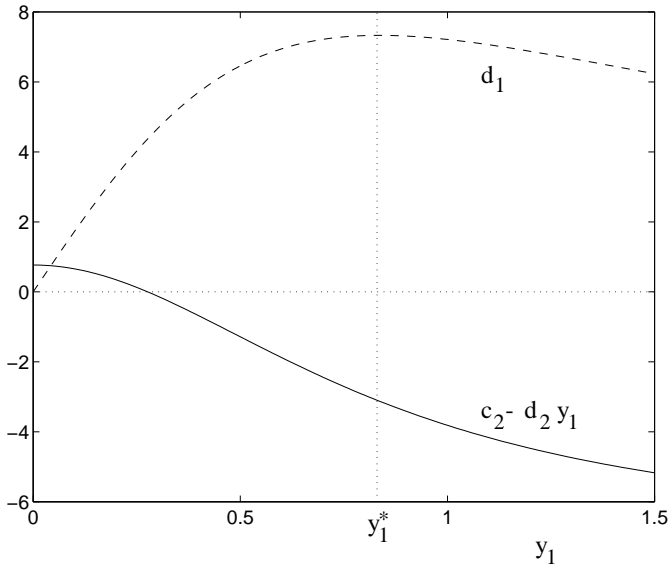


FIGURE 9. Dashed: the coefficient of interaction,  $d_1$ , between the jet stream pattern and the wave patterns. Solid: the effective damping coefficient of  $y_{2,3}$ . If we fix  $y_1 = y_1^* = \bar{C}/\kappa$  model (32) is equivalent to the Lorenz-84 model described in section (6)

the energy transfer increases. Beyond  $y_1 \approx 0.276$ , the effective damping coefficient is negative, and baroclinic waves can grow. When  $y_1 = \bar{C}/\kappa \approx 0.83$ , the phase shift,  $\gamma$ , is maximal and the waves are optimally baroclinic. They extract energy from the jet stream and  $y_1$  decreases. Then the waves decay and become decreasingly baroclinic in the process.

In order to see, if system (32) behaves qualitatively the same as system (15), we study the bifurcation diagram. It is shown in figure (8)(bottom). All the bifurcations displayed in diagram (8)(top) are present here, too. Therefore, the qualitative behaviour of the reduced system (32) is the same as that of the full system (15). The essence of the extra degrees of freedom in the six dimensional model can be captured by the variable coefficients in the three dimensional model.

## 6. Reduction to the Lorenz-84 model

As a final simplification of our model, we fix the coefficients in equations (32). The choice

$$A = A(\bar{C}/\kappa) = 0 \quad B = B(\bar{C}/\kappa) = 1$$

maximizes the efficiency of the energy transfer between the baroclinic waves and the jet stream. The phase shift is fixed to  $\gamma = \pi/2$ . Equivalently, we can reduce model (15) to the tangent space  $T_{(\mathbf{x}^*, \mathbf{y}^*)}W_0$ , where  $(\mathbf{x}^*, \mathbf{y}^*) = (\bar{C}/\kappa, 0, 0, \bar{C}/\kappa, 0, 0)$ . In other words, we linearise  $\phi_0$  around the Hadley state.

We then scale  $\mathbf{y}$  and  $t$  according to

$$\begin{aligned} t &= [c_2 + c_3 \frac{d_2}{d_3}]^{-1} t' & y_1 &= \frac{1}{d_2} [c_2 + c_3 \frac{d_2}{d_3}] x - \frac{c_3}{d_3} \\ y_2 &= [c_2 + c_3 \frac{d_2}{d_3}] \frac{1}{\sqrt{d_1 d_2}} y & y_3 &= [c_2 + c_3 \frac{d_2}{d_3}] \frac{1}{\sqrt{d_1 d_2}} z \end{aligned} \quad (36)$$

and find

$$\dot{x} = -y^2 - z^2 - ax + aF \quad (37.1)$$

$$\dot{y} = xy - bxz - y + G \quad (37.2)$$

$$\dot{z} = bxy + xz - z \quad (37.3)$$

which is the model introduced by Lorenz [1984]. For the parameters we find

$$\begin{aligned} F &= d_2 [c_2 + c_3 \frac{d_2}{d_3}]^{-2} (\bar{T}_1 + \frac{c_1 c_3}{d_3}) & G &= \sqrt{d_1 d_2} [c_2 + c_3 \frac{d_2}{d_3}]^{-2} \bar{T}_2 \\ a &= c_1 [c_2 + c_3 \frac{d_2}{d_3}]^{-1} & b &= \frac{d_3}{d_2} \end{aligned} \quad (38)$$

With the parameters as specified in section (4.1), we thus obtain

$$a \approx 0.35 \quad b \approx 1.33 \quad (39)$$

in contrast to the traditional values  $a = 1/4$  and  $b = 4$ . Diagram (10)(top) has been obtained by setting the parameters according to (39). There still is a strong similarity to diagram (8)(top). However, the neutral saddle focus transitions have disappeared. Along both homoclinic bifurcation curves only a stable cycle is created. The accumulation of 1 : 2 resonance points is still there and, although homoclinic curve  $H_1$  moves farther away, the branch switching mechanism along  $fp_2$  works as described in section (4.1).

**6.1. Continuation in  $a$  and  $b$ .** Finally, we continue the bifurcations in diagram (10)(top) in parameters  $a$  and  $b$  in order to establish the relation to the diagram at traditional parameter values, presented in Shilnikov et al. [1995].

Changing  $a$  to its traditional value,  $a = 1/4$ , does not change the bifurcation diagram qualitatively. When changing  $b$  two changes are apparent. Shown in figure (10)(bottom) is the diagram obtained for  $a = 1/4$  and  $b = 3.24$ . The second torus bifurcation line,  $tr_2$ , connecting two 1 : 2 resonance points in diagram (10)(top), is now tangent to flip bifurcation line  $f_2$  at point  $r$  and connects to the fold line  $fp_2$ . These two meet in a 1 : 1 resonance points, also called Bogdanov-Takens point.

Also, a pair of cusp points, marked  $c_{1,2}$ , has developed on fold line  $fp_2$ . These cusps denote creation and vanishing of successive wiggles on the branch of periodic solutions connected to homoclinic curve  $H_1$ .

Figure (11)(top) shows the bifurcation diagram at parameter values  $a = 1/4$  and  $b = 4$ . This diagram was presented by Shilnikov et al. [1995]. The torus bifurcation line  $tr_2$  no longer connects to flip bifurcation line  $f_2$  and, consequently, has developed an angular degeneracy (Peckham et al. [1995]) at point  $D$ . Along curve  $tr_2$  the multipliers of the periodic orbit are given by  $\exp(\pm i\phi)$ , where  $\phi$  is the phase angle. At point  $D$  it has a maximum given by  $\phi \approx 0.8\pi$ .

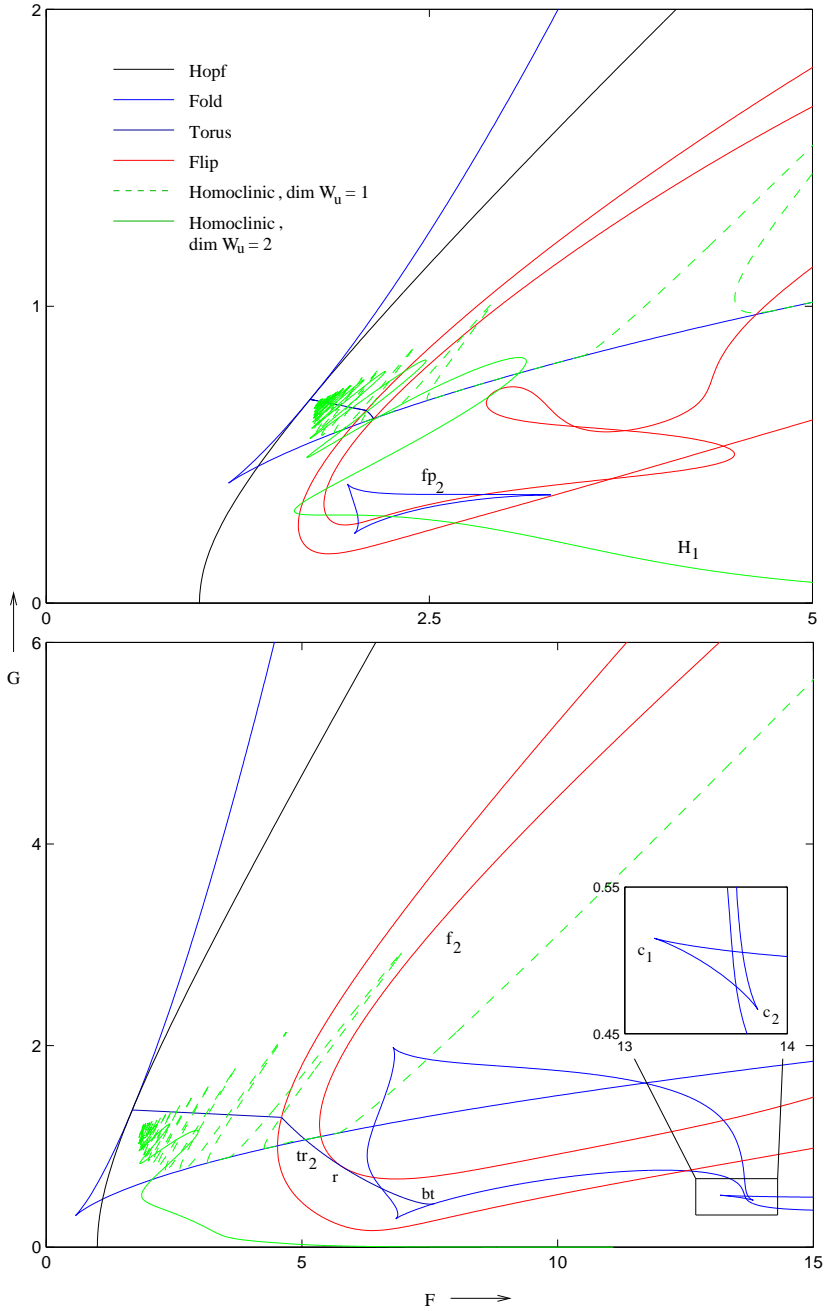


FIGURE 10. Top: bifurcation diagram of system (37), with  $a$  and  $b$  as calculated from the physical parameters  $C$ ,  $C'$ ,  $h_N$  and  $\alpha$ . Bottom: with  $a = 1/4$  and  $b = 3.24$ . Torus bifurcation line  $tr_2$  and flip bifurcation line  $f_2$  are tangent at point  $r$ .  $tr_2$  ends in a 1 : 1 resonance point, marked  $bt$ . The enlargement shows that extra cusps,  $c_{1,2}$ , have developed on saddle node line  $fp_2$ .

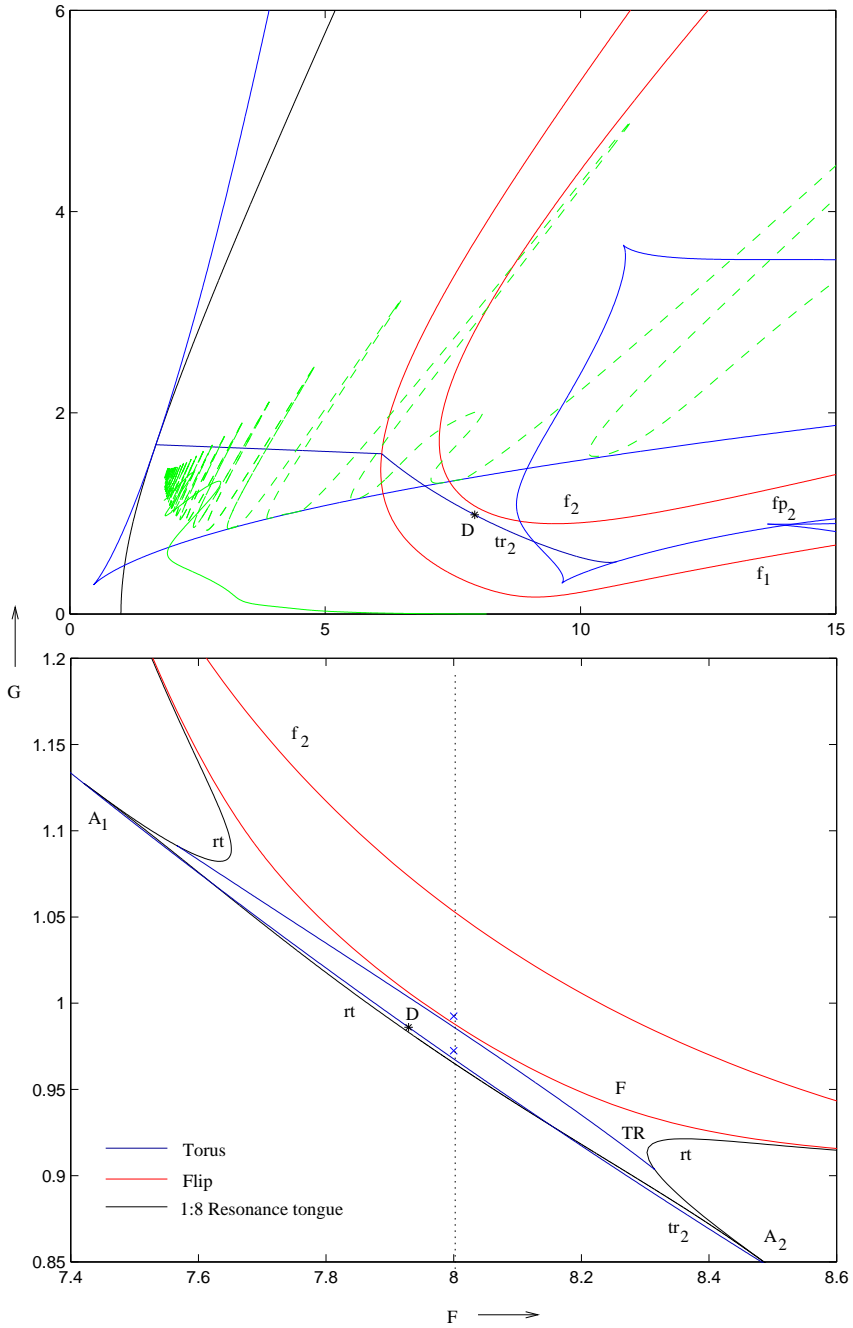


FIGURE 11. Top: bifurcation diagram of system (37) at  $a = 1/4$  and  $b = 4$ , with angular degeneracy point  $D$ . Bottom: detail, with boundaries of the 8:1 resonance tongue and a torus and flip bifurcation of the period 8 orbit. The crosses mark the parameter values of Poincaré sections in figure (12).

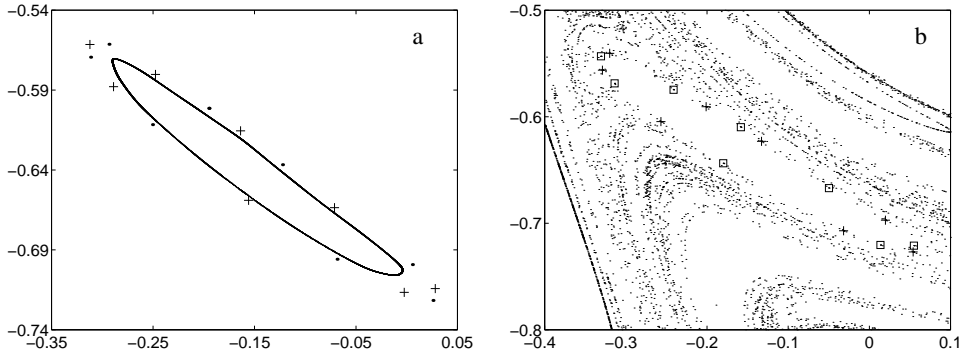


FIGURE 12. Poincaré sections of the Lorenz-84 model with  $a = 1/4$  and  $b = 4$  in the  $y, z$ -plane. a:  $(F, G) = (8, 0.9725)$ . Two coexisting invariant tori, one with the period 8 orbits, one with quasiperiodic dynamics. The thick dots denote the stable orbit, the crosses the saddle type orbit. b:  $(F, G) = (8, 0.99)$ . Beyond the torus and flip bifurcations TR and F. Both orbits, marked with crosses and boxes are now of saddle type.

If the forcing is set to  $(F, G) = (8, 1)$  the model is known to behave chaotically (e.g. Lorenz [1984]). An important, unanswered question is how this chaotic behaviour is brought about. With the derivation of the model and the bifurcation analysis in mind, we discuss four different possible routes to chaos in the following subsections.

6.1.1. *Period doubling cascades.* The flip bifurcation lines  $f_{1,2}$  in diagram (11) (top) still are the first of an infinite sequence. However, as explained in section (4.1), figure (4), a cross section with  $F$  fixed does not show a period doubling cascade followed by an inverse cascade, due to branch switching along the cusped saddle node line  $fp_2$ . The flip bifurcation lines  $f_{1,2,\dots}$ , extending beyond the limits of diagrams (10) and (11), are closed curves. As can be seen in diagram (10)(top), these curves form unnnested islands. In accordance with the claim to general applicability of the analysis presented in Wieczorek et al. [2001], the bifurcation diagram of the Lorenz-84 model has much in common with that of their rate equation model. Chaotic attractors can be created and destroyed through different routes, including period doubling cascades, the Ruelle-Takens scenario and intermittency.

6.1.2. *Ruelle-Takens scenario.* Another possible route to chaos was proposed by Ruelle and Takens [1971]. In this scenario, an invariant torus is created first. Then a periodic orbit appears on the torus, when crossing the boundary of an Arnold resonance tongue. If this periodic orbit bifurcates, a chaotic attractor can be created. This scenario can be observed in the Lorenz-84 model. We will concentrate on the chaotic behaviour at parameter values  $(F, G) = (8, 1)$ , close to the angular degeneracy point D.

If we fix  $F = 8$  and increase  $G$  from below  $tr_2$ , we find the attracting period two orbit first, then quasiperiodic behaviour in a small interval, then a period 8 orbit on the invariant torus. Figure (11)(bottom) shows a detail of diagram (11)(top), with

the boundaries of the 8:1 resonance tongue and two subsequent bifurcations, a torus and a flip bifurcation, of the period 8 orbit.

The phase angle crosses the point  $\phi = 3\pi/4$  twice, at resonance points  $A_{1,2}$ . One edge of the resonance tongue connects these points. It appears that the invariant torus itself goes through two subsequent fold bifurcations, so that the edge of the resonance tongue can cross  $\text{tr}_2$ , and in a narrow band two stable tori coexist. This is shown in figure (12a). On the inner torus the dynamics is quasiperiodic, on the outer torus the period 8 orbits exist. If we further increase  $G$ , the period 8 orbit loses its stability in a torus bifurcation, directly followed by a flip bifurcation, as one of the multipliers crosses back into the unit circle through  $-1$ . Beyond these bifurcations, a chaotic attractor appears. The corresponding Poincaré section is shown in figure (12b). The whole picture is more involved, as the tori shown in figure (12)a coexist with several tori with phase locked orbits of higher period.

Scenarios for the creation of a chaotic attractor through the bifurcation of a periodic orbit on an invariant torus are described in Broer et al. [1998]. The Ruelle-Takens scenario in the vicinity of an angular degeneracy was recently found in an electronic model by Algaba et al. [2001].

6.1.3. *Shil'nikov bifurcations.* The neutral saddle focus transitions, found in the six dimensional model, (15), and the approximate reduced model, (32), are not present in diagrams (10)(top)-(11)(top). Therefore, no Shil'nikov type chaos occurs in the Lorenz-84 model for these parameter values. We can, however, retrace the transition points for different values of  $b$ . As the continuation package HomCont (Doedel et al. [1986]) allows for three parameter continuation of codimension two points on homoclinic curves, it is possible to calculate a curve of neutral saddle focus transitions in the space of parameters  $b$ ,  $F$  and  $G$ . It turns out, that two transition points appear on curve  $H_1$  if  $b < 0.419$ . Just like in diagram (8)(bottom), on a small segment the saddle value becomes negative. Therefore, for  $b < 0.419$  Shil'nikov type chaos can be encountered in the Lorenz-84 model.

6.1.4. *Intermittency.* The last route to chaos described here is through intermittency. If we keep  $F = 8$  fixed and increase  $G$ , we find a periodic window around  $G \approx 1.167$ . At  $G = 1.16742$ , the stable periodic orbit undergoes a saddle node bifurcation. Beyond this point, the behaviour is intermittent. In terms of Pomeau and Manneville [1980], this is type I intermittency. Two time series in the intermittent regime are shown in figure (13). In Wiczeorek et al. [2001] the same type of intermittency is found and pictures of the stable and unstable manifolds of the saddle type orbit are shown.

## 7. Conclusion

The starting point of the analysis in this paper is the truncation to six degrees of freedom of a QG two level model of atmospheric flow. Period doubling cascades and Shil'nikov bifurcations are identified as routes to chaos in the bifurcation diagram of this model. A measurement of the dimension of the chaotic attractor along a section of the bifurcation diagram reveals that it is less than three dimensional, hinting at the existence of a three dimensional invariant manifold which captures the dynamics.

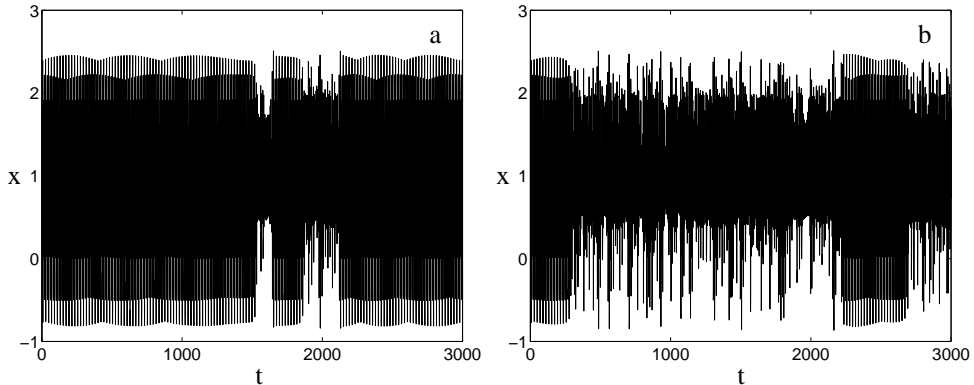


FIGURE 13. Intermittency in the Lorenz-84 model. a:  $(F, G) = (8, 1.16743)$ .  
 b:  $(F, G) = (8, 1.1675)$ .

In order to approximate this invariant manifold we have introduced a small parameter,  $\epsilon$ , into the equations. In the limit of  $\epsilon \downarrow 0$  an exact solution was presented. This solution has a clear physical interpretation in terms of energy exchange between the zonally symmetric jet stream mode and the traveling waves. Numerical evidence for the existence of this manifold for finite  $\epsilon$  was found implementing a variant of the graph transform algorithm of Broer et al. [1997].

We have shown that we can set  $\epsilon = 0$  without destroying the qualitative dynamics. The bifurcation diagram of the reduced model in this limit agrees well with the diagram of the six dimensional model. The invariant manifold at  $\epsilon = 0$  can be linearised around the Hadley state. If the six dimensional model is reduced to this linear approximation of the invariant manifold, the Lorenz-84 model is found. The parameters of the Lorenz-84 model can then be calculated from the physical parameters of the QG model. One of them comes out significantly different. We have compared the bifurcation diagram of the Lorenz-84 model at physical parameters to that of the six dimensional model and to the diagram at traditional parameter values, first presented in Shilnikov et al. [1995].

Finally, we have discussed four possible routes to chaos in the Lorenz-84 model. Period doubling cascades appear both in the six dimensional model and in the Lorenz-84 model. Shil'nikov bifurcations are only found in the Lorenz-84 model for parameter values far away from those considered here. A route to chaos not considered before in this model is the Ruelle-Takens scenario. We have presented evidence that the creation and destruction of invariant tori and the presence of resonance tongues lead to chaos in the Lorenz-84 model. Finally, an intermittent transition has been presented. The overall picture of chaotic attractors being created and destroyed via different routes is reminiscent of the dynamics described in Wicczorek et al. [2001].

The link between a Galerkin truncation of a QG baroclinic model and the Lorenz-84 model justifies the use of the latter in conceptual studies of atmosphere and climate dynamics. It is remarkable how much of the bifurcation structure of



the six dimensional truncation is preserved, notwithstanding rough approximations, namely setting  $\epsilon = 0$  and linearising the three dimensional invariant manifold. Probably, this is because the six dimensional model isolates one aspect of midlatitude, synoptic flow: the energy exchange between the jet stream and the baroclinic waves. When reducing to three degrees of freedom, and subsequently to the Lorenz-84 model, this process is modeled qualitatively correctly.

### **8. Acknowledgments**

The author wishes to thank Ferdinand Verhulst, Theo Opsteegh, Ulrich Achatz, Yuri Kuznetsov and Renato Vitolo for useful discussions and proofreading. This work is part of the NWO project ‘a conceptual approach to climate variability’ (nr. 61-620-367).



## Bibliography

- Achatz, U. & Branstator, G. [1999] “A two-layer model with empirical linear corrections and reduced order for studies of internal climate variability,” *J. Atmos. Sci.* **56**, 3140–3160.
- Algaba, A., Merino, M. & Rodríguez-Luis, A. J. [2001] “Takens-Bogdanov bifurcations of periodic orbits and Arnold’s tongues in a three dimensional electronic model,” *Internat. J. Bifur. Chaos* **2**, 513–531.
- Anderson, J. L. & Hubeny, V. [1997] “A reexamination of methods for evaluating the predictability of the atmosphere,” *Nonlin. Proc. Geophys.* **4**, 157–165.
- Broer, H. W., Osinga, H. M. & Vegter, G. [1997] “Algorithms for computing normally hyperbolic invariant manifolds,” *Z. angew. Math. Phys.* **48**, 480–524.
- Broer, H. W., Simó, C. & Tatjer, J. C. [1998] “Towards global models near homoclinic tangencies of dissipative diffeomorphisms,” *Nonlinearity* **11**, 667–770.
- Broer, H. W., Simó, C. & Vitolo, R. [2001] “Bifurcations and strange attractors in the Lorenz-84 climate model with seasonal forcing,” IWI preprint 2001-3-03, to appear in *Nonlinearity*.
- Champneys, A. R. & Kuznetsov, Yu. A. [1994] “Numerical detection and continuation of codimension-two homoclinic bifurcations,” *Internat. J. Bifur. Chaos* **4**, 785–822.
- De Swart, H. E. [1988] “Low order spectral models of the atmospheric circulation: a survey,” *Acta Appl. Math.* **11**, 49–96.
- Doedel, E., Champneys, A., Fairgrieve, T., Kuznetsov, Yu. A., Sandstede, B. & Wang, X.J. [1986] *AUTO97: Continuation and bifurcation software for ordinary differential equations (with HomCont)* Computer Science, Concordia University, Montreal, Canada.
- Foias, C., Jolly, M. S., Kevrekidis, I. G., Sell, G. R. & Titi, E. S. [1988] “On the computation of inertial manifolds,” *Phys. Lett. A* **131**, 433–436.
- Frisius, T. [1998] “A mechanism for the barotropic equilibration of baroclinic waves,” *J. Atmos. Sci.* **55**, 2918–2936.
- Glendinning, P. & Sparrow, C. [1984] “Local and global behavior near homoclinic orbits,” *J. Stat Phys.* **35**, 645–696.
- González-Miranda, J. M. [1997] “Predictability in the Lorenz low-order general atmospheric circulation model,” *Phys. Lett. A* **233**, 347–354.
- Holton, J.R. [1992] *Introduction to dynamic meteorology* (Academic press).
- Itoh, H. & Kimoto, M. [1996] “Multiple attractors and chaotic itinerancy in a quasi-geostrophic model with realistic topography: implications for weather regimes and

- low-frequency variability,” *J. Atmos. Sci.* **53**, 2217–2231.
- Kuznetsov, Yu. A. [1998] *Elements of applied bifurcation theory* (Springer, New York).
- Kuznetsov, Yu. A. [1999] “Numerical normalization techniques for all codim 2 bifurcations of equilibria in ode’s,” *SIAM J. Numer. Anal.* **36**, 1104–1124.
- Kuznetsov, Yu. A. & Levitin, V. V. [1997] *CONTENT: A multiplatform environment for analyzing dynamical systems* Centrum voor Wiskunde en Informatica, Amsterdam.
- Lorenz, E. N. [1960] “Energy and numerical weather prediction,” *Tellus* **12**(4), 364–373.
- Lorenz, E. N. [1963] “Deterministic non-periodic flows,” *J. Atmos. Sci.* **20**, 130–141.
- Lorenz, E.N. [1984] “Irregularity: a fundamental property of the atmosphere,” *Tellus* **36A**, 98–110.
- Peckham, B. B., Frouzakis, C. E. & Kevrekidis, G. [1995] “Bananas and banana splits: a parametric degeneracy in the hopf bifurcation for maps,” *SIAM J. Math. Anal.* **26**, 190–217.
- Peixoto, J. P. & Oort, A. H. [1992] *Physics of climate* (Springer, New York).
- Pelino, V. & Pasini, A. [2001] “Dissipation in Lie-Poisson systems and the Lorenz-84 model,” *Phys. Lett. A* **291**, 389–396.
- Philips, N. A. [1954] “Energy transformations and meridional circulations associated with simple baroclinic waves in a two-level, quasi-geostrophic model,” *Tellus* **6**, 273–286.
- Pielke, R. & Zeng, X. [1994] “Long-term variability of climate,” *J. Atmos. Sci.* **51**, 155–159.
- Pomeau, Y. & Manneville, P. [1980] “Intermittent transition to turbulence in dissipative dynamical systems,” *Commun. Math. Phys.* **74**, 189–197.
- Roebber, P.J. [1995] “Climate variability in a low-order coupled atmosphere-ocean model,” *Tellus* **47A**, 473–494.
- Ruelle, D. & Takens, F. [1971] “On the nature of turbulence,” *Commun. math. Phys.* **20**, 167–192.
- Saltzman, B. [1962] “Finite amplitude free convection as an initial value problem,” *J. Atmos. Sci.* **19**, 329.
- Shilnikov, A., Nicolis, G. & Nicolis, C. [1995] “Bifurcation and predictability analysis of a low-order atmospheric circulation model,” *Internat. J. Bifur. Chaos* **5**(6), 1701–1711.
- Veen, L.van , Opsteegh, T. & Verhulst, F. [2001] “Active and passive ocean regimes in a low-order climate model,” *Tellus* **53A**, 616–627 (chapter 3 of this thesis).
- Wieczorek, S., Krauskopf, B. & Lenstra, D. [2001] “Unnested islands of period doublings in an injected semiconductor laser,” *Phys. Rev. E* **64**, 056204.
- Wiin-Nielsen, A. [1992] “Comparisons of low-order atmospheric dynamical systems,” *Atmosfera* **5**, 135–155.
- Wiin-Nielsen, A. [1994] “Nonlinear studies of quasi-geostrophic systems,” *Physica D* **77**, 33–59.

## CHAPTER 3

# Active and passive ocean regimes in a low-order climate model

*Tellus* **53A**, 2001, 616-627.

ABSTRACT. A low order climate model is studied which combines the Lorenz-84 model for the atmosphere on a fast time scale and a box model for the ocean on a slow time scale. In this climate model, the ocean is forced strongly by the atmosphere. The feedback to the atmosphere is weak. The behaviour of the model is studied as a function of the feedback parameters. We find regions in parameter space with dominant atmospheric dynamics, i.e. a passive ocean, as well as regions with an active ocean, where the oceanic feedback is essential for the qualitative dynamics. The ocean is passive if the coupled system is fully chaotic. This is illustrated by comparing the Kaplan-Yorke dimension and the correlation dimension of the chaotic attractor to the values found in the uncoupled Lorenz-84 model. The active ocean behaviour occurs at parameter values between fully chaotic and stable periodic motion. Here, intermittency is observed. By means of bifurcation analysis of periodic orbits, the intermittent behaviour, and the role played by the ocean model, is clarified. A comparison of power spectra in the active ocean regime and the passive ocean regime clearly shows an increase of energy in the low frequency modes of the atmospheric variables. The results are discussed in terms of itinerancy and quasi-stationary states observed in realistic atmosphere and climate models.

### 1. Introduction

On a time scale of days or weeks, the atmospheric component of the earth's climate system is dominant. Therefore, for short range weather forecasts, oceanic variables, such as the sea surface temperature, can often be considered fixed. On a much longer time scale the ocean's dynamics can play an important role. It has to be taken into account when studying for instance decadal climate variability or anthropogenic influences like the enhanced greenhouse effect. For such purposes state-of-the-art climate models are often used, which possess millions of degrees of freedom. The results of experiments with such models are analysed statistically, as they are out of reach of the ordinary analysis of dynamical systems theory. As much understanding of atmosphere models has been gained by looking at extremely low dimensional truncations, our aim is to do the same for coupled models.

The issue we will focus on is the interplay of the short time scale variability of the atmospheric, intrinsically chaotic, component, and the long time scale of the oceanic component. In climatological terms, the question is whether the ocean is passive or active. If it is passive, it simply integrates the atmospheric signal, as if there is a one

way coupling. If it is active, there are notable feedback effects in the atmospheric dynamics. Even though the forcing of the atmosphere by the ocean is intrinsically weak, it may produce, for instance, decadal variability in atmospheric observables. Whether the ocean really is passive or active is still a matter of debate. Latif and Barnett [1994] found decadal variability induced by an active ocean. Other studies, such as Frankignoul et al. [2000], using complex, state-of-the-art climate models, or Saravanan and Mc Williams [1997] and Selten et al. [1999], who used models of intermediate complexity, give evidence for a passive ocean. In this paper we investigate the atmosphere-ocean interaction in a low-dimensional coupled model applicable to midlatitudes. We will show, that the ocean can be passive or active, depending on small changes in the coupling parameters. This may explain the different conclusions reached in studies with more realistic, complex models.

The low-order model studied in this paper is based on a proposal by Roebber (1995). He coupled the Lorenz-84 model, which is a metaphor for the general circulation of the atmosphere [Lorenz, 1984], to Stommel's box model for a single ocean basin [Stommel, 1961]. Roebber uses numerical integrations and power spectra to characterise the coupled dynamics, without the exploration of bifurcation analysis and other tools of dynamical systems theory. In the fully coupled system, subject to periodic forcing, he finds increased energy in low frequency atmospheric modes when compared to one way coupling, i.e. without oceanic feedback to the atmosphere. In this paper, we investigate the coupled dynamics in detail.

In sections (2) and (3) the Lorenz-84 model and Stommel's box model are briefly introduced. When coupling these models, as described in section (4), we take into account that experiments with realistic climate models, such as Grötzner et al. [1998], indicate that the circulation of the ocean is largely driven by atmospheric dynamics and solar forcing. In contrast, the oceanic feedback to the atmosphere is rather weak, and only notable on intrinsic time scales of the ocean. Therefore, we assume that the coupling terms in the ocean model are of the same order of magnitude as its internal dynamics, while the coupling terms in the atmosphere model are taken to be small perturbations of the atmosphere's internal dynamics. Thus, a small parameter is introduced into the equations. The ratio of time scales of the atmosphere and the ocean model is a second small parameter. The consequences of the presence of small parameters, in the light of perturbation theory, are discussed in section (5). The behaviour of the coupled system is then investigated as a function of the coupling parameters in the atmosphere model.

In section (6) a bifurcation analysis of the equilibria of the coupled model is presented. The coexistence of attracting equilibria is inherited from the uncoupled box model. These equilibria describe two different orientations of the thermohaline circulation (THC).

For a range of parameter values chaotic attractors exist. In section (7), numerical estimates of the Kaplan-Yorke dimension and the correlation dimension of these attractors are given. They are compared to the corresponding quantities for the uncoupled Lorenz-84 model. It is shown that, in the chaotic regime, the ocean can be considered passive. It is slaved by the atmospheric forcing.

A new property of the coupled model is the intermittent behaviour, which is observed at parameter values between fully chaotic and stable periodic regions in parameter space. In section (8) this behaviour is studied in detail by means of bifurcation analysis of periodic solutions. It is shown that the slow dynamics of the ocean model play an important role here. Therefore, the ocean can be considered active in this regime.

Finally, in section (9), we compare power spectra of the atmospheric component of the coupled model in the passive and the active regime. In the active regime, the spectral power in the low frequency modes, on the intrinsic time scale of the ocean, is considerably increased.

## 2. The Lorenz-84 general circulation model

Like the Lorenz-63 model, the Lorenz-84 model is related to a Galerkin truncation of the Navier-Stokes equations. Where the '63 model describes convection, the '84 model gives the simplest approximation to the general atmospheric circulation at midlatitude. The approximation is applicable on an  $f$ -plane, placed over the North Atlantic ocean.

We can give a physical interpretation of the variables of the Lorenz-84 model:  $x$  is the intensity of the westerly circulation,  $y$  and  $z$  are the sine and cosine components of a large traveling wave. The time derivatives are given by

$$\dot{x} = -y^2 - z^2 - ax + aF \quad (1.1)$$

$$\dot{y} = xy - bxz - y + G \quad (1.2)$$

$$\dot{z} = bxy + xz - z \quad (1.3)$$

where  $F$  and  $G$  are forcing terms due to the average north-south temperature contrast and the earth-sea temperature contrast, respectively. Conventionally we take  $a = 1/4$  and  $b = 4$ .

The behaviour of this model has been studied extensively since its introduction by Lorenz [1984]. Numerical and analytical explorations can be found in Masoller et al. [1995] and Sicardi and Masoller [1996], a bifurcation analysis is presented in Shilnikov et al. [1995]. The bifurcation diagram of this model is quite rich. It brings forth equilibrium points, periodic and quasi periodic orbits as well as chaotic motion. Qualitatively the behaviour can be sketched by looking at the energy transfer between the westerly circulation and the traveling wave. The energy content of the westerly circulation tends to grow, forced by solar heating. Above a certain value however this circulation becomes unstable and energy is transferred to traveling waves, and then dissipated. The energy content of the westerly circulation decreases rapidly and the cycle repeats itself in a periodic or irregular fashion. In figure (1) one can see that the orbit tends to spiral around the  $x$ -axis towards a critical value of  $x$ , then drops towards the  $y, z$ -plane.

At parameter values  $(F, G) = (6, 1)$  two stable periodic solutions coexist. These parameter values are called summer conditions. For  $(F, G) = (8, 1)$  the behaviour is chaotic (see figure (1)). These parameter values are called winter conditions. As argued in Lorenz [1990], the north-south temperature contrast,  $F$ , is larger during

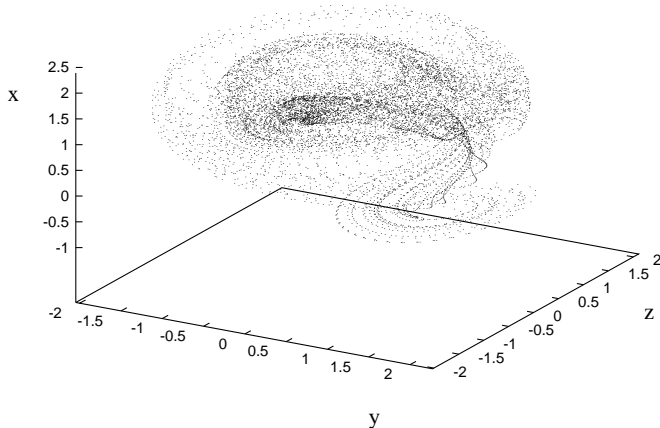


FIGURE 1. Chaotic motion in the Lorenz-84 model for  $(F, G) = (8, 1)$ : about  $10^4$  points on the attractor.

winters. This results in strong baroclinic wave activity, reflected by chaotic motion in the Lorenz-84 model. The periodic motion under summer conditions reflects less turbulent large scale dynamics due to a smaller north-south temperature contrast.

If we fix these forcing parameters to summer conditions in the coupled model, described below, no complex dynamics arise. When varying the coupling parameters we see only equilibrium points and periodic solutions. In our investigations we will take  $(F, G) = (8, 1)$ , i.e. we will consider perpetual winter conditions.

### 3. The box model for a single ocean basin

The ocean-box model was introduced by Stommel [1961]. It is a simple model of a single ocean basin, the North Atlantic. This basin is divided in two boxes, one at the equator and one at the north pole. Within the boxes the water is supposed to be perfectly mixed, so that the temperature and salinity are constant within each box but may differ between them. This drives a circulation between the boxes which represents the THC. Water evaporates from the equatorial box and precipitates into the polar box. Thus the salinity difference between the boxes is enhanced. The temperature difference is maintained by the difference in heat flux from the sun. Thus, the salinity and the temperature difference drive a circulation in opposite directions. For a suitable choice of parameters, both the circulation driven by salinity and the circulation driven by temperature occur as stable solutions in this model [Stommel, 1961]. In contrast to the Lorenz model, no complex dynamics arise.

Figure (2) shows the setting of the model. The volume of water is kept equal, but its density may differ between the boxes. Using a linearised equation of state and some assumptions on the damping, dynamical equations for the temperature difference  $T = T_e - T_p$  and the salinity difference  $S = S_e - S_p$  can be derived. They



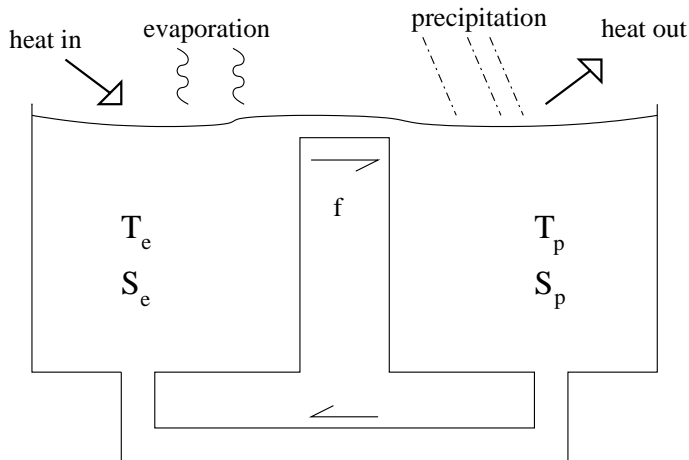


FIGURE 2. The two box model. Water evaporates from the warmer equatorial box on the left and is transported through the atmosphere to the polar box on the right. The flow  $f$  is positive when directed northward.

are

$$\dot{T} = k_a(T_a - T) - |f(T, S)|T - k_w T \quad (2.1)$$

$$\dot{S} = \delta - |f(T, S)|S - k_w S \quad (2.2)$$

$$f = \omega T - \xi S \quad (2.3)$$

where  $k_a$  is the coefficient of heat exchange between ocean and atmosphere,  $k_w$  is the coefficient of internal diffusion and  $\omega$  and  $\xi$  derive from the linearised equation of state. The flow,  $f$ , represents the THC. It is positive when temperature driven and negative when salinity driven. The inhomogeneous forcing by solar heating and atmospheric water transport are given by  $T_a$  and  $\delta$ , respectively. When coupling the box model to the Lorenz-84 model, we will use the estimates in Roebber [1995] for the parameters in equations (2). The volume of the deep ocean box, not present in our model, is simply divided between the polar and the equatorial box.

The absolute value in (2.1) and (2.2) was put there by Stommel, arguing that the mixing of the water should be independent of the direction of the flow. A more straightforward derivation of the equations of motion of a simple ocean model related to the box model indicates that this is indeed the case, although the term comes out quadratic instead of piecewise linear [Maas, 1994]. If we take this term to be quadratic in the coupled model, described below, the average values of  $T$  and  $S$  change significantly, but we find qualitatively the same behaviour.

#### 4. The coupled equations

Having described these simple models for atmospheric and oceanic circulation, and the physical interpretation of their variables, we can now identify three mechanisms by which they interact:

- (1) The atmospheric pole-equator temperature contrast is supposed to be in permanent equilibrium with the zonal wind strength  $x$ , i.e. we put  $T_a \propto x$ . Also, the forcing of the atmosphere by the north-south temperature contrast in (1.1) is modified by the ocean temperature contrast, so we put  $F \rightarrow F_0 + F_1 T$ . This expresses the simplest geostrophic equilibrium: a north-south temperature gradient which drives a east-west atmospheric circulation.
- (2) The inhomogeneous forcing by land-sea temperature contrast in (1.2) should decrease with increasing temperature difference  $T$ . It is assumed that in the polar region the sea water temperature is higher than the temperature over land, while in the equatorial region it is lower. A higher temperature difference  $T$  thus means a lower land-sea temperature contrast. This influence is described as a fluctuation upon a fixed forcing:  $G \rightarrow G_0 + G_1(T_{av} - T)$ .
- (3) The water transport through the atmosphere is taken to be linear in the energy content of the traveling wave:  $\delta \rightarrow \delta_0 + \delta_1(y^2 + z^2)$ .

Combining (1) and (2) with the proposed coupling terms we obtain

$$\dot{x} = -y^2 - z^2 - ax + a(F_0 + F_1 T) \quad (3.1)$$

$$\dot{y} = xy - bxz - y + G_0 + G_1(T_{av} - T) \quad (3.2)$$

$$\dot{z} = bxy + xz - z \quad (3.3)$$

$$\dot{T} = k_a(\gamma x - T) - |f(T, S)|T - k_w T \quad (3.4)$$

$$\dot{S} = \delta_0 + \delta_1(y^2 + z^2) - |f(T, S)|S - k_w S \quad (3.5)$$

with  $f$  as in (2.3). With the coupling some new constants have been introduced. They are  $T_{av}$ , the standard temperature contrast between the polar and the equatorial box,  $\gamma$ , the proportionality constant of the westerly wind strength and the north-south temperature contrast and  $\delta_1$ , a measure for the rate of water transport through the atmosphere. When exploring the dynamical behaviour of the model we take  $F_1$  and  $G_1$  as free parameters. As motivated in the introduction, we consider small coupling to the atmosphere model. This is the case if we take  $(F_1, G_1) \in [0, 0.1] \times [0, 0.1]$ . In table (1) the parameters are listed. In this scaling, one unit of time in the model corresponds to the typical damping time scale of the planetary waves, estimated to be five to ten days.

$a$	$1/4$	$\delta_0$	$7.8 \cdot 10^{-7}$
$b$	$4$	$k_w$	$1.8 \cdot 10^{-5}$
$F_0$	$8$	$k_a$	$1.8 \cdot 10^{-4}$
$G_0$	$1$	$\xi$	$1.1 \cdot 10^{-3}$
$\gamma$	$30$	$\omega$	$1.3 \cdot 10^{-4}$
$\delta_1$	$9.6 \cdot 10^{-8}$	$T_{av}$	$30$

TABLE 1. The constants of the coupled model. With these constants the ocean and the atmosphere model have time scales that differ by a factor of about one thousand. See Roebber [1995].

### 5. Perturbation theory

If we denote the atmospheric variables by  $\mathbf{x} \in \mathbb{R}^3$  and the oceanic variables by  $\mathbf{y} \in \mathbb{R}^2$ , we can write the system (3) as

$$\begin{aligned}\dot{\mathbf{x}} &= f_0(\mathbf{x}) + \epsilon_1 f_1(\mathbf{y}) \\ \dot{\mathbf{y}} &= \epsilon_2 g_0(\mathbf{x}) + \epsilon_2 g_1(\mathbf{y})\end{aligned}\quad (4)$$

where  $\epsilon_1$  and  $\epsilon_2$  are small parameters. Putting  $\epsilon_1 = \epsilon_2 = 0$  yields the Lorenz-84 model. Hyperbolic equilibria in the Lorenz-84 equations correspond to a first approximation of a slow manifold in the full system (4) as a consequence of Fenichel' theorem [Wiggins, 1994]. In our case the slow manifold is unstable and not physically interesting.

Instead we focus on periodic and chaotic solutions of the Lorenz-84 equations and the phenomenon of intermittency in the coupled system. Note, that the existence of the periodic solutions and their corresponding Floquet spectrum, which determines the stability properties, is described by the Poincaré expansion theorem [see Verhulst, 1996]. The Floquet multipliers of periodic orbits in the coupled system are expected to be  $O(\epsilon_1, \epsilon_2)$  perturbations of the corresponding multipliers in the uncoupled system. This information will be used when describing the intermittent behaviour.

### 6. Bifurcations of equilibrium points

The equilibrium points of system (3) can be found after some algebraic manipulations, as roots of a high order polynomial equation. For each set of parameter values, the equilibria can be calculated along with their spectra. In addition, the bifurcations of these equilibria can be found using the continuation package AUTO [Doedel et al., 1986]. On a plane in phase space, defined by  $f = 0$ , the vector field is not differentiable. There is an equilibrium point on this plane if

$$G_1 = \frac{-G_0 \pm \sqrt{a(F_0 + F_1 T_0 - x_0)(1 - 2x_0 + (1 + b^2)x_0^2)}}{T_{av} - T_0}. \quad (5)$$

with equilibrium values  $x_0 = (\delta_0 + a\delta_1 F_0)(k_a + k_w)\xi / (\omega k_w k_a \gamma + a\delta_1 \xi [k_a + k_w - F_1 \gamma k_a])$  and  $T_0 = k_a \gamma x_0 / (k_a + k_w)$ . On the curve in parameter space, defined by (5), a bifurcation occurs. When crossing it, increasing  $G_1$ , two equilibrium points appear, one with a positive value of  $f$ , and one with a negative value. The latter is stable. In fact, for any  $G_1$  greater than the right hand side in (5) there is an attracting equilibrium or periodic solution on which  $f$  is negative, i.e. the THC is salinity driven. At such an equilibrium, most of the energy in the atmosphere model is stored in the wave activity, whereas the jetstream intensity is low (i.e.  $y^2 + z^2 \gg x^2$ ). This results in a large freshwater flux through the atmosphere. The ocean's response is a weak, inverted, THC, a small negative temperature difference  $T$  and a relatively large salinity difference  $S$ .

The results of the bifurcation and stability analysis are shown in diagram (3). The stability of the equilibrium points is indicated in the diagram. As can be seen,

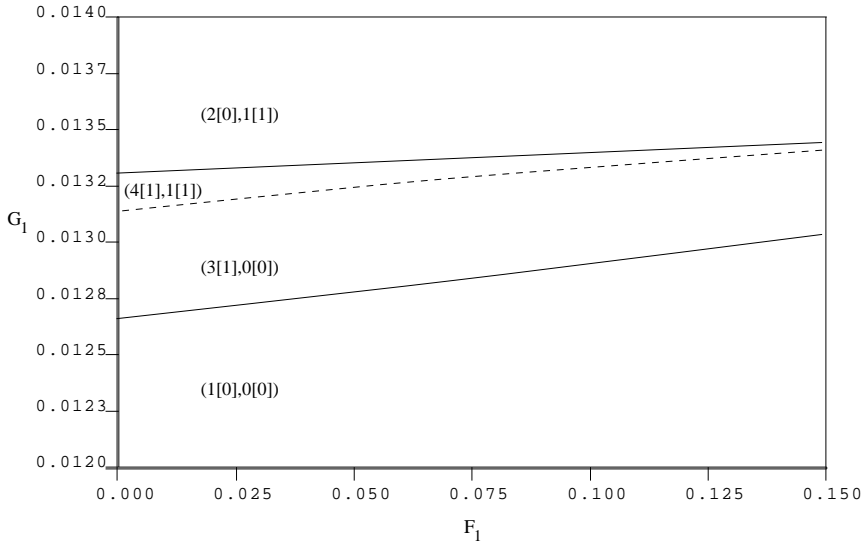


FIGURE 3. Saddle node bifurcations (solid lines) and the bifurcation at  $f = 0$ , given by (5) (dashed line). Between brackets the number of equilibria with  $f > 0$  and  $f < 0$ , respectively. Between square brackets the corresponding number of *stable* equilibria.

only in a small window in parameter space there exists a stable equilibrium with positive flow. Other stable solutions with positive flow are periodic or chaotic.

## 7. Chaotic attractors

As mentioned in section (5), the coupled model can be regarded as a perturbation of the Lorenz-84 model. The parameters  $F_0$  and  $G_0$  of the uncoupled Lorenz-84 model have been chosen in a fully chaotic regime. Therefore, we cannot expect a complete insight in the bifurcations and the behaviour of the coupled model as a function of the coupling parameters. Still, through a combination of time integrations and bifurcation analysis, we can clarify our model's dynamics to a large extent.

It is found that for many parameter values the behaviour is chaotic. Using the algorithm described by Wolf et al. [1985] we can approximate the Kaplan-Yorke dimension of the chaotic attractors. We can also numerically estimate their correlation dimension. A description of the algorithms and a discussion of the physical interpretation of these dimensions can be found in Nayfeh and Balachandran [1995].

For several parameter values the Kaplan-Yorke dimension is found to be about 4.3, compared to the typical value of about 2.4 for the uncoupled Lorenz-84 model. The Kaplan-Yorke dimension, however, only characterises the geometry of the attractor. Even though the Kaplan-Yorke dimension is increased by 1.9, there might be little variability in the oceanic variables. In order to see if the ocean model plays

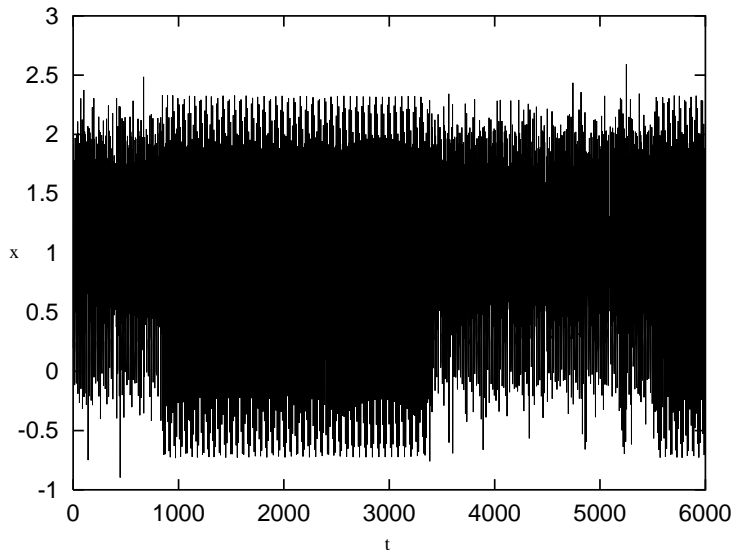


FIGURE 4. Intermittent time series  $x(t)$  at parameter values  $(F_1, G_1) = (0.021685, 0.01)$ .

an important role, we can calculate the correlation dimension. This quantity is calculated from an orbit on the chaotic attractor, sampled at equal time intervals. If there is a lower dimensional subset of the attractor which is visited relatively often, the correlation dimension will be smaller than the Kaplan-Yorke dimension. This is an indication that the Kaplan-Yorke dimension overestimates the variability of the system.

Indeed, for the uncoupled Lorenz model the correlation dimension is typically about 2.3 [Anastassiades, 1995], compared to  $3.4 \pm 0.2$  for the coupled model. The difference in correlation dimension is significantly smaller than the difference in Kaplan-Yorke dimension. We conclude that the attractor of the coupled system is much more inhomogeneous than that of the Lorenz-84 system.

The ocean is passive in the chaotic regime. The qualitative behaviour of the atmospheric variables is similar to the uncoupled behaviour and the inhomogeneity of the attractor shows that there is little variability in the oceanic variables. In the following we describe a regime in parameter space in which the ocean is manifestly active, as it dictates the qualitative behaviour of the system.

## 8. Intermittency

Inbetween fully chaotic and stable periodic regions in parameter space, intermittency can be observed. In figure (4) an example of an intermittent time series of system (3) is shown. On some time intervals the curve looks chaotic, on the other time intervals it looks periodic. This behaviour occurs near a bifurcation point at which a periodic orbit loses its stability. The systematic study of this phenomenon

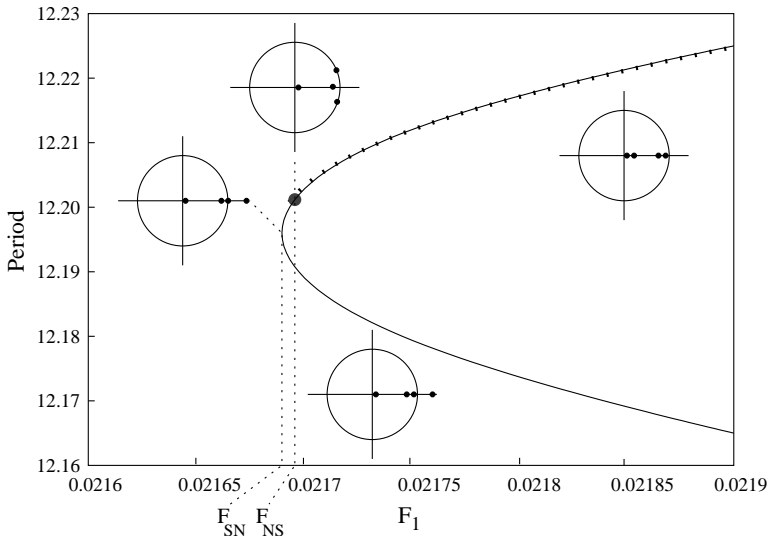


FIGURE 5. Continuation of the periodic solution approached during the periodic interval in (4). The Floquet multipliers are drawn in the complex plane. The bifurcation points are indicated by SN for saddle node and NS for Neimark-Sacker. This picture was obtained applying the algorithm described in Simó [1989]. The stable branch has been marked with dots.

in dynamical systems was initiated by Pomeau and Manneville [1980]. Here, we describe the underlying bifurcation structure.

Note, that the phenomenon of intermittency is not restricted to alternating periodic and chaotic motion in low-order models. It is also found in models with multiplicative noise [Shapiro, 1993] or additive noise [Eckmann et al., 1981]. Furthermore, in so called cycling chaos [Dellnitz et al., 1995] two, or more, chaotic sets are involved, instead of a chaotic set and a periodic orbit. Our case, described below, is called type II intermittency [Pomeau and Manneville, 1980].

**8.1. The theory of intermittency.** In order to explain the intermittent behaviour and the role of the slow, oceanic, variables in detail we did a numerical bifurcation analysis of the relevant periodic orbit. This was done following the algorithm described in Simó [1989]. An approximation of the periodic orbit can be obtained from a time series such as the one shown in figure (4). This orbit is then followed in one parameter by a prediction-correction method. Generically the periodic orbit will undergo saddle node, period doubling and Neimark-Sacker bifurcations, at which its stability properties change [see, e.g. Wiggins, 1990, chapter 3].

The result of this analysis is shown in figure (5). At the saddle node bifurcation (SN) two periodic orbits come into existence. Initially both are unstable. Increasing parameter  $F_1$  slightly, the upper branch passes through a Neimark-Sacker bifurcation (NS), after which all Floquet multipliers lie within the unit circle, indicating that the periodic orbit is stable. Beyond this point, for  $F_1 > F_{NS}$ , periodic motion sets

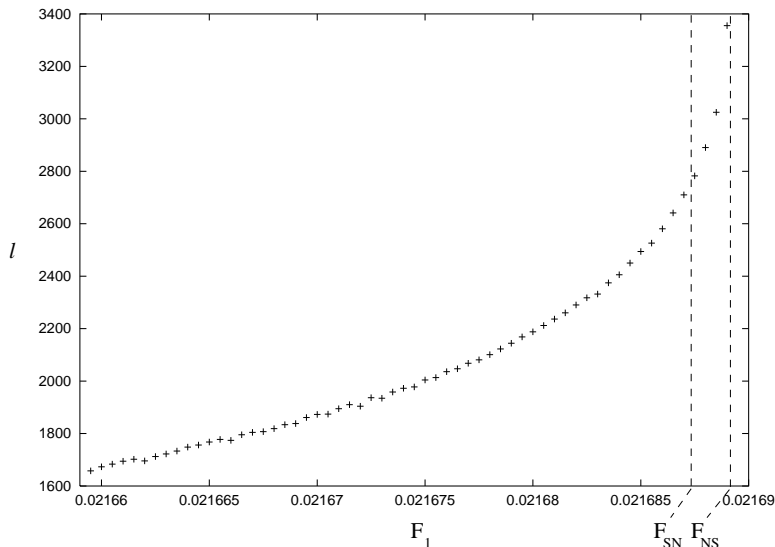


FIGURE 6. The expectation value  $l$  of the length of the periodic intervals as a function of  $F_1$  for  $G_1 = 0.01$ . The integration time for each measurement was  $\Delta t = 5 \cdot 10^6 \approx 9.6 \cdot 10^4$ yr. The bifurcation points of figure (5) have been labelled  $F_{SN}$  and  $F_{NS}$ .

in. For  $F_{SN} < F_1 < F_{NS}$  there is no stable periodic orbit for the system to settle on. Instead the periodic orbit has a stable and an unstable manifold attached to it [see Wiggins, 1990, chapter 1]. The solution of system (3.1)-(3.5) approaches the periodic orbit closely following the stable manifold, and moves away from it closely following the unstable manifold. This is what happens during a periodic interval. Sufficiently far away from the unstable periodic orbit in phase space, the solution wanders about chaotically until it comes close to the stable manifold again and the cycle repeats.

The intermittent behaviour persists to the left of the saddle node point, i.e. for  $F_1 < F_{SN}$ . This is because both the saddle node and the Neimark-Sacker bifurcation are local, meaning that some distance away from the bifurcating orbit in phase space, the vector field remains essentially the same. Although the periodic orbits have collided and disappeared, their ‘ghosts’ still influence the dynamics.

The farther left of the saddle node point parameter  $F_1$  is chosen, the less the influence of the ghost structure. This can be quantified by measuring the length of the periodic intervals, or rather its distribution, for a number of parameter values. To obtain these data, integrations of  $5 \times 10^6$  in units of  $t$  (about  $9.6 \times 10^4$  years) were done, during which more than 600 periodic intervals were registered for each parameter value. The length of the periodic intervals in each integration run is approximately normally distributed. In figure (6), the expectation value  $l$  has been plotted against parameter  $F_1$ . Beyond the Neimark-Sacker bifurcation, for  $F_1 > F_{NS}$ , the periodic behaviour is stable and therefore  $l$  diverges. The rate

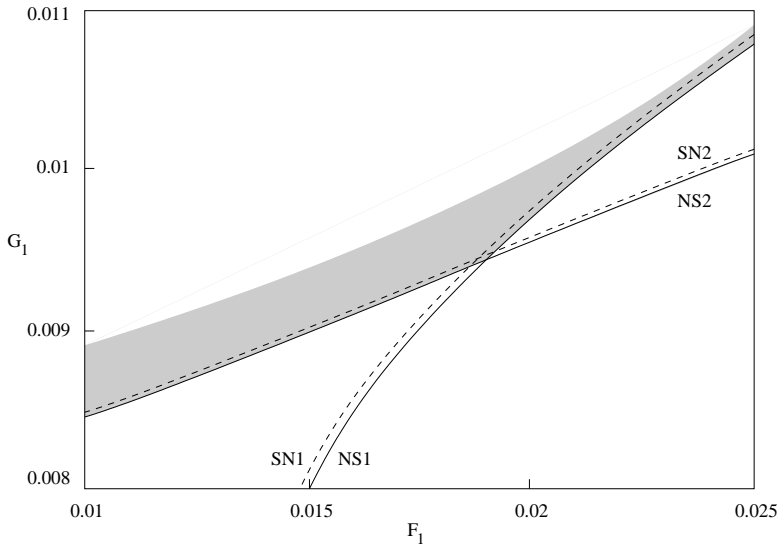


FIGURE 7. Two parameter continuation of the bifurcations described in section (8). The saddle-node lines are dashed and the Neimark-Sacker lines are solid. In the shaded region intermittency takes place. Directly to the right of NS1 and below NS2 the behaviour is periodic.

of divergence was numerically estimated by Pomeau and Manneville [1980]. They found the power law  $l \propto \epsilon^{-\alpha}$ , where  $\epsilon$  is the distance to the bifurcation point, in our case  $F_{NS} - F_1$ , and  $\alpha \approx 0.04$ . In our experiments we find  $\alpha \approx 0.06$ , in reasonable agreement.

The Neimark-Sacker bifurcation, at which the behaviour becomes periodic, can be continued in two parameters in order to find a window in parameter space in which intermittency takes place. Such a window is shown in figure (7). The saddle-node and Neimark-Sacker bifurcations of figure (5) have been labeled SN1 and NS1, respectively. At SN2 another periodic orbit becomes stable, following the same scenario as described above. Directly to the right of NS1 and below NS2 the behaviour is periodic. In the shaded region the behaviour is intermittent.

**8.2. The driven Lorenz-84 model.** In order to study the behaviour of the slow variables,  $T$  and  $S$ , in the intermittent regime, we made a Poincaré plot of the coupled system. The plane of intersection in phase space is defined as  $\mathcal{S}_x = \{(x, y, z, T, S) \in \mathbb{R}^5 | x = 1\}$ . In figure (8) the intersection points are shown, projected onto the  $T, S$ -plane. The intersections of the unstable periodic orbit with  $\mathcal{S}$  have been marked with crosses. The arrows indicate the direction of the flow in  $\mathcal{S}_x$  near the intersections of the unstable periodic orbit. The qualitative behaviour, as described above, is neatly illustrated. On the left hand side of the picture the solution of equations (3) approaches the periodic solution, closely following its stable manifold. This happens during a periodic interval. At the top of the picture the solution moves away from the periodic solution closely following the unstable



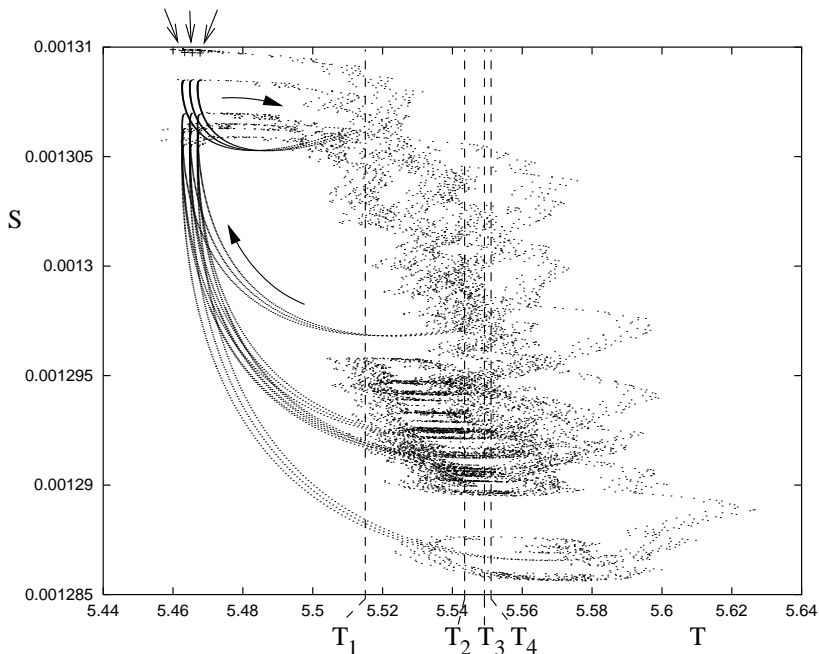


FIGURE 8. Poincaré section  $S_x$ , at  $(F_1, G_1) = (0.021685, 0.01)$ : projection onto the  $(T, S)$ -plane. The intersections of the unstable periodic solution with  $S_x$  have been marked with crosses in the top-left corner. The solid arrows indicate the direction of the flow.  $T_{1,2,3,4}$  denote the period doubling bifurcations of the driven Lorenz-84 model.

manifold. The average values of  $T$  and  $S$  clearly differ between the periodic and the chaotic intervals.

It seems natural to study the uncoupled Lorenz-84 model (1.1)-(1.3) with the effective parameters  $F = F_0 + F_{int}T_{eff}$  and  $G = G_0 + G_{int}(T_{av} - T_{eff})$ , where  $F_{int}$  and  $G_{int}$  are coupling parameters for which we observe intermittency. The effective temperature contrast  $T_{eff}$  can be taken fixed, which would correspond to the limit of  $\epsilon_2 \downarrow 0$  in section (5), or slowly varying. A bifurcation analysis of the Lorenz-84 model with these effective parameters, and  $T_{eff}$  as the bifurcation parameter, yields an alternative explanation of the intermittency.

If we set  $T_{eff}$  equal to the average value of  $T$  during a periodic interval, we find a stable periodic orbit in the uncoupled Lorenz-84 model. This orbit is strongly attracting and the transient time from an arbitrary initial condition is short. If we let  $T_{eff}$  vary on the time scale of the ocean model, as a second approximation to the coupled system, this orbit persists.

If we continue the attracting orbit to higher values of  $T_{eff}$  it undergoes a period doubling cascade, resulting in chaotic behaviour. The first four period doublings have been marked  $T_{1,2,3,4}$  in figure (8). At these period doublings, weakly attracting orbits of high period are created. The transient time from an arbitrary initial condition

is rather long. Therefore, these orbits do not persist in the second approximation, with a slowly varying  $T_{eff}$ . In the second approximation the behaviour is chaotic beyond the first period doubling.

To the right of the culmination point of the period doubling cascade, close to  $T_4$ , the behaviour is chaotic with fixed or slowly varying  $T_{eff}$ . If  $T_{eff}$  follows the behaviour of  $T$  during the intermittency, it repeatedly drives the Lorenz-84 model through the period doubling bifurcations, into the chaotic region, and back to the periodic region. This gives an intuitive picture of the intermittent behaviour.

### 9. Power spectra in the passive and the active regime

An illustrative way to show the influence of the active ocean component on the coupled dynamics is to look at power spectra. In figure (9) the power spectrum of the atmospheric variable  $x$ , averaged over  $t_{av} = 15 \approx 3$  months, is shown. The data have been taken from integrations spanning some  $7.7 \cdot 10^3$  yrs. The top picture shows the spectrum in the passive, chaotic, regime at parameter values  $(F_1, G_1) = (0.02, 0.01)$ . The bottom picture, on the same scale, shows the spectrum in the active, intermittent, regime, at parameter values  $(F_1, G_1) = (0.021685, 0.01)$ . The three sharp peaks on the left are caused by the periodic intervals. Compared to the spectrum in the passive regime, a lot of energy is present in low frequency modes, associated with the recurrence of periodic intervals. These are modes on the thermal damping time scale of the ocean model.

### 10. Conclusion and discussion

The behaviour of the coupled model has been studied as a function of the coupling parameters in the atmosphere model. A bifurcation analysis of the equilibrium states reveals that, for a range of parameter values, there exists a stable equilibrium which describes a salinity driven THC. This property is inherited from the uncoupled ocean box-model. Other attractors of the coupled model are chaotic or periodic. Depending on small changes in the coupling parameters, the ocean can be passive or active.

The passive behaviour occurs if the coupled model is fully chaotic. Here, the ocean basically integrates the atmospheric forcing. As illustrated by comparing attractor dimensions of the coupled model to those of the Lorenz-84 model, there is not much variability in the oceanic variables in this case.

Active behaviour is found near a bifurcation of the coupled system. On one side of this bifurcation the behaviour is periodic, on the other side it is intermittent. In the intermittent regime the slow time scale of the ocean model plays an important role in the dynamics, as illustrated by the power spectrum of the atmospheric variables. This can be explained from the theory of intermittency, and the motion along the stable and unstable manifolds of the periodic orbit. Alternatively, the intermittency can be described as the behaviour of the Lorenz-84 model with slowly varying, effective parameters. The effective parameters vary on the time scale of the ocean model and repeatedly push the Lorenz-84 model through a sequence of bifurcations at which the stability of periodic motion is lost.

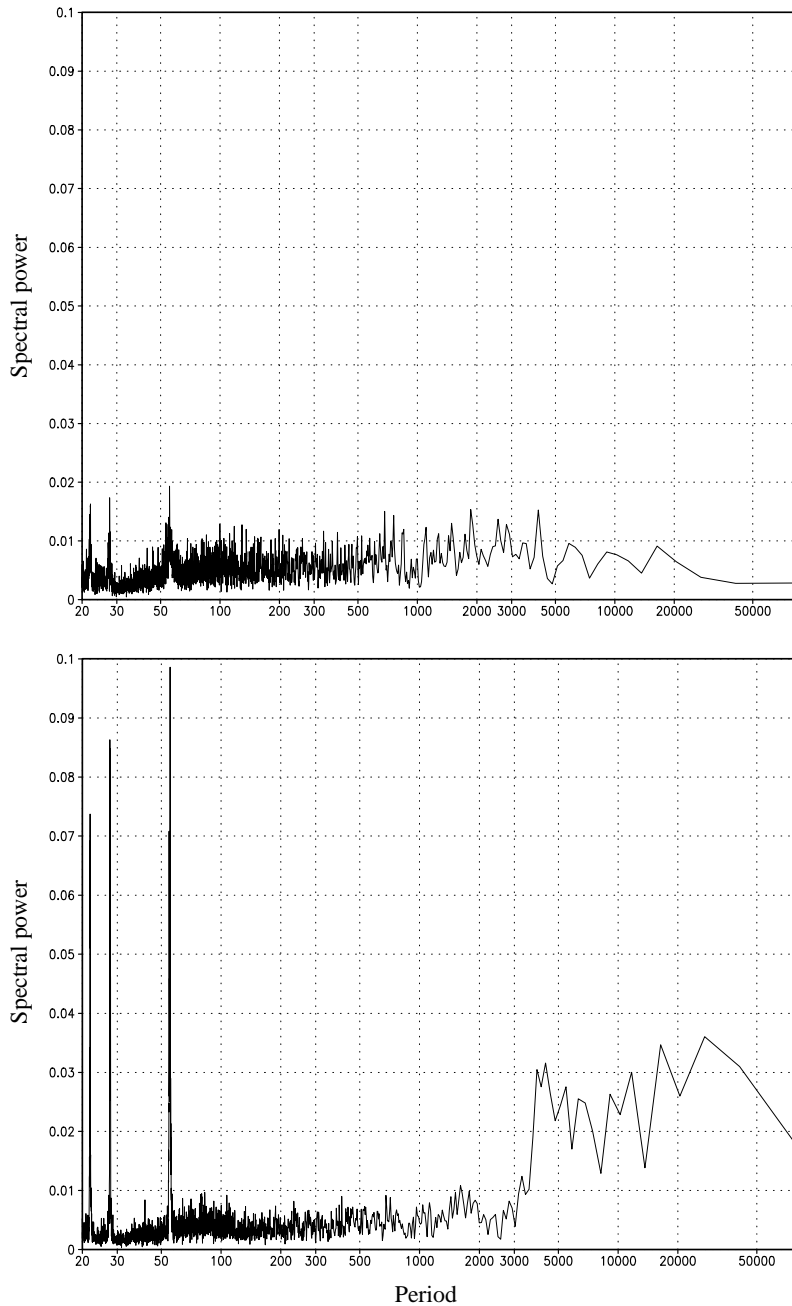


FIGURE 9. Power spectra of  $x(t)$  in the passive ocean (chaotic) regime (top) and the active ocean (intermittent) regime (bottom). Period in weeks (see section (4)).

In order to make a connection to more realistic climate models, two points should be made clear. First of all, stable equilibria or periodic orbits are not commonly found in the state space of realistic, high resolution, models. The invariant structures in high dimensional state spaces are usually much more complicated. A useful analogy is provided by the method of Probability Density Functions [PDF's, see Molteni et al., 1990, and references therein]. Figure (8) is the analogue of a bimodal PDF, with one regime near the saddle type periodic orbit (upper left corner) and one chaotic regime (bottom right corner). In fact, applying the method of PDF's for intermittent parameter values would yield such a bimodal distribution. The expectation value of the length of the periodic intervals, plotted in figure (6), then measures the residence time in the regimes. In this context, the intermittency can be regarded as itinerancy, switching back and forth between climate regimes. The time scale of motion within each of the regimes is set by the fast, atmospheric, component of the model while the time scale of migration between the regimes is set by the slow, oceanic component.

Itinerancy and the related notion of quasi-stationary states [see, e.g. Marshall and Molteni, 1993], have been proposed as a possible mechanism generating low frequency variability. Itoh and Kimoto [1996] found evidence for itinerancy in an atmosphere model up to fairly high resolution (T21). In their case the transitions between regimes are noise-induced, as described in De Swart and Grasman [1987], and describe internal low-frequency variability of the atmosphere. Schopf and Suarez [1988] found vacillation in a coupled model, generating variability on a time scale of years, related to the transit time of traveling waves in the ocean models rectangular domain. In our case, the long time scale is set by fluctuations in the THC, generating decadal variability.

The second point is that, in our model, the coupling of the ocean to the atmosphere is on a conceptual level and depends only on two parameters. In reality, the ocean-atmosphere feedback is highly complex, which results in a large amount of parameterisations in realistic models. This makes it very hard to identify the relevant parameters for a sensitivity experiment. The goal of such an experiment would be to find transitions from unimodal to multimodal PDF's, analogous to the bifurcation scheme presented in section (8.1). Alternatively, an experiment in the fashion of section (8.2) might be conducted, in which the dependence of the atmospheric PDF on prescribed Sea Surface Temperature (SST) patterns is tested.

In classical studies such as Palmer and Sun [1985], the response of the atmospheric circulation to SST anomalies is measured in terms of time mean quantities. However, in order to detect a qualitative change in behaviour, namely a crossover to another regime, it may be necessary to extract more information, in the form of PDF's. In the experiment we propose, the atmospheric PDF, projected onto a few relevant indicators, should be measured as a function of the amplitude of a typical SST anomaly pattern. Relevant indicators can be, for instance, the amplitudes of the leading empirical orthogonal functions of surface pressure. If a qualitative change in the PDF is detected at a reasonable amplitude of the SST anomaly forcing, this indicates that the atmosphere is sensitive to oceanic feedback. Whether or not itinerancy, and the associated variability on oceanic time scales, will be found

in a subsequent coupled integration depends on the forcing of the ocean by the atmosphere in the preferred flow regimes. If, in an ocean only run, driven by one of the centroids of the atmospheric PDF, the amplitude of the SST anomaly is driven through its critical value, the feedback loop is complete and itinerancy can occur in a fully coupled integration.

Evidence for sensitivity of the atmospheric PDF to SST anomalies was found in Selten et al. [1999]. In an atmosphere only run they found that a North Atlantic Oscillation (NAO) related SST anomaly induced a preference for one sign of the model's NAO pattern. Also, Kharin [1995] showed that SST can have a nonlinear effect on the atmospheric circulation.

The discussion about the active or passive role of the ocean in coupled climate models and in the real climate systems is still going on [for a review, see Latif, 1997]. We think, that the description of intermittent behaviour in a low-order climate model and the analogy to itinerancy in realistic models gives a possible explanation for the different results in recent literature. An experiment as proposed above might reveal that active and passive ocean behaviour can occur in one model at different parameter values. Recent sensitivity studies, such as performed by Rahmstorf and Ganopolsky [1999], indicate that at critical values of coupling parameters major climatic changes can occur. It is at such critical points that coupling of the atmosphere to other components of the climate system can be crucial.

## 11. Acknowledgments

Part of the work by the first author (section (8)) was done at the Department of Applied Mathematics and Analysis of the University of Barcelona. The hospitality and helpfulness of Carles Simó and the dynamical systems group is gratefully acknowledged. Contributions were also made by F.A. Bakker, G. Zondervan, F.M. Selten and R.J. Haarsma at the KNMI. This work is part of the NWO project 'a conceptual approach to climate variability' (nr. 61-620-367).



## Bibliography

- Anastassiades, L. [1995] “Numerical studies on the Lorenz-84 atmosphere model,” Report wr 95-05, KNMI, de Bilt, Netherlands.
- De Swart, H. E. & Grasman, J. [1987] “Effect of stochastic perturbations on a low-order spectral model of the atmospheric circulation,” *Tellus* **39A**, 10–24.
- Dellnitz, M., Field, M., Golubitsky, M., Ma, J. & Hohmann, A. [1995] “Cycling chaos,” *Int. J. of Bifurcation and Chaos* **5**, 1243–1247.
- Doedel, E., Champneys, A., Fairgrieve, T., Kuznetsov, Yu. A., Sandstede, B. & Wang, X.J. [1986] *AUTO97: Continuation and bifurcation software for ordinary differential equations (with HomCont)* Computer Science, Concordia University, Montreal, Canada.
- Eckmann, J-P., Thomas, L. & Wittwer, P. [1981] “Intermittency in the presence of noise,” *J. Phys. A: Math. Gen.* **14**, 3153–3168.
- Frankignoul, C., Kestenare, E., Sennéchaël, N., de Coëtlogon, G. & D’Andrea, F. [2000] “On decadal-scale ocean-atmosphere interactions in the extended ECHAM1/LSG climate simulation,” *Climate Dynamics* **16**, 333–354.
- Grötzner, A., Latif, M. & Barnett, T. P. [1998] “A decadal climate cycle in the North Atlantic ocean as simulated by the ECHO coupled GCM,” *J. of Climate* **11**, 831–847.
- Itoh, H. & Kimoto, M. [1996] “Multiple attractors and chaotic itinerancy in a quasi-geostrophic model with realistic topography: implications for weather regimes and low-frequency variability,” *J. Atmos. Sci.* **53**, 2217–2231.
- Kharin, V. V. [1995] “The relationship between sea surface temperature anomalies and atmospheric circulation in GCM experiments,” *Climate Dynamics* **11**, 359–375.
- Latif, M. [1997] “Dynamics of interdecadal variability in coupled ocean-atmosphere models,” *J. of Climate* **11**, 602–624.
- Latif, M. & Barnett, T. P. [1994] “Causes of decadal climate variability over the North Pacific and North America,” *Science* **266**, 634–637.
- Lorenz, E. N. [1984] “Irregularity: a fundamental property of the atmosphere,” *Tellus* **36A**, 98–110.
- Lorenz, E.N. [1990] “Can chaos and intransitivity lead to interannual variability?,” *Tellus* **42A**, 378–389.
- Maas, L. R. M. [1994] “A simple model for the three-dimensional, thermally and wind-driven ocean circulation,” *Tellus* **46A**, 671–680.

- Marshall, J. & Molteni, F. [1993] "Toward a dynamical understanding of planetary-scale flow regimes," *J. Atmos. Sci.* **50**, 1792–1818.
- Masoller, C., Schifano, A. C. S. & Romanelli, L. [1995] "Characterization of strange attractors of the Lorenz model of general circulation of the atmosphere," *Chaos, Solitons & Fractals* **6**, 357–366.
- Molteni, F., Tibaldi, S. & Palmer, T. N. [1990] "Regimes in wintertime circulation over northern extratropics I: Observational evidence," *Q. J. R. Meteorol. Soc.* **116**, 31–67.
- Nayfeh, A. H. & Balachandran, B. [1995] *Applied nonlinear dynamics* (Wiley).
- Palmer, T. N. & Sun, Z. [1985] "A modelling and observational study of the relationship between sea surface temperature in the north-west Atlantic and the atmospheric general circulation," *Q. J. R. Meteorol. Soc.* **111**, 947–975.
- Pomeau, Y. & Manneville, P. [1980] "Intermittent transition to turbulence in dissipative dynamical systems," *Commun. Math. Phys.* **74**, 189–197.
- Rahmstorf, S. & Ganopolsky, A. [1999] "Long term global warming scenarios computed with an efficient coupled climate model," *Climatic Change* **43**, 353–367.
- Roebber, P. J. [1995] "Climate variability in a low-order coupled atmosphere-ocean model," *Tellus* **47A**, 473–494.
- Saravanan, R. & Mc Williams, J. [1997] "Stochasticity and spatial resonance in interdecadal climate fluctuations," *J. of Climate* **10**, 2299–2320.
- Schopf, P. S. & Suarez, M. J. [1988] "Vacillations in a coupled ocean-atmosphere model," *J. Atmos. Sci.* **45**, 549–568.
- Selten, F. M., Haarsma, R. J. & Opsteegh, J. D. [1999] "On the mechanism of North Atlantic decadal variability," *J. of Climate* **12**, 1956–1973.
- Shapiro, V. E. [1993] "Systems near a critical point under multiplicative noise and the concept of effective potential," *Phys. Rev. E* **48**, 109–120.
- Shilnikov, A., Nicolis, G. & Nicolis, C. [1995] "Bifurcation and predictability analysis of a low-order atmospheric circulation model," *Int. J. of Bifurcation and Chaos* **5**, 1701–1711.
- Sicardi, A. C. & Masoller, C. [1996] "Analytical study of the codimension two bifurcation of the new Lorenz system," *Instabilities and Nonequilibrium Structures V*, 345–348.
- Simó, C. [1989] *On the analytical and numerical approximation of invariant manifolds*, chapter in *Les Méthodes Modernes de la Mécanique Céleste*, ed. Benest, D. and Froeschlé, C., pp 285–329 Goutelas.
- Stommel, H. [1961] "Thermohaline convection with two stable regimes of flow," *Tellus* **13**, 224–230.
- Verhulst, F. [1996] *Nonlinear differential equations and dynamical systems* (Springer Verlag).
- Wiggins, S. [1990] *Introduction to applied nonlinear dynamical systems and chaos* (Springer-Verlag).
- Wiggins, S. [1994] *Normally hyperbolic invariant manifolds in dynamical systems* (Springer Verlag).
- Wolf, A, Swift, J. B., Swinney, H. L. & Vastano, J. A. [1985] "Determining Lyapunov exponents from a time series," *Physica D* **16**, 285–317.



# Overturning and wind driven circulation in a low-order ocean-atmosphere model

Submitted to *Dyn. Atmos. Oceans*.

ABSTRACT. A low-order ocean-atmosphere model is presented which combines coupling through heat exchange at the interface and wind stress forcing. The coupling terms are derived from the boundary conditions and the forcing terms of the constituents. Both the ocean and the atmosphere model are based on Galerkin truncations of the basic fluid dynamical equations. Hence, the coupled model can readily be extended to include more physics and more detail. The model presented here is the simplest of a hierarchy of low-order ocean-atmosphere models. The behaviour of the coupled model is investigated by means of geometric singular perturbation theory and bifurcation analysis. Two ways are found in which the slow time scales can play a role in the coupled dynamics. In the first scenario, a limit cycle on the overturning time scale is created. The associated oscillatory behaviour is governed by internal ocean dynamics. In the second scenario intermittent behaviour occurs between periodic and chaotic regimes in parameter space.

## 1. Introduction

Until recently, the study of ocean models of low order has been restricted to a rather conceptual level. A variety of models have been constructed using the idea of Stommel [1961], dividing the ocean, or rather a meridional plane, into compartments. Within each compartment, the temperature and salinity of the sea water are constant and the flux of these quantities is based on diffusion-like dynamics. Such models are used to investigate the stability of the overturning circulation. Coexisting equilibria then represent different orientations of the overturning. Extensions of Stommel's model have been constructed to allow for oscillatory behaviour [Welander, 1982; Titz et al., 2002] and to mimic wind driven circulation [Huang and Stommel, 1992]. Low-order climate models usually rely on Stommel type ocean models, such as in Nakamura et al. [1994]; Roebber [1995]; van Veen et al. [2001]. Distinct disadvantages of such models are that they cannot be derived from the physical equations by means of Galerkin truncation and they cannot include rotation.

The wind driven circulation has also been investigated by means of low-order models. Veronis [1963], for instance, studied multiple equilibria and oscillatory behaviour in a model with four degrees of freedom. His findings were validated by comparison to a model of intermediate complexity [Jerley and Sheremet, 1995]. In

that work the two dimensional Navier-Stokes equations govern the flow. Consequently the overturning circulation is absent.

The Maas [1994] model, in contrast, allows for the study of both overturning and wind driven circulation in a low-order setting. Also, its formulation in terms of a Galerkin truncation of the angular momentum and density fields links it directly to the governing fluid dynamical equations.

We couple the angular momentum based ocean model to the Lorenz-84 model for the atmosphere. As shown in van Veen [2002], the latter model approximates the dynamics of a baroclinic atmosphere model. The physical processes thus represented in the coupled model are thermally induced overturning, wind driven gyre circulation and, in the atmosphere, baroclinic wave activity.

The aim of this paper is twofold: firstly to describe the scaling and the coupling of the model in some detail and secondly to explore the dynamics of the coupled system by means of perturbation theory and bifurcation analysis.

In section (2) the ocean-atmosphere interaction terms are calculated from the surface integrals which appear in the ocean's boundary conditions and the atmosphere's forcing terms. The difference in time scales between the wind driven, the overturning and the atmospheric dynamics, as well as the coupling strengths, follow from the physically relevant scaling. The coupled model, presented here, is in a sense the simplest of a family of low-order ocean-atmosphere models. In the concluding section a number of possible extensions is listed.

In section (3), we explore the behaviour of the model by means of Fenichel theory, or, more specifically, Geometric Singular Perturbation (GSP) theory. A bifurcation analysis is conducted in section (4). In this analysis, the focus is on the question how the slow dynamics of the ocean model can show up in the dynamics of the coupled model.

GSP theory is applied in the regime where the atmosphere is in an equilibrium state. In this case, no instabilities are excited in the ocean model, except when the atmosphere's equilibrium is nearly critical. In that case, a Hopf bifurcation can occur which produces a weakly unstable cycle on the overturning time scale. The occurrence of this Hopf bifurcation is connected to the presence of a Bogdanov-Takens point at nearby parameter values. The unfolding of this point and the consequences for the coupled dynamics are discussed in section (4.1). The oscillatory behaviour induced by the cycle is generated by internal ocean dynamics.

A window in parameter space is shown to exist where the behaviour is chaotic, with tiny periodic intervals. In the fully chaotic regime the climatology of the model is studied. The physical processes represented in the model are simulated to reasonable accuracy. Near the boundary of stable periodic motion, intermittency can occur. Here, the slow subsystem, i.e. the ocean, can cause the fast subsystem, i.e. the atmosphere, to pass through a sequence of bifurcations repeatedly. This phenomenon was already observed in the Lorenz-Stommel model [van Veen, 2002]. Thus, the slow time scale shows up in the transition time between regimes of qualitatively different behaviour. This is a second way for the slow dynamics to influence the behaviour of the coupled system.

To the author's knowledge, no low-order ocean-atmosphere model which combines wind driven and overturning circulation has been studied before. The model analysis presented here is far from exhaustive. The presence of small parameters in the model suggests the use of perturbation theory, also in the regime where the atmosphere is not in equilibrium. Such a perturbation theory involves averaging over the fast time scale [Rödenbeck et al., 2001]. In future research, this technique will be applied to the Lorenz-Maas model [Arnold and Olbers, 2002]. Also, the coupled system might be compared to the Maas model with stochastic forcing [Monahan, 2001]. The computation of Lyapunov exponents and attractor dimensions might reveal to what extent chaotic, deterministic forcing is different from forcing by noise.

## 2. Description of the model

The ocean model was formulated in Maas [1994, 2002]. The atmosphere model is due to Lorenz [1984] and was provided with a physical basis in van Veen [2002]. Here, we will show how the coupling terms and multiple time scales are introduced.

**2.1. Scaling of the low order models.** The ocean model is valid in a rectangular domain with width and length  $L$  and height  $H$ . This basin is assumed to have a rigid lid. We choose Cartesian coordinates about the basin's geometric centre. The fluid motion is governed by the Navier-Stokes equations in the Boussinesq approximation on an  $f$ -plane. It is described by the basin averaged angular momentum and the linear variations of the density field,  $\rho$ , defined respectively as

$$\mathbf{L} = \frac{1}{V} \int \mathbf{x} \times \mathbf{u} dV \quad \rho_x = \frac{\int x \rho dV}{\int x^2 dV} \quad \rho_y = \frac{\int y \rho dV}{\int y^2 dV} \quad \rho_z = \frac{\int z \rho dV}{\int z^2 dV} \quad (1)$$

Here  $V = L^2 H$  is the volume of the domain,  $\mathbf{u}$  is the velocity of the fluid and the density field is defined as  $\rho = (\rho_* - \rho_0) / \delta\rho$ , i.e. the difference between the dimensional field,  $\rho_*$  and a constant reference field,  $\rho_0$ , scaled by a typical fluctuation,  $\delta\rho$ . The salinity of the ocean is not taken into account, so that the density is determined by the temperature alone. We define the non-dimensional temperature by  $T = \alpha(T_* - T_0) / \delta\rho$ , where  $\alpha$  is the thermal expansion coefficient. Thus, we have

$$\rho = x\rho_x + y\rho_y + z\rho_z \quad \text{and} \quad T = -\rho. \quad (2)$$

In this approximation the model has six degrees of freedom. In a scaling appropriate for overturning dynamics, however, we see that the inertia of the horizontal angular momentum can be neglected.

The dynamical equations for  $\mathbf{L}$  and  $\rho_{x,y,z}$  are

$$\frac{d}{dt}\mathbf{L} = -\frac{f}{2}\mathbf{k} \times \mathbf{L} + \frac{H^2 g \delta \rho}{12 \rho_0} (-\rho_y \mathbf{i} + \rho_x \mathbf{j}) - (r_h L_1, r_h L_2, r_v L_3)^T + \mathbf{T} \quad (3.1)$$

$$\frac{L^2}{12} \frac{d}{dt} \rho_x = -\frac{1}{2} L_3 \rho_y + \frac{1}{2} L_2 \rho_z - K_h \rho_x + F^{(x)} \quad (3.2)$$

$$\frac{L^2}{12} \frac{d}{dt} \rho_y = -\frac{1}{2} L_1 \rho_z + \frac{1}{2} L_3 \rho_x - K_h \rho_y + F^{(y)} \quad (3.3)$$

$$\frac{H^2}{12} \frac{d}{dt} \rho_z = -\frac{1}{2} L_2 \rho_x + \frac{1}{2} L_1 \rho_y - K_v \rho_z + F^{(z)} \quad (3.4)$$

where  $\mathbf{i}, \mathbf{j}, \mathbf{k}$  are the unit vectors in the  $x, y$  and  $z$  direction,  $f$  is the Coriolis parameter,  $g$  is the acceleration of gravity,  $r_h$  and  $r_v$  are the horizontal and vertical Rayleigh damping coefficients and  $K_h$  and  $K_v$  are the horizontal and vertical eddy diffusivity constants. The forcing terms  $\mathbf{T}$  and  $\mathbf{F}$  stand for the wind stress torque and the buoyancy flux at the surface. In the following we will assume that  $F^{(x)} = F^{(z)} = 0$  and  $T_1 = T_2 = 0$ . The remaining forcing terms,  $F^{(y)}$  and  $T_3$  represent meridional differential heating and wind shear forcing, respectively.

The Cartesian coordinates will be scaled as  $[x, y, z] = [L, L, H]$ , and the density fluctuations as  $[\delta \rho] = [12 \rho_0 r_h K_h / g H]$ . The time scale of interest is different for the overturning, the wind driven and the atmospheric dynamics in the coupled model. As described below, this difference of time scales leads to the introduction of a small parameter in the model.

A typical time scale for the overturning dynamics, described by the horizontal components of the angular momentum,  $L_{1,2}$ , is given by  $\Sigma_1^{-1} = L^2 / K_h$ . Let  $t_1 = \Sigma_1 t$  and let primes denote non-dimensional quantities, then we find from equation (3.1) that

$$\begin{aligned} \frac{1}{Pr} \frac{d}{dt_1} L'_1 &= f' L'_2 - \delta \rho' \rho'_y - L'_1 \\ \frac{1}{Pr} \frac{d}{dt_1} L'_2 &= -f' L'_1 + \delta \rho' \rho'_x - L'_2 \end{aligned} \quad (4)$$

where  $f' = f/2r_h$  is the scaled Coriolis parameter and  $Pr = r_h L^2 / K_h$  is the Prandtl number. A realistic value of  $Pr$  is  $O(10^5)$ . Therefore, we consider the limit  $Pr \rightarrow \infty$ , obtaining

$$\begin{pmatrix} L'_1 \\ L'_2 \end{pmatrix} = \frac{\delta \rho'}{1 + f'^2} \begin{pmatrix} f' & -1 \\ 1 & f' \end{pmatrix} \begin{pmatrix} \rho'_x \\ \rho'_y \end{pmatrix} \quad (5)$$

The vertical component of the angular momentum is driven by wind shear forcing. Therefore, we introduce a second time scale, reasonable for the ocean's boundary layer. It is given by  $\Sigma_2^{-1} = r_v^{-1}$ . With  $L'_3 = L_3 / L^2 \Sigma_1$  and  $t_2 = \Sigma_2 t$  we have

$$\frac{d}{dt_2} L'_3 = -L'_3 + T'_3 \quad (6)$$

where  $T'_3 = T_3 / L^2 \Sigma_1 \Sigma_2$  is the dimensionless torque due to wind stress. Note, that we have scaled  $L_3$  by a factor  $\Sigma_1$  and its tendency by a factor  $\Sigma_2$ . This hybrid formulation is necessary to make up for the absence of an explicit boundary layer

in the model. The wind shear directly drives the basin averaged vertical angular momentum. In reality, the influence of the wind stress is manifest in a boundary layer of thickness  $h$ , and rapidly decreases below that. Therefore, we will include a factor of  $h/H$  in the forcing strength, as discussed below.

In order to get rid of the numerical factors in equations (3.2-4) we rescale  $t_1$  by a factor  $1/12$ ,  $\mathbf{u}$  by a factor 2 and set  $\delta\rho' = 2$ . Then, using relation (5) to eliminate  $L_{1,2}$ , we obtain

$$\frac{d}{dt_1}\rho'_x = -\rho'_y L'_3 + \frac{1}{1+f'^2}(\rho'_x + f'\rho'_y)\rho'_z - \rho'_x \quad (7.1)$$

$$\frac{d}{dt_1}\rho'_y = \rho'_x L'_3 - \frac{1}{1+f'^2}(f'\rho'_x - \rho'_y)\rho'_z - \rho'_y + F^{(y)'} \quad (7.2)$$

$$\frac{d}{dt_1}\rho'_z = -\rho'^2_x - \rho'^2_y - \mu\rho'_z \quad (7.3)$$

Where  $\mu = K_v L^2 / K_h H^2$ . The set of equations (6) and (7) forms the ocean model. It will be coupled to the atmosphere model through the wind stress torque,  $T_3$  and the differential heating term  $F^{(y)}$ . The coupling will be discussed in section (2.2)

The horizontal spatial scale of the atmosphere model is identical to that of the ocean model. The time scale of the Lorenz-84 model is set to  $\Sigma_3^{-1}$ , the damping time scale of baroclinic waves. The model's equations are

$$\dot{X} = -Y^2 - Z^2 - aX + aF \quad (8.1)$$

$$\dot{Y} = XY - bXZ - Y + G \quad (8.2)$$

$$\dot{Z} = bXY + XZ - Z \quad (8.3)$$

where  $F$  stands for forcing by differential heating in the meridional direction and  $G$  in the zonal direction, e.g. through land-sea contrast. The damping time scale of the zonally symmetric westerlies with respect to that of the baroclinic waves is set by  $a$  while  $b$  determines the strength of passive advection relative to the exchange of energy between the baroclinic waves and the westerlies, i.e. the jet stream.

As shown in van Veen [2002], equations (8.1-3) approximate the dynamics of a severe truncation of a quasi-geostrophic two layer model on an  $f$ -plane. The mean and shear streamfunctions,  $\Psi$  and  $\tau$ , consist of a zonally symmetric part, representing the jet stream, and a sinusoidal wave. They are related to  $X$ ,  $Y$  and  $Z$  through

$$\Psi' = -X \sin \pi y' + \sqrt{2} \cos \pi y' (Y \sin \pi x' + Z \cos \pi x') \quad (9.1)$$

$$\tau' = -X \sin \pi y' + \sqrt{2} \cos \pi y' (Z \sin \pi x' - Y \cos \pi x') \quad (9.2)$$

with  $\Psi'$  and  $\tau'$  in units  $[L^2 \Sigma_3]$  and  $(x', y') \in [-1, 1] \times [-1/2, 1/2]$ . The jet stream pattern is equivalent barotropic whereas the wave is optimally baroclinic. The mean potential temperature,  $\Theta$ , can be calculated from the shear stream function using the thermal wind relation. Let  $\Theta = \Theta_{av} + \theta$ , where  $\Theta_{av}$  is the average potential temperature over the whole domain, and  $\theta$  is the local departure. Then we have

$$\theta' = \tau' \quad (10)$$

with  $\theta'$  in units  $[\Theta] = [f\Sigma_3 L^2 / dc_p^a]$ . Here,  $c_p^a$  is the specific heat of dry air at constant pressure and the non-dimensional constant  $d = 0.124$  results from the vertical discretisation. The vertical gradient of potential temperature,  $\sigma$ , is kept constant. The feedback to the atmosphere will be represented by a modulation of the meridional heating gradient, induced by heat exchange at the ocean's surface.

**2.2. Coupling terms.** We consider two kinds of interaction between ocean and atmosphere: wind driven circulation and heat flux at the ocean's surface. The former interaction is represented by the forcing term  $T_3$  in equation (6) for the evolution of the vertical angular momentum. The latter is represented by a modification of the forcing terms representing differential heating in the meridional direction,  $F^{(y)}$  in equation (7.2) and  $F$  in equation (8.1). The effect of baroclinic waves in the atmosphere on the wind driven circulation is excluded, and so is the effect of the zonal gradient of heat exchange.

The angular momentum-based ocean model is capable of representing a single, wind driven gyre. We associate it with the larger, clockwise gyre in the Atlantic basin, south of the gulf stream. Under winter conditions, the centre of this gyre is located at about  $30^\circ N$ . The maximum of the jet stream intensity is located at about  $30^\circ N$  and 10km height. At the earth's surface, however, the maximum intensity of the zonal wind is located at about  $40^\circ N$  [Peixoto and Oort, 1992]. Therefore, it drives the ocean gyre in a clockwise direction.

The height dependence of the maximal intensity of the zonal wind is not resolved in the two layer model, nor is the atmospheric boundary layer. Therefore we pose a diagnostic relation to obtain the surface winds from the mean streamfunction, consistent with the observed climatology. As the zonally symmetric pattern, i.e. the jet stream, is equivalent barotropic, we include a scale factor,  $s$ , to tune the magnitude of the surface winds. The maximum of the zonal wind is displaced northward by a distance  $\Delta$ . This yields

$$\bar{U}'_s = -s \frac{\partial}{\partial y'} \bar{\Psi}'(x', y' - \Delta') = \pi s X \cos \pi(y' - \Delta') \quad (11)$$

where  $U_s$  is the zonal wind component at 10m height and bars denote zonal averages. This setup is sketched in figure (1). The easterlies along the southern lower boundary of the domain may be thought of as subtropical trade winds. From equation (11) we can calculate the wind stress,  $\tau_1$ , which in turn determines the forcing torque  $T_3$  in equation (6). The wind stress is related to the surface winds through

$$\tau_1 = \frac{\rho_a}{\rho_0} C_d U_* \bar{U}_s \quad (12)$$

where  $\rho_a$  is the atmospheric density,  $C_d$  is the non-dimensional drag coefficient and  $U_*$  is the typical (time and zonal average) magnitude of the zonal wind component at the surface.

The forcing due to the wind stress,  $\tau$ , is given by

$$T_3 = \frac{-1}{V} \iint y \tau_1 dx dy = -\frac{2}{\pi} \frac{\rho_a}{\rho_0} C_d s X U_*' \frac{L}{H} \Sigma_3^2 L^2 \sin \pi \Delta' \quad (13)$$

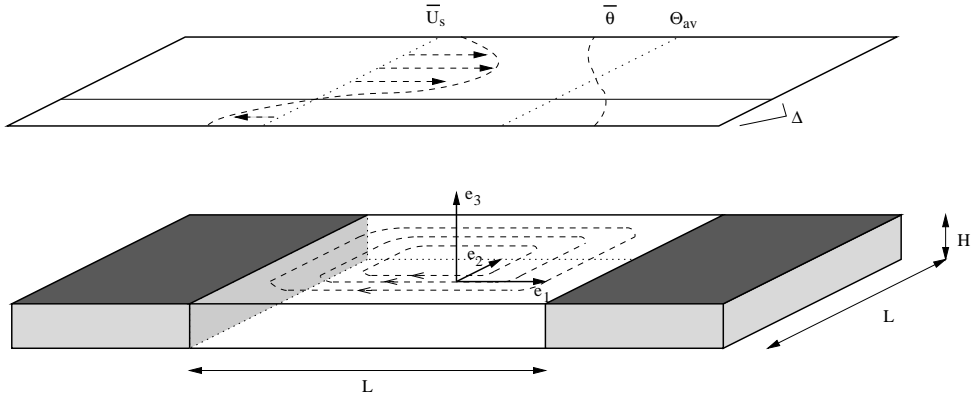


FIGURE 1. Sketch of the geometry of the coupled model. The centre of the jet stream is displaced northward by a distance  $\Delta$  with respect to the geometrical centre of the ocean basin. Thus, the zonally averaged zonal wind,  $\bar{U}$  drives a clockwise circulation in the ocean basin, indicated with dashed lines. Also shown is the profile of  $\bar{\theta}$ , the zonally averaged departure from the average potential temperature  $\Theta_{av}$ .

As explained in section (2.1), we need to include a factor of  $h/H$ , the relative depth of the mixed layer in the ocean, in the non-dimensional torque  $T'_3$ . The rescaling of  $\mathbf{u}$  introduces a factor of  $1/2$ . This finally results in

$$T'_3 = -\frac{1}{\pi} \frac{\rho_a}{\rho_0} C_{ds} X U_*' \frac{L}{H} \frac{\Sigma_3^2}{\Sigma_1 \Sigma_2} \frac{h}{H} \sin \pi \Delta' \quad (14)$$

The buoyancy forcing consists of a constant part,  $F_0^{(y)}$ , due to solar heating, and a part due to exchange of sensible heat with the atmosphere,  $F_1^{(y)}$ . It is given by the surface integral

$$F^{(y)} = \frac{K_v}{V} \iint y \frac{\partial \rho}{\partial z} \Big|_{\frac{H}{2}} dx dy = \frac{\alpha}{V \widehat{\delta \rho} \rho_0 c_p^o} \iint y (-Q + F_{SH}) dx dy = F_0^{(y)} + F_1^{(y)} \quad (15)$$

where  $c_p^o$  is the specific heat of the ocean and  $\widehat{\delta \rho}$  is the scale of density variations in the mixed layer. The flux of sensible heat, directed out of the ocean,  $F_{SH}$ , and the solar heat flux,  $Q$ , are in units  $[W/m^2]$ . We assume that  $Q = -y Q_s q / L$ , i.e. the solar heating is linear in the latitude with amplitude  $Q_s q$ , where  $Q_s$  is a scale for the meridional gradient in solar heating and  $q$  is the non-dimensional forcing strength. This yields

$$F_0^{(y)'} = \frac{1}{12 L \Sigma_1} \frac{L}{H} \frac{\alpha Q_s q}{\widehat{\delta \rho} \rho_0 c_p^o} \quad (16)$$

In terms of the temperature difference between the top of the ocean and the bottom of the atmosphere,  $F_{SH}$  is given by

$$F_{SH} = -\rho_a c_p^a C_H U_*' (\Theta_s - \Theta^o) \quad (17)$$

where  $\rho_a$  is the atmospheric density at the surface and  $C_H$  is the dimensionless heat transfer coefficient. For the potential temperature at the 10m level,  $\Theta_s$ , and the surface potential temperature of the ocean,  $\Theta^o$ , we substitute

$$\Theta_s = \Theta_{av} + \theta = \Theta_{av} + [\Theta]\tau' \quad (18.1)$$

$$\Theta^o = T_0 - [\Theta^o]\rho(x, y, \frac{H}{2}) = T_0 - [\Theta^o](x\rho_x + y\rho_y + \frac{H}{2}\rho_z) \quad (18.2)$$

where  $[\Theta^o] = \widehat{\delta\rho}/\alpha$  is the scale of temperature perturbations in the mixed layer. Using equations (9.2), (18) and (17) we can evaluate the surface integral in equation (15). The result is

$$F_1^{(y)'} = \frac{L}{H} \frac{\rho_a c_p^a}{\rho_0 c_p^o} C_H U_* \left( \frac{2}{\pi^2} \frac{[\Theta]}{[\Theta^o]} X - \frac{1}{12} \rho_y' \right) \quad (19)$$

Note, that we assume a dry atmosphere, and  $F_1^{(y)}$  describes sensible heat flux. However, in reality the latent heat flux is larger, of the same order of magnitude as the direct solar forcing. Thus, the flux  $F_1^{(y)}$  must be thought of as the sum of sensible and latent heat flux, although there is no explicit evaporation and precipitation in the model.

Finally, there is a feedback term in the atmospheric equations. The forcing term in equation (8.1) consists of a constant part,  $F_0$ , representing the meridional gradient in solar heating, and  $F_1$ , forcing due to heat exchange with the ocean. We assume that the mass in a unit column of air is given by  $M/L^2$ , where  $M = p_0 L^2 f / 2g \Sigma_3 \sigma'$  is the mass scale, defined in van Veen [2002]. Thus, the rate of change of the atmospheric temperature due to heat exchange at the ocean's surface is given by  $L^2 F_{SH} / c_p^a M$ . By the thermal wind relation, (10), this yields a forcing term in the tendency of the shear stream function,  $\tau$ . The non-dimensional projection onto the zonally symmetric pattern is given by

$$F_1 = - \frac{L^2}{\Sigma_3 [\Theta] c_p^a M} \frac{1}{L^2} \iint F_{SH} \sin \pi y \, dx dy = \frac{L^2 \rho_a C_H U_*}{\Sigma_3 M} \left( \frac{2}{\pi^2} \frac{[\Theta^o]}{[\Theta]} \rho_y' - \frac{1}{2} X \right) \quad (20)$$

In table (1) we have listed all physical constants along with their value in SI units. The scales for length, time, density and temperature have been listed in table (2). With these parameters, the forcing terms (14), (15) and (20) are approximately given by

$$\begin{aligned} T_3' &\approx -X \\ F_1^{(y)'} &\approx 4.6q + 21.7(X - 0.06\rho_y') \\ F_1 &\approx 0.02(0.06\rho_y' - X) \end{aligned} \quad (21)$$



Finally, we redefine the density gradients, dividing them by a factor of  $1 + f'^2$ . Dropping the primes, the resulting dimensionless equations are

$$\frac{d}{dt_1}\rho_x = -\rho_y L_3 + (\rho_x + f'\rho_y)\rho_z - \rho_x \quad (22.1)$$

$$\frac{d}{dt_1}\rho_y = \rho_x L_3 - (f'\rho_x - \rho_y)\rho_z - \rho_y + k_1 q + k_2(X - k_3\rho_y) \quad (22.2)$$

$$\frac{d}{dt_1}\rho_z = -\rho_x^2 - \rho_y^2 - \mu\rho_z \quad (22.3)$$

$$\frac{d}{dt_2}L_3 = -L_3 - k_4 X \quad (22.4)$$

$$\frac{d}{dt_3}X = -Y^2 - Z^2 - aX + aF_0 + \epsilon_1(k_3\rho_y - X) \quad (22.5)$$

$$\frac{d}{dt_3}Y = XY - bXZ - Y + G \quad (22.6)$$

$$\frac{d}{dt_3}Z = bXY + XZ - Z \quad (22.7)$$

where  $f' = 3.65$ ,  $k_1 = 0.32$ ,  $k_2 = 1.5$ ,  $k_3 = 0.86$ ,  $k_4 = 1$  and  $\epsilon_1 = 0.02$ . The parameters of the atmosphere model are set to  $a = 1/4$ ,  $b = 4$  and  $G = 1$ . The forcing terms  $q$  and  $F_0$  and the coupling strength  $\epsilon_1$  will be used as bifurcation parameters.

In equations (22.1-7) we have written derivatives with respect to different time variables. They are related by

$$\frac{d}{dt_3} = \frac{\Sigma_1}{\Sigma_3} \frac{d}{dt_1} \equiv \epsilon_2 \frac{d}{dt_1} \quad \frac{d}{dt_3} = \frac{\Sigma_2}{\Sigma_3} \frac{d}{dt_2} \equiv \epsilon_3 \frac{d}{dt_2} \quad (23)$$

where we have introduced two more small parameters,  $\epsilon_{2,3}$ , alongside the coupling parameter  $\epsilon_1$ . In section (3) an asymptotic analysis will be presented, exploiting the time scale separation and the weak feedback.

System (22) has a feature common for Galerkin truncations of fluid dynamical equations. The linear terms are dissipative, the nonlinear terms are quadratic and conserve the quadratic sum of variables and the forcing terms are constant. A suitable Lyapunov function is given by

$$\mathcal{L} = \rho_x^2 + \rho_y^2 + \rho_z^2 + X^2 + Y^2 + Z^2 \quad (24)$$

A trapping region is then given by

$$\mathcal{L} < \frac{1}{\epsilon_2}(k_1^2 q^2 + F_0^2 + G^2) \equiv R^2 \quad (25)$$

Note, that the vertical angular momentum,  $L_3$ , is not taken into account. This is because the coupling term in equation (22.4) has no counterpart in equation (22.5). This is reasonable because the atmospheric loss of energy due to wind shear forcing is small compared to the heat flux. However, from equation (22.4) it follows that

$$L_3^2 \leq k_4^2 R^2 \quad (26)$$

defines a trapping region for  $L_3$ . Hence, all solutions of system (22) are bounded.

Parameter	Meaning	Value	Unit
$L$	Length of the basin	$5 \cdot 10^6$	$m$
$H$	Depth of the basin	$5 \cdot 10^3$	$m$
$h$	Depth of the mixed layer	50	$m$
$f$	Coriolis parameter	$7.3 \cdot 10^{-5}$	$s^{-1}$
$g$	Acceleration of gravity	10	$m s^{-2}$
$\alpha$	Thermal expansion coefficient	0.14	$kg m^{-3} K^{-1}$
$c_p^a$	Specific heat of the dry atmosphere	$10^3$	$J kg^{-1} K^{-1}$
$c_p^o$	Specific heat of the ocean	$4.19 \cdot 10^3$	$J kg^{-1} K^{-1}$
$p_0$	Atmospheric pressure at the surface	$10^5$	$Pa$
$\rho_a$	Atmospheric density at the surface	1.2	$kg m^{-3}$
$\rho_o$	Reference density in the ocean	$10^3$	$kg m^{-3}$
$r_h$	Horizontal Rayleigh damping coefficient	$10^{-5}$	$s^{-1}$
$r_v$	Vertical Rayleigh damping coefficient	$3 \cdot 10^{-8}$	$s^{-1}$
$K_h$	Horizontal eddy diffusivity coefficient	$10^2$	$m^2 s^{-1}$
$K_v$	Vertical eddy diffusivity coefficient	$10^{-4}$	$m^2 s^{-1}$
$\Delta$	Displacement of the zonal jet at the surface	$10^6$	$m$
$C_d$	Surface drag coefficient	$1.3 \cdot 10^{-3}$	
$C_H$	Heat transfer coefficient	$1.3 \cdot 10^{-3}$	
$U_*$	Typical zonal wind velocity at the surface	10	$m s^{-1}$
$Q_s$	Meridional difference in solar heating	200	$W m^{-2}$
$s$	Vertical scale factor of the zonal wind	0.2	
$\sigma$	Static stability of the atmosphere	22	$K$

TABLE 1. Parameters in the coupled model. Numerical values taken from Maas [1994], van der Schrier and Maas [1998] and Peixoto and Oort [1992]. Note, that  $r_h$  has been chosen large in order to yield a realistic density scale. In van der Schrier and Maas [1998]  $r_h$  is smaller, but the scaling factor  $1 + f'^2$  is of order  $10^3$ , so that a comparable effective density scale is used.

### 3. Asymptotic analysis with a passive atmosphere

As we have seen, the weak feedback to the atmosphere and the difference in time scales introduce small parameters in the coupled model. For simplicity, we scale them with a single small parameter:

$$\epsilon_1 = 2 \cdot 10^{-2} = O(\epsilon) \quad \epsilon_2 = 3 \cdot 10^{-5} = O(\epsilon^2) \quad \epsilon_3 = 2 \cdot 10^{-2} = O(\epsilon) \quad (27)$$

System (22) can then be written as

$$\begin{aligned} \frac{d}{dt_1} \mathbf{Y} &= \mathbf{g}(\mathbf{Y}, L_3, \mathbf{X}_1) \\ \epsilon \frac{d}{dt_1} L_3 &= -L_3 - k_4 \mathbf{X}_1 \\ \epsilon^2 \frac{d}{dt_1} \mathbf{X} &= \mathbf{f}_0(\mathbf{X}) + \epsilon \mathbf{f}_1(\mathbf{X}_1, \mathbf{Y}_2) \end{aligned} \quad (28)$$

Length			
	horizontal	$L$	$5 \cdot 10^3 \text{ km}$
	vertical	$H$	$5 \text{ km}$
Time			
	overturning	$\Sigma_1^{-1} = L^2/12K_h$	$500 \text{ years}$
	wind driven	$\Sigma_2^{-1} = r_v^{-1}$	$1 \text{ year}$
	atmospheric	$\Sigma_3^{-1}$	$7 \text{ days}$
Density variations			
	interior	$[\hat{\delta}\rho] = 12\rho_0 r_h K_h / gH$	$2.4 \cdot 10^{-4} \text{ kg m}^{-3}$
	mixed layer	$[\hat{\delta}\rho] = \alpha Q_s f L^2 / \rho_0 g c_p^o h^2$	$0.5 \text{ kg m}^{-3}$
Temperature			
	atmosphere	$[\Theta] = f \Sigma_3 L^2 / d c_p$	$24 \text{ K}$
	mixed layer	$[\Theta^o] = \hat{\delta}\rho / \alpha$	$3.6 \text{ K}$
Mass			
	atmosphere	$M = p_0 L^2 f [\Theta] / 2g \Sigma_3 \sigma$	$7.7 \cdot 10^{18} \text{ kg}$

TABLE 2. Scales for the ocean and the atmosphere model. The atmospheric time scale is the damping time scale of baroclinic waves due to Hamiltonian cooling and interlayer friction, see van Veen [2002]. In the right column the order of magnitude.

where we have introduced  $\mathbf{Y} = (\rho_x, \rho_y, \rho_z)^T$  and  $\mathbf{X} = (X, Y, Z)^T$ . As a consequence of Fenichel's theorem [Wiggins, 1994], hyperbolic equilibria of the system with  $\epsilon = 0$  give a first approximation of a slow manifold in the system with nonzero  $\epsilon$ . In order to asymptotically approximate the dynamics on the slow manifold, we substitute the regular expansion

$$L_3 = L_3^{(0)} + \epsilon L_3^{(1)} + \dots \quad \mathbf{X} = \mathbf{X}^{(0)} + \epsilon \mathbf{X}^{(1)} + \dots \quad (29)$$

In the limit  $\epsilon \downarrow 0$  we find

$$\mathbf{f}_0(\mathbf{X}^{(0)}; F_0) = 0 \quad (30)$$

Thus, a three dimensional slow manifold of equations (28) is approximated by the equilibria of the uncoupled Lorenz model. The solutions of equation (30), and their linear stability, can be found explicitly as the roots of a third order polynomial equation [Sicardi and Masoller, 1996; Shilnikov et al., 1995]. In figure (2) the branch of equilibria is shown. Two saddle node bifurcations occur, so that there is one equilibrium or there are three. The Hopf bifurcation, labeled HB, represents the baroclinic instability in the Lorenz model. Away from the saddle node bifurcations,  $\mathbf{f}_0$  can locally be inverted so that we can write  $\mathbf{X}^{(0)} = \phi(F_0)$ , with  $\mathbf{f}_0(\phi; F_0) = 0$ . On the intermediary time scale  $L_3^{(0)}$  relaxes towards an equilibrium with  $\mathbf{X}^{(0)}$ , given by

$$L_3^{(0)} = -k_4 \mathbf{X}_1^{(0)} \quad (31)$$

Together, equations (30) and (31) approximate an extended, four dimensional slow manifold of the coupled system.

The slow dynamics is described by  $\dot{\mathbf{Y}} = \mathbf{g}(\mathbf{Y}, -k_4\phi_1, \phi_1)$ . A familiar form of these equations is obtained if we first shift  $\mathbf{Y}_3 \rightarrow \bar{\mathbf{Y}}_3 = \mathbf{Y}_3 + k_4\phi_1/f'$  and subsequently scale time and  $\mathbf{Y}$  by a factor  $1 + k_4\phi_1/f'$ . This yields

$$\frac{d}{dt_1} \mathbf{Y}_1 = -\mathbf{Y}_1 + \mathbf{Y}_1 \bar{\mathbf{Y}}_3 + B \mathbf{Y}_2 \bar{\mathbf{Y}}_3 \quad (32.1)$$

$$\frac{d}{dt_1} \mathbf{Y}_2 = -\mathbf{Y}_2 + \mathbf{Y}_2 \bar{\mathbf{Y}}_3 - B \mathbf{Y}_1 \bar{\mathbf{Y}}_3 + \mathcal{G} - C \mathbf{Y}_2 \quad (32.2)$$

$$\frac{d}{dt_1} \bar{\mathbf{Y}}_3 = -\mathbf{Y}_1^2 - \mathbf{Y}_2^2 - A \bar{\mathbf{Y}}_3 + A \mathcal{F} \quad (32.3)$$

Apart from the extra damping term in equation (32.2), these are the equations of the Lorenz model (8), with parameters depending on  $\phi$  according to

$$\begin{aligned} A &= \frac{f' \mu}{f' + k_4 \phi_1} & C &= \frac{f' k_2 k_3}{f' + k_4 \phi_1} & \mathcal{G} &= \frac{f' k_1 q + f' k_2 \phi_1}{f' + k_4 \phi_1} \\ B &= f' & \mathcal{F} &= \frac{k_4 \phi_1}{f'} \end{aligned} \quad (33)$$

The similarity between the ocean model and the Lorenz model was already pointed out in Maas [1994]. There, the choice of parameters guaranteed that no complex behaviour occurred. Here, this is not clear from the outset as we have an extra damping term and forcing that depends on the atmospheric parameters through  $\phi_1$ . Because of the extra damping term we cannot exactly solve for the equilibria of system (32), as this involves finding roots of a fifth order polynomial equation. We can, however, check numerically what kind of dynamics arise as we vary  $F_0$ , thereby altering the atmosphere's equilibrium state,  $\phi$ . Continuation, by means of software package AUTO [Doedel et al., 1986], indicates that a stable equilibrium state is the unique limit set of system (32) for  $0 < F_0 < 100$  and  $q = 1$ . This equilibrium state corresponds to a statically stable state of the ocean, i.e.  $\rho_z < 0$ .

The first order terms are given by

$$L_3^{(1)} + k_4 \mathbf{X}_1^{(1)} = 0 \quad \mathbf{X}^{(1)} = -D\mathbf{f}_0^{-1} \mathbf{f}_1(\phi_1, \mathbf{Y}_2) \quad (34)$$

Here, the inverse of the Jacobian matrix at  $\phi$  enters the equations. As long as  $\mathbf{X}^{(1)}$  is of order one, the dynamically and statically stable equilibrium state of the ocean model, found in the lowest order approximation, will persist. If, however,  $F_0$  is chosen near a saddle node bifurcation of the atmospheric equilibrium,  $D\mathbf{f}_0$  becomes nearly singular and the ocean's equilibrium state might bifurcate. In this situation the feedback loop in system (22), otherwise weak because of the small parameter  $\epsilon_1$ , becomes strong due to the sensitive dependence of the atmosphere's equilibrium state on the feedback,  $\mathbf{f}_1$ .

Thus, GSP analysis shows that we have four possibilities for the behaviour of the coupled model, depending on the equilibria of the Lorenz-84 model, labeled 1 to 4 in figure (2):

- (1) There is one stable equilibrium. This equilibrium corresponds to a stable slow manifold in the coupled system. The dynamics on this slow manifold consists of a relaxation towards a statically stable equilibrium state in the ocean model.

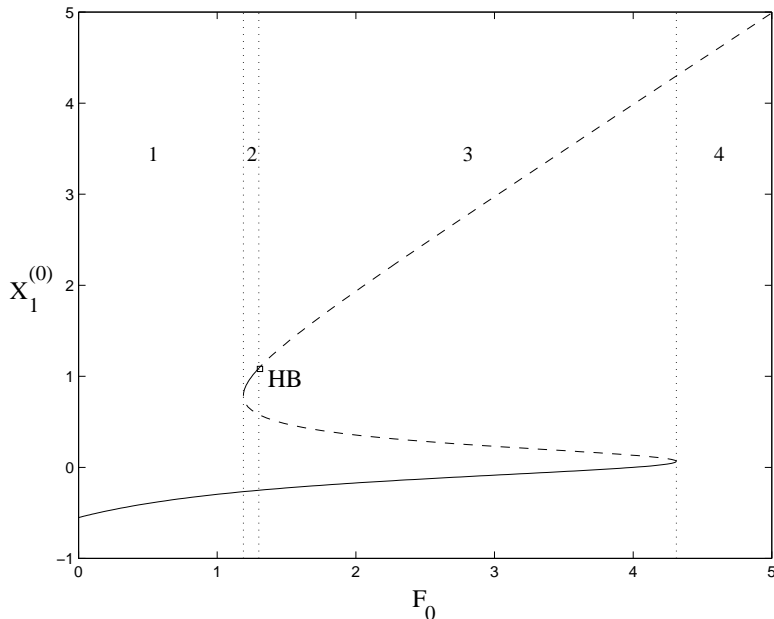


FIGURE 2. Continuation of the equilibria of the Lorenz-84 model for  $G = 1$ . The numbers 1 to 4 denote the different cases listed in section 3. Solid branches are stable and dashed branches are unstable.

- (2) There are three equilibria, one is of saddle type whereas the other two are stable. Each of these equilibria corresponds to a slow manifold in the coupled system, two of which are stable. The dynamics on a slow manifold consists of a relaxation towards a statically stable equilibrium state in the ocean model. Only if the corresponding atmospheric equilibrium is nearly critical, the ocean model's equilibrium can bifurcate and periodic oscillations can occur on the slowest time scale. This situation is described in section (4.1).
- (3) There are three equilibria, one of which is stable whereas the other two are of saddle type. This situation occurs beyond Hopf bifurcation HB, where a stable cycle is produced. Depending on the initial conditions, the coupled system can either settle on the slow manifold corresponding to the stable equilibrium or be attracted to the stable cycle on the fast time scale. As shown in section (4), no bifurcations of the ocean model's equilibrium occur on the stable slow manifold.
- (4) There is one equilibrium of saddle type. The corresponding slow manifold is unstable and the coupled system is attracted to the stable cycle on the fast time scale. For higher values of  $F_0$ , this cycle bifurcates and more complex behaviour sets in, as shown in section (4.2).

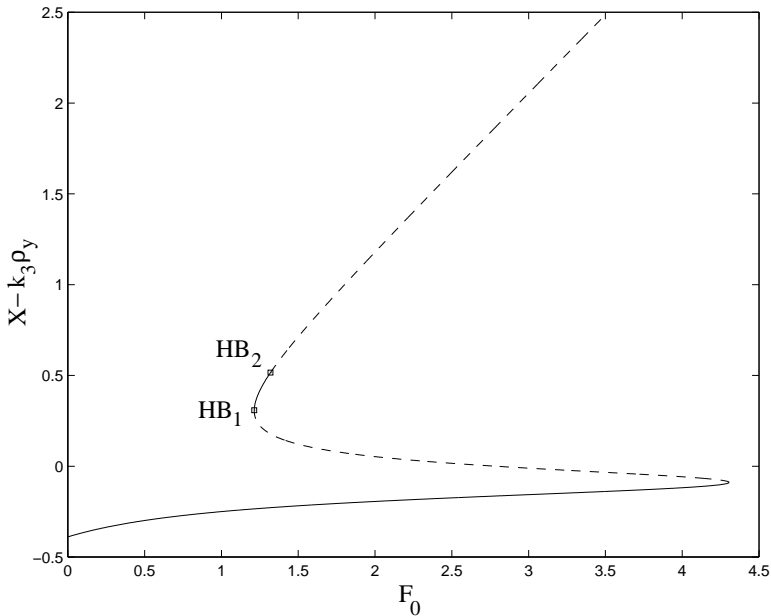


FIGURE 3. Continuation of the equilibrium state of the Lorenz-Maas model. Solid lines represent stable branches, dashed lines represent unstable branches. Hopf bifurcations have been labeled  $HB_{1,2}$ .

#### 4. Bifurcation analysis of the coupled system

In figure (3) the branch of equilibria of the coupled system (22) is shown. We have fixed  $q = 1$  and  $\epsilon_1 = 0.02$  and increased  $F_0$  from zero. On the vertical axis we have plotted the meridional gradient of the heat flux at the ocean's surface. In the lower, stable, branch of equilibria this flux strengthens the zonal jet in the atmosphere, i.e.  $F_1 > 0$ . In the upper branch it weakens the zonal jet, i.e.  $F_1 < 0$ . The latter situation agrees with the annual mean distribution of sensible heat flux at the surface [Peixoto and Oort, 1992, chapter 10].

The first Hopf bifurcation, labeled  $HB_1$ , occurs near a saddle node bifurcation and is not present in the uncoupled Lorenz model. It corresponds to case 2 discussed in section (3). Here, an unstable cycle with a period of order one in units  $\Sigma_1^{-1}$  is created. In section (4.1) it is shown that the presence of this Hopf bifurcation near the saddle node bifurcation is connected to a Bogdanov-Takens point, at which the equilibrium has two zero eigenvalues.

The rightmost Hopf bifurcation, labeled  $HB_2$ , represents the atmosphere model's baroclinic instability. It produces a cycle with a period of order one in units  $\Sigma_3^{-1}$ , which represents a traveling baroclinic wave. If the forcing is increased this cycle bifurcates and complex behaviour arises. The route to chaos through bifurcations of the cycle and intermittent behaviour are described in sections (4.2) and (4.2), respectively.

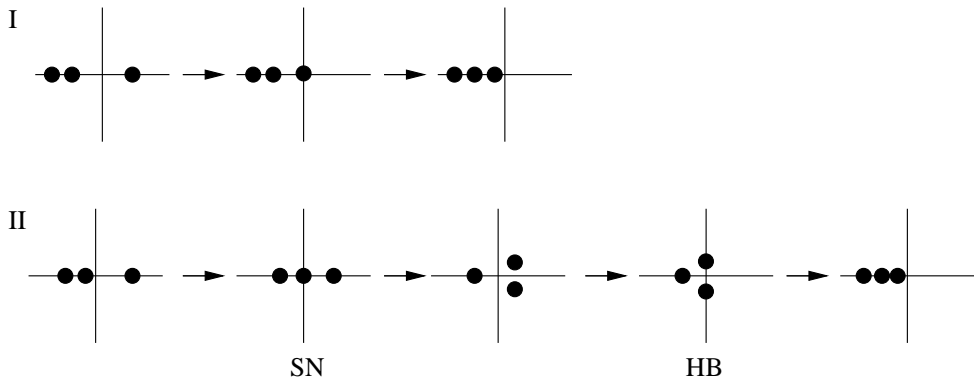


FIGURE 4. Bifurcation scenario along the branch of equilibria of the Lorenz model (I) and the Lorenz-Maas model (II): eigenvalues in the complex plane. The saddle node (fold) bifurcation has been labeled SN and the Hopf bifurcation  $HB$ . In scenario II only the leading eigenvalues are shown. Compare to figures (2) and (3).

**4.1. The Bogdanov-Takens singularity.** At Hopf bifurcation  $HB_1$  a cycle is created with a period of about 500 years, the overturning time scale  $\Sigma_1^{-1}$ . The behaviour of the eigenvalues along the branch of equilibria, shown in figure (3), is portrayed in figure (4). The periodic orbit exists to the right of  $HB_1$  and has one unstable multiplier. If  $F_0$  is increased slightly, it becomes homoclinic to the saddle type equilibrium. This can be understood from the unfolding of the Bogdanov-Takens singularity which occurs if the fold and Hopf bifurcations in scenario II coincide. The unfolding of this singularity is described in Kuznetsov [1998], chapter 8. As predicted by the asymptotic analysis of section (3), the distance between the bifurcation points in parameter space is rather small, about  $2 \cdot 10^{-5}$  and thus of the order of  $\epsilon_2$ . The clearest picture is obtained by unfolding the codimension two singularity in parameters  $q$  and  $\epsilon_1$ , i.e. the solar forcing in the ocean model and one coupling parameter, as shown in figure (5). When increasing  $\epsilon_1$  from zero, at first there is no Hopf bifurcation. Scenario I is followed when we continue the equilibrium in parameter  $q$ . At the critical value of  $\epsilon_1$  a pair of zero eigenvalues appears. This is the codimension two Bogdanov-Takens point. At this point a Hopf curve and a homoclinic bifurcation curve originate. If we increase  $\epsilon_1$  further, scenario II is followed.

Along the homoclinic bifurcation line, the saddle value, i.e. the sum of the unstable eigenvalue and the (real part of the) leading stable eigenvalue, is small ( $\lesssim 10^{-2}$ ) but positive. Therefore, the homoclinic connection and the periodic orbit that connects to the Hopf line are weakly unstable. In figure (6) the homoclinic connection is shown, along with an 50.000 year integration, started near the saddle type equilibrium. On the long time scale,  $\Sigma_3^{-1}$ , the system relaxes towards the stable focus on the upper branch in diagram (3), with the realistic surface flux. In terms of phase relations between the density gradients  $\rho_{x,y,z}$ , this damped oscillation is similar to the oscillatory cycle found in the uncoupled Maas model [Maas, 1994]. In

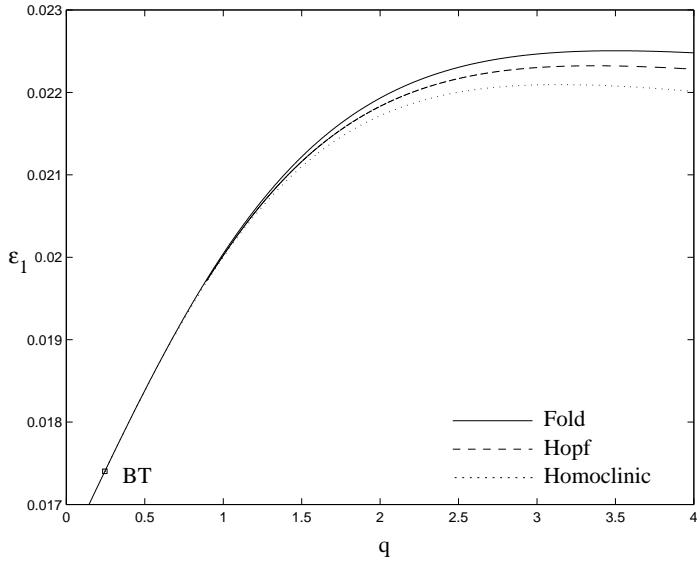


FIGURE 5. Unfolding of the Bogdanov-Takens singularity in  $q$  and  $\epsilon_1$ , for  $F_0 = 1.21374$ . On the Hopf line an unstable periodic orbit is created which becomes homoclinic to the saddle type equilibrium, i.e. the middle branch in figure (3).

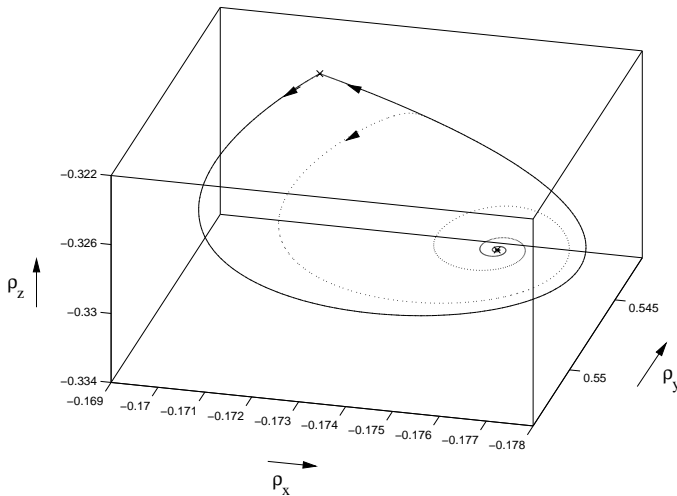


FIGURE 6. Damped oscillation on the time scale  $\Sigma_1^{-1}$ , for  $\epsilon_1 = 0.0217$  and  $q = 2$ . The solid line is the homoclinic connection, the dashed line is forward integration. The saddle, in the top left corner, and the stable focus, in the bottom right corner, have been marked with crosses. The integration time was  $\Delta t_1 = 100$ .



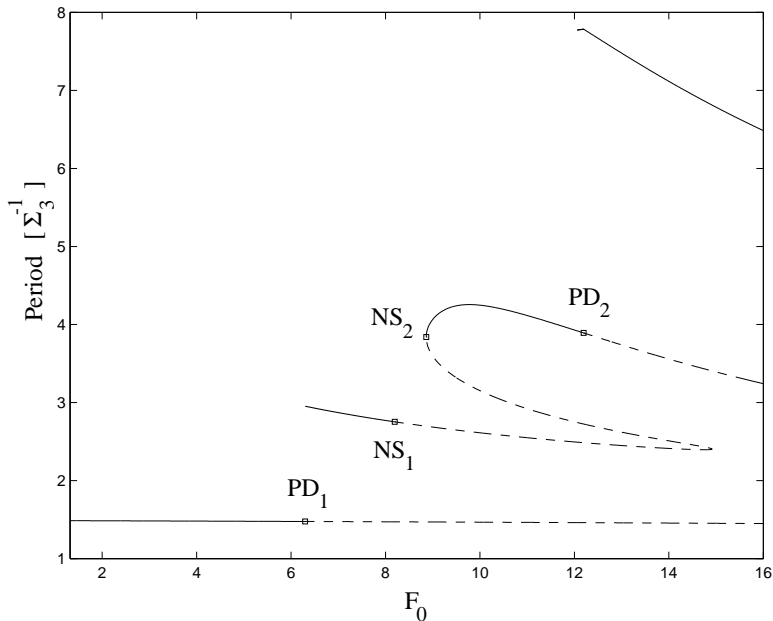


FIGURE 7. Continuation of the cycle produced at  $HB_2$ . Solid lines denote stable branches, dashed lines denote unstable branches. Period doubling bifurcations have been marked  $PD_{1,2}$  and Neimark-Sacker bifurcations  $NS_{1,2}$ . For values of  $F_0$  between bifurcation points  $NS_1$  and  $NS_2$  the behaviour is chaotic, periodic with high period ( $O(10) [\Sigma_3^{-1}]$ ) or intermittent.

one phase of the oscillation the meridional density gradient,  $\rho_y$  is relatively low, and the zonal density gradient,  $\rho_x$ , relaxes due to friction and dissipation. The overturning circulation weakens. In the second phase, the differential solar heating builds up the meridional density gradient, which strengthens the overturning through the geostrophic coupling to  $\rho_x$ . The overturning circulation then weakens the meridional gradient and the cycle is closed. It might be expected that this cycle can not occur if the coupling through the vertical angular momentum,  $L_3$ , is strong. In that case, the horizontal components of the density gradient will be mixed and the interplay between the damped overturning circulation and the forcing due to meridional differential heating will be destroyed. Indeed, if  $k_4$  is increased to about 1.5, the Hopf bifurcation  $HB_1$  disappears. As prescribed by GSP theory, discussed in section (3), the fast, atmospheric, variables are slaved during the oscillation, in instantaneous balance with the feedback term  $\mathbf{f}_1$ .

**4.2. Bifurcations of limit cycles and chaos.** In diagram (7), the continuation of the cycle, originating at  $HB_2$ , is shown. Initially it is stable. At the first period doubling bifurcation, labeled  $PD_1$ , a stable cycle of twice the period is created. This cycle becomes unstable through a Neimark-Sacker bifurcation, labeled  $NS_1$ . The period doublings  $PD_{1,2}$  and Neimark-Sacker bifurcation  $NS_1$  are also

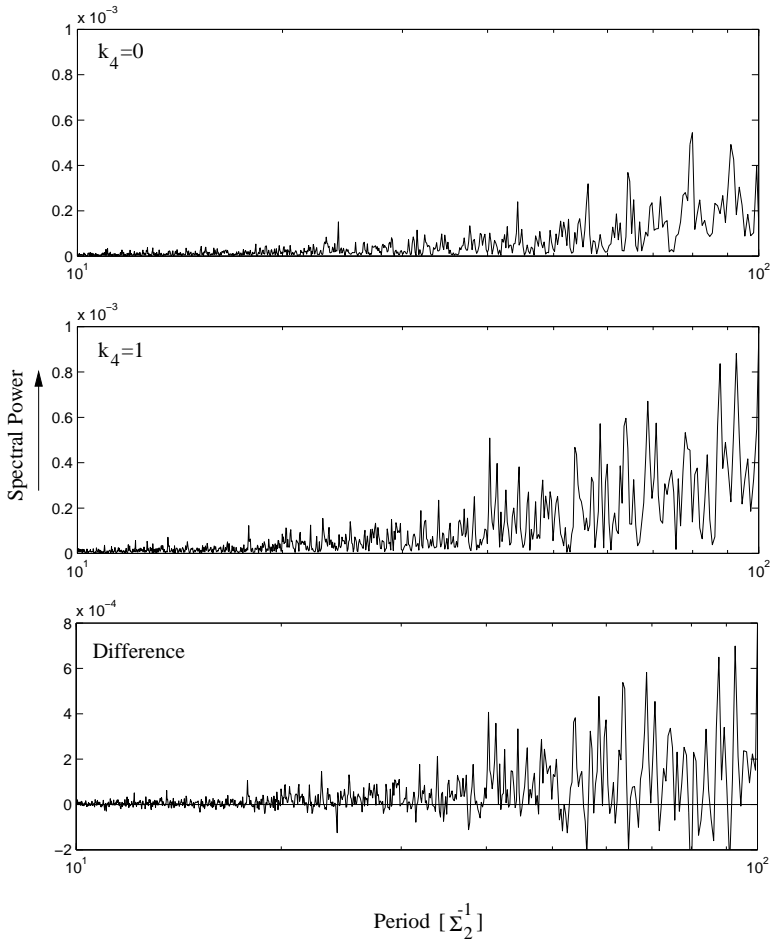


FIGURE 8. Power spectra of  $\rho_y$  from a 15.000 year integration in the chaotic regime with  $F_0 = 8.25$ . Top:  $k_4 = 0$ , middle:  $k_4 = 1$ , bottom: difference. Note, that the vertical scales are almost the same. The horizontal scale is logarithmic, spanning  $10 - 100 [\Sigma_2^{-1}] \approx 10 - 100 \text{ yrs}$ .

present in the uncoupled Lorenz model [Shilnikov et al., 1995]. In van Veen [2002] it was shown that beyond  $NS_1$  a sudden transition to chaos occurs following the Ruelle-Takens scenario [Ruelle and Takens, 1971]. This also happens in the coupled model. The behaviour becomes chaotic, with tiny periodic intervals in parameter space. This behaviour is similar to that of the Lorenz-Stommel model, as described in Roebber [1995]; van Veen et al. [2001]. In the chaotic regime, there is very little variability in the slow subsystem. Therefore, it can be characterised as a regime with a passive ocean.

The regime with a chaotic atmosphere and a passive ocean can be regarded as the model's representation of the real climate. Therefore, we list a number of average

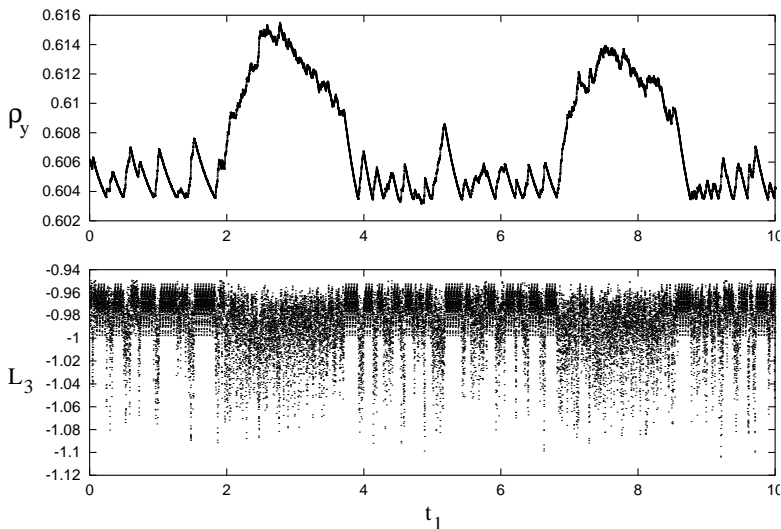


FIGURE 9. Intermittency in the Lorenz-Maas model. The meridional density gradient,  $\rho_y$ , and the vertical angular momentum,  $L_3$ , against  $t_1$ .

physical quantities to validate the model. The average values were obtained from a 15.000 year integration at  $F_0 = 8.25$ . The vertical mean intensity of the zonal jet is about  $26 \text{ ms}^{-1}$ , which yields a maximal zonal wind at the surface of about  $5.2 \text{ ms}^{-1}$  with an associated surface wind stress of about  $8.1 \text{ Pa}$ . The meridional density difference in the ocean's mixed layer is about  $4.3 \text{ kgm}^{-3}$ , corresponding to a difference in sea surface temperature of about  $30 \text{ K}$ . The meridional difference in heat flux into the atmosphere is about  $260 \text{ W}$ . Finally, a measure for the overturning circulation is given by  $\sqrt{L_1^2 + L_2^2} \approx 1.1 \cdot 10^4 \text{ m}^2 \text{ s}^{-1}$ . These values agree reasonably well with climatological means [Peixoto and Oort, 1992], although the zonal jet intensity and the sea surface temperature difference are exaggerated by a factor of about 1.2. Considering the few degrees of freedom of the coupled model it reproduces the climatological values well.

The deviation from the mean value of the meridional sea surface temperature difference is slightly underestimated: typically about  $0.2 \text{ K}$  compared to a measured standard deviation induced by synoptic-scale eddies of  $0.5 \text{ K}$ . The deviation from the mean value of the vertical mean zonal jet intensity agrees with the measured value of about  $8 \text{ ms}^{-1}$ .

In order to investigate the influence of the coupling through the wind driven circulation in this regime, we produced power spectra of a 15.000 year integration with  $k_4 = 1$  and  $k_4 = 0$ , shown in figure (8). In the latter case only the coupling through heat exchange remains. As  $L_3$  forces the density gradients through advection, we expect to see an increase in the spectral power of  $\rho_y$  on a decadal time scale if the coupling is switched on. This is best visible in the bottom picture, the difference of the spectra with and without wind driven circulation. The difference is of the same order of magnitude as the power in the individual spectra.

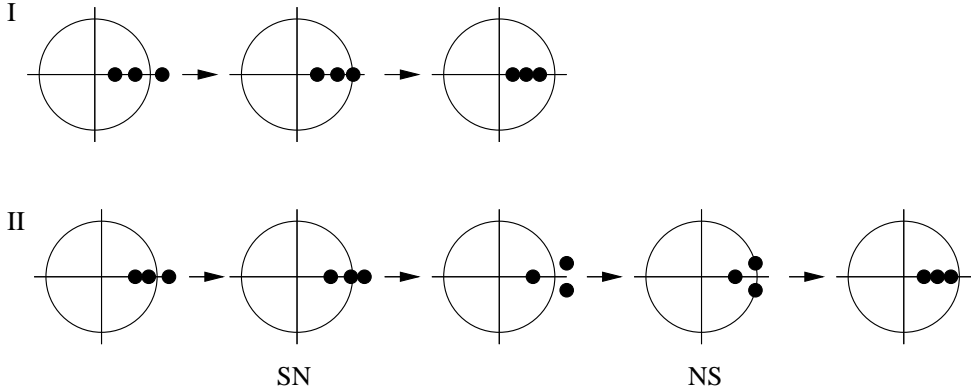


FIGURE 10. Bifurcation scenario along a branch of periodic solutions of the Lorenz-84 model (I) and the Lorenz-Maas model (II): Floquet multipliers in the complex plane. The saddle node (fold) bifurcation has been labeled SN and the Neimark-Sacker bifurcation *NS*. In scenario II only the leading multipliers are shown.

**4.3. Ocean-atmosphere interaction through intermittency.** The ocean plays an active role near the boundaries of the periodic intervals, where intermittency can occur. Ample discussion of this behaviour was given in van Veen et al. [2001]. In figure (9) we show an intermittent time series of the Lorenz-Maas model, obtained from a 5.000 year integration. As in the Lorenz-Stommel model, the intermittency is of type II in terms of the classification by Pomeau and Manneville [1980], meaning that the periodic orbit involved loses its stability through a Neimark-Sacker bifurcation. In the coupled model, Neimark-Sacker bifurcations tend to occur close to fold bifurcations. This scenario is illustrated in figure (10). In the uncoupled Lorenz model, scenario I, a single, real Floquet multiplier crosses the unit circle. In the coupled model, scenario II, a real multiplier crosses the unit circle in the opposite direction and forms a complex pair with the unstable multiplier. The complex pair crosses back into the unit circle, causing a Neimark-Sacker bifurcation. The distance in parameter space between the fold and the Neimark-Sacker bifurcations is typically of the same order of magnitude as the ratio of time scales  $\epsilon_2 = \Sigma_3/\Sigma_1 \approx 10^{-5}$ . This scenario is also followed around bifurcation point  $NS_2$ , on the second branch of periodic orbits in figure (7). The long time scale,  $\Sigma_1^{-1}$ , shows up in the intermittent dynamics because the rate of convergence to, and departure from the saddle type periodic orbit is set by the leading multipliers, two of which are associated with the slow subsystem.

The bifurcation scenarios for periodic orbits, shown in figure (10), are analogous to those of equilibria, discussed in section (4.1). Again, the ocean can play an active role in the coupled dynamics near a bifurcation point of the model.

## 5. Conclusion

We have presented a low-order ocean-atmosphere model which combines wind driven and overturning circulation. The coupling terms, both through wind torque forcing and heat exchange at the interface, have been derived from the boundary conditions of the ocean model. The model describes the clockwise gyre, south of the gulf stream in the North Atlantic, coupled to a midlatitude, geostrophic atmosphere with baroclinic waves.

Due to the difference in time scales of wind driven, overturning and atmospheric dynamics, as well as to the weak feedback to the atmosphere, small parameters appear in the model. By means of GSP theory, the coupled model is reduced to an approximate slow manifold. Analysis of the reduced dynamics shows that, as long as the atmospheric equilibrium is not near a saddle-node bifurcation, only relaxation towards a dynamically and statically stable equilibrium can occur in the ocean model. If the atmospheric equilibrium becomes nearly critical, a Hopf instability can be induced in the slow dynamics.

At this Hopf bifurcation a cycle, with a period on the overturning time scale, is created. A bifurcation analysis in two parameters leads to a Bogdanov-Takens point, where the saddle-node and the Hopf bifurcations coincide. The unfolding of this codimension two point shows, that the Hopf bifurcation disappears if the feedback parameter is smaller than a critical value and if the coupling through wind driven circulation is stronger than a critical value. It also shows, that the cycle, created at the Hopf bifurcation, becomes homoclinic if the forcing is increased slightly. The homoclinic connection is weakly unstable, and integrations show damped oscillations towards a stable equilibrium on the slow (overturning) time scale. During these oscillations the atmospheric variables are passive, in instantaneous balance with the ocean's feedback.

If the solar forcing parameter in the atmosphere model is increased, its equilibrium state becomes unstable through a Hopf bifurcation which represents the baroclinic instability. A stable cycle is created with a period of the order of one week. The continuation of this cycle to higher values of the solar forcing shows that, in a window in parameter space, chaotic behaviour arises. Some averaged physical quantities, obtained from a forward integration in the chaotic regime, are compared to their observed climatological means. In spite of its simplicity, the coupled model reproduces the observed values well. The intensity of the zonal jet in the atmosphere and the meridional sea surface temperature difference are slightly exaggerated. A comparison of power spectra with and without wind driven circulation reveals that the coupling through wind stress forcing adds to the energy in decadal modes of the ocean's variables.

Typically, tiny windows of periodicity exist amidst the chaos. Near the boundary of stability of such windows, intermittency is observed. This situation is very similar to the one found in van Veen [2002]. In the fully chaotic regime, the ocean can be considered passive. The slow variables have very small amplitude and merely integrate the atmospheric forcing. During the intermittent behaviour, the ocean

plays an active role, as it repeatedly pushes the atmosphere through the boundary of periodic and chaotic behaviour.

The low-order climate model presented here can readily be extended to include more physics and more detail. In contrast to, e.g. Nakamura et al. [1994] and van Veen [2002], both constituents of the model are scalable, i.e. based on Galerkin truncation. Extensions of the model, to be studied in future research, include:

- Taking into account salinity in the ocean model, after van der Schrier and Maas [1998], allowing for a study of the full thermohaline circulation. A parameterisation of water vapour transport in the atmosphere then has to be designed. Thus, the effect of the meridional profile of precipitation can be studied. Also, the ocean model with salinity can display chaotic behaviour and thus play a more active role in the coupled dynamics.
- Adding more modes to the atmosphere model, allowing for more complex internal atmosphere dynamics such as vacillation [De Swart, 1989]. The internal dynamics of the atmosphere then includes a wider range of time scales, overlapping with the time scale of wind driven circulation.
- Adding more modes to the ocean model in order to extend it to a double gyre or two hemispheres. Inclusion of nonlinear modes is, however, not straightforward in view of the treatment of the pressure torque [Maas, 2002].
- Explicitly representing the ocean's mixed layer such as to avoid some of the parameterisations in section (2.2). This may lead to a better description of the coupling between wind driven and overturning circulation through advection of sea surface temperature anomalies.

Thus, a family of low-order models is set up which allows for the mathematical analysis of important feedback loops in the climate system.

## 6. Acknowledgments

The author would like to thank Ferdinand Verhulst, Theo Opsteegh, Leo Maas, Gerard van der Schrier, Frank Selten and Reindert Haarsma for useful discussions and proofreading. This work is part of the NWO project 'a conceptual approach to climate variability' (nr. 61-620-367).

## Bibliography

- Arnold, L. & Olbers, D. [2002] Private communications.
- De Swart, H. E. [1989] “Analysis of a six-component atmospheric spectral model: chaos, predictability and vacillation,” *Physica D* **36**, 222–234.
- Doedel, E., Champneys, A., Fairgrieve, T., Kuznetsov, Yu. A., Sandstede, B. & Wang, X.J. [1986] *AUTO97: Continuation and bifurcation software for ordinary differential equations (with HomCont)* Computer Science, Concordia University, Montreal, Canada.
- Huang, R. X. & Stommel, H. M. [1992] “Convective flow patterns in an eight-box cube driven by combined windstress, thermal and saline forcing,” *J. Geophys. Res.* **97**, 2347–2364.
- Ierley, G. R. & Sheremet, V. A. [1995] “Multiple solutions and advection-dominated flows in the wind-driven circulation. part I: Slip,” *J. Mar. Res.* **53**, 703–737.
- Kuznetsov, Yu. A. [1998] *Elements of applied bifurcation theory* (Springer, New York).
- Lorenz, E. N. [1984] “Irregularity: a fundamental property of the atmosphere,” *Tellus* **36A**, 98–110.
- Maas, L. R. M. [1994] “A simple model for the three-dimensional, thermally and wind-driven ocean circulation,” *Tellus* **46A**, 671–680.
- Maas, L. R. M. [2002] “Basin scale dynamics of a stratified rotating fluid,” In preparation.
- Monahan, A. H. [2001] “Lyapunov exponents of a simple stochastic model of the thermally and wind-driven ocean circulation,” Submitted to *Dyn. Atmos. Ocean.*
- Nakamura, M., Stone, P. H. & Marotzke, J. [1994] “Destabilization of the thermohaline circulation by atmospheric eddy transports,” *Journal of Climate* **7**, 1870–1882.
- Peixoto, J.P. & Oort, A.H. [1992] *Physics of climate* (American Institute of Physics).
- Pomeau, Y. & Manneville, P. [1980] “Intermittent transition to turbulence in dissipative dynamical systems,” *Commun. Math. Phys.* **74**, 189–197.
- Rödenbeck, C., Beck, C. & Kantz, H. “Dynamical systems with time scale separation: averaging, stochastic modelling and central limit theorems,” In Imkeller, P. & von Storch, J. S., editors, *Stochastic climate models*. Birkhauser, [2001].
- Roebber, P. J. [1995] “Climate variability in a low-order coupled atmosphere-ocean model,” *Tellus* **47A**, 473–494.
- Ruelle, D. & Takens, F. [1971] “On the nature of turbulence,” *Commun. math. Phys.* **20**, 167–192.

- Shilnikov, A., Nicolis, G. & Nicolis, C. [1995] “Bifurcation and predictability analysis of a low-order atmospheric circulation model,” *Internat. J. Bifur. Chaos* **5(6)**, 1701–1711.
- Sicardi, A. C. & Masoller, C. [1996] “Analytical study of the codimension two bifurcation of the new Lorenz system,” *Instabilities and Nonequilibrium Structures V*, 345–348.
- Stommel, H. [1961] “Thermohaline convection with two stable regimes of flow,” *Tellus* **13**, 224–230.
- Titz, S., Kuhlbrodt, T., Rahmstorf, S. & Feudel, U. [2002] “On freshwater-dependent bifurcations in box models of the interhemisphere thermohaline circulation,” *Tellus* **54A**, 89–98.
- Schrier, G. van der & Maas, L. R. M. [1998] “Chaos in a simple model of the three-dimensional salt-dominated ocean circulation,” *Climate Dynamics* **14**, 489–502.
- Veen, L. van [2002] “Baroclinic flow and the Lorenz-84 model,” *Internat. J. Bifur. Chaos*. To appear (chapter 2 of this thesis).
- Veen, L. van , Opsteegh, T. & Verhulst, F. [2001] “Active and passive ocean regimes in a low-order climate model,” *Tellus* **53A**, 616–627 (chapter 3 of this thesis).
- Veronis, G. [1963] “An analysis of wind-driven ocean circulation with a limited number of Fourier components,” *J. Atmos. Sci.* **20**, 577–593.
- Welander, P. [1982] “A simple heat-salt oscillator,” *Dyn. Atmos. Ocean.* **6**, 233–242.
- Wiggins, S. [1994] *Normally hyperbolic invariant manifolds in dynamical systems* (Springer Verlag).



## Samenvatting

Onderzoek naar klimaatvariabiliteit heeft in de afgelopen decennia veel aandacht getrokken. De observatie van een globale temperatuurstijging, die rond het begin van de twintigste eeuw inzette, vraagt om een verklaring. Het ligt voor de hand, een verband te leggen met de industriële revolutie en de daarmee samenhangende milieubelasting. Volgens welke mechanismen deze menselijke invloed zich kan doen gelden is echter slechts ten dele bekend. Daarnaast rijst de vraag, tot op welke hoogte klimaatverandering door menselijk ingrijpen onderscheiden kan worden van natuurlijke variabiliteit. Helaas gaan metingen niet veel verder terug in de tijd dan honderd jaar, zodat het ondoenlijk is de gemeten temperatuurstijging op significantie te beoordelen aan de hand van empirie.

Als mogelijke oplossing van dit probleem kunnen we een model van het klimaat opstellen en dit representeren als computerprogramma. De fysische basisvergelijkingen voor zo'n model zijn klassieke vergelijkingen uit de stromingsleer, eventueel aangevuld met een beschrijving van chemische processen, dynamica van ijsmassa's, enzovoorts. Met behulp van de computer kunnen we het klimaat in het model naar believen voor- en achteruit in de tijd laten evolueren. Zo kan worden getest, of het model meetwaarden goed reproduceert en kunnen voorspellingen worden gedaan.

Probleem is, dat het model in de computer discreet gerepresenteerd is. Met andere woorden: relevante grootheden, zoals temperatuur en windsnelheid, worden op een eindig aantal roosterpunten berekend en ook in de tijd worden discrete stappen gezet. Dit introduceert een fout, aangezien de structuur van, bijvoorbeeld, het temperatuurveld op kleine schaal verwaarloosd wordt. Deze fout is inherent aan het doen van numerieke berekeningen. De keuze van een rooster, en daarmee van het oplossend vermogen, van het computermodel bepaald mede met welke fysische effecten rekening moet worden gehouden bij het opstellen van de modelvergelijkingen. Processen die zich afspelen op een schaal, kleiner dan de roosterafstand, worden niet beschreven.

Over het algemeen zal de fout in de berekeningen kleiner zijn als gekozen wordt voor een fijner rooster en een navenant groter aantal opgeloste fysische processen. Deze keuze brengt met zich mee, dat het computermodel groter wordt. Het aantal variabelen, en daarmee het aantal vergelijkingen dat bij iedere stap in de berekening simultaan moet worden opgelost, groeit snel met het aantal roosterpunten. Dit geeft twee problemen. Het eerste is dat berekeningen aan een groot model een zware wissel trekken op de computer. Dit probleem kunnen we voor ons uit schuiven door steeds snellere computers met grotere geheugens te bouwen. Het tweede probleem, dat in de ijver het eerste vooruit te schuiven soms vergeten wordt, is dat data, gegenereerd door een groot model, moeilijk interpreteerbaar zijn. Door de veelheid aan wisselwerkingen raken causale verbanden ondergesneeuwd. Zulke data worden dan ook doorgaans geanalyseerd met behulp van statistische methoden. Zo worden gemiddelden en spreidingen berekend, alsmede correlaties tussen verschillende variabelen. Door afwisselend aan verschillende parameters te draaien, zoals CO<sub>2</sub>-uitstoot, zonnestraling en degelijke, wordt gepoogd de fysische mechanismen die leiden tot structurele klimaatverandering te destilleren.

Een volledige wiskundige beschrijving van het gedrag van zo'n groot model is ondoenlijk. Daardoor blijft de vraag, hoe robuust conclusies zijn waartoe modelberekeningen leiden, onbeantwoord. Maar al te vaak blijken voorspellingen voor het toekomstige klimaat kritiek afhankelijk van het model of de analysetechniek die wordt gebruikt. De studie van lage orde modellen is een poging dit probleem te vermijden. Lage orde wil zeggen dat het oplossend vermogen van het model bewust laag wordt gehouden. Zodoende wordt de fijnstructuur niet beschreven en worden veel kleinschalige processen verwaarloosd. De vereenvoudiging van het model houdt daarmee een selectie in van de relevante tijdschalen en ruimtelijke schalen. Zonder de pretentie een realistische beschrijving van het klimaat te geven kan in lage orde modellen worden gezocht naar causale verbanden en kwalitatief gedrag met een zekere mate van universaliteit.

Een voorbeeld van universeel gedrag, dat voor het eerst werd beschreven met behulp van lage orde modellen, is chaos. Edward Lorenz ontdekte chaotisch gedrag, oftewel gevoelige afhankelijkheid van begincondities, in een lage orde model voor atmosferische stroming. Ofschoon het model, dat hij bestudeerde, zo sterk vereenvoudigd was dat geen meteoroloog het serieus kan nemen, leidde zijn ontdekking tot een nieuw paradigma in de meteorologie. De studie van lage orde klimaatmodellen, zoals betracht in dit proefschrift, is een poging universeel gedrag op te sporen dat generiek is voor het klimaatsysteem.

Een pregnante eigenschap van klimaatmodellen, van welke complexiteit dan ook, is de aanwezigheid van sterk uiteenlopende tijdschalen. De atmosferische gesteldheid verandert van dag tot dag, terwijl bijvoorbeeld de grootschalige oceaanstrooming pas op een tijdschaal van maanden varieert. De typische tijdschaal van variabiliteit loopt op tot eeuwen als we kijken naar stroming in de diepe oceaan en dynamica van ijskappen. Ten opzichte van weersvoorspelling brengt dit een nieuwe vraag met zich mee: hoe kunnen processen, die zich op zulke uiteenlopende tijdschalen voordoen, elkaar beïnvloeden?

De lage orde klimaatmodellen, die hier bestudeerd worden, zijn oceaan-atmosfeer modellen. De oceaan is de langzame component en de atmosfeer is de snelle component. Is er geen essentiële interactie tussen de componenten, dan noemen we de oceaan passief. Forcering van de oceaan door de atmosfeer is dan niet te onderscheiden van forcering door witte ruis. Het kan voorkomen, dat de koppeling tussen de componenten een belangrijke rol speelt. In dat geval noemen de oceaan actief. Processen die zich in de oceaan afspelen drukken dan hun stempel op de evolutie van het klimaat.

In hoofdstuk 2 van dit proefschrift wordt een lage orde atmosfeermodel afgeleid, dat in hoofdstukken 3 en 4 aan twee verschillende oceaanmodellen wordt gekoppeld. Met behulp van bifurcatie-analyse wordt gezocht naar mechanismen door welke het oceaanmodel een actieve rol kan spelen. Bifurcatie-analyse beschrijft de afhankelijkheid van het gedrag van een model van zijn parameters. Deze parameters zijn geassocieerd met fysische grootheden als de instraling van zonnearmte en wrijving aan het aardoppervlak. Een kwalitatieve verandering van het gedrag van een model dient zich aan op een bifurcatiepunt, oftewel bij kritieke waarden van de parameters. De algemene conclusie, die kan worden getrokken uit hoofdstukken 3 en 4, is dat

juist in de buurt van zo'n kritiek punt de langzame component, de oceaan dus, een actieve rol kan spelen. Op afstand van zo'n kritiek punt is de oceaan passief.

De implicaties van deze conclusie voor grote modellen zijn niet direct duidelijk. Hoewel er de laatste tijd grote vooruitgang is geboekt is het nog steeds niet haalbaar om realistische modellen van hoge orde met bifurcatie-analyse te ontleden. Wel zijn er studies verricht met hoge orde modellen die het hier geschetste beeld bevestigen. Er zijn zekere realistische keuzes van de parameters bij welke het model zeer gevoelig is voor de koppeling tussen langzame en snelle componenten. Door de onderliggende bifurcatiestructuur van dit fenomeen te beschrijven in een hiërarchie van modellen met een toenemend aantal variabelen, kan uiteindelijk wellicht een verklaring worden gegeven voor de verschillen in prognoses verkregen met actuele, realistische klimaatmodellen.



*Time wounds all heels.*  
Groucho Marx

## Dankwoord

Ten eerste dank ik Jan en Marian. Mijn ouders.

Dan ben ik dank verschuldigd aan Ferdinand en Theo, die dit project mogelijk hebben gemaakt.

Vervolgens gaat mijn dank uit naar Sander, Tobias, Steven, Daan, Barbara, Richard, Henk, Menno, Theo, Luis, Bob, Philipp, Maarten, Mischja, Arno, Yuri, Thierry, Leo, Wijnand, Gerard, Odo, Anna, Vaughn, Arnoud, Tessa, Erica, Hanna, David, Rudi, Viktor, Mark, Siti, Liesbeth, Mark, Niels, Natascha, Gert-Jan, Kirsten, Erik-Paul, Caroline, Bruce, Agaath, Axel, André, Harold, Vincent, Bart, Geertje, Rainer, Ulrich, Charlotte, Frank, Reindert, Christine, Andrey, Renato, Marie-José, Martijn, Emmanuelle, Gregory, Carles, Martijn, Aleksandra, Jo, Jeroen, Henk en Cor.  
Zonder jullie was er niks aan.



# Curriculum Vitae

Lennaert van Veen werd geboren op 27 maart 1972 in Leiden. In 1990 haalde hij zijn VWO diploma aan het Rijnlands Lyceum in Oegstgeest. Daarna volgde een studie natuurkunde aan de universiteit van Amsterdam, in 1996 afgesloten met het doctoraalexamen. Dit proefschrift is het resultaat van een promotieonderzoek, uitgevoerd aan de universiteit van Utrecht en het KNMI.